A NUMERICAL SOLUTION FOR THE INTERACTION OF A MOVING SHOCK WAVE WITH A TURBULENT MIXING REGION

By

WILLIAM FRED WALKER

Bachelor of Science
The University of Texas
Austin, Texas
1960

Master of Science
The University of Texas
Austin, Texas
1961

Submitted to the Faculty of the Graduate School
of the Oklahoma State University
in partial fulfillment of the requirements
for the degree of
DOCTOR OF PHILOSOPHY
May, 1966

A NUMERICAL SOLUTION FOR THE INTERACTION OF A MOVING SHOCK WAVE WITH A TURBULENT MIXING REGION

Thesis Approved:

Glen W. Zumwalt
Thesis Adviser

Jerald D. Parker

Ladislaus J Fila

R V Beal

J. W. Boggs
Dean of the Graduate School

PREFACE

A method has been devised whereby the interaction of a moving shock wave with a turbulent mixing region can be studied. The method has been applied to a relatively simple two-dimensional problem and qualitative experimental verification has been obtained.

This work was completed under the sponsorship of the Sandia Corporation, Albuquerque, New Mexico. The study constitutes a single phase in the overall program of developing a capability for predicting the phenomenon which occurs when a blast wave intercepts a ballistic vehicle. Investigations into other facets of the blast intercept problem are presently being conducted at Oklahoma State University. Mr. R. J. Damkevala is performing an experimental study of the interaction of a moving shock wave with a free flight conical projectile. Mr. R. R. Eaton is performing an analysis in order to describe the exiting of a vehicle from a blast sphere. The results of these studies, as well as the results provided from the present investigation, should provide useful information with regard to the ultimate solution of the complex blast intercept problem.

The author wishes to express his deepest appreciation to Dr. G. W. Zumwalt for the giving of his valuable time to serve as thesis adviser. Dr. Zumwalt's ability to understand the physical side of a complex problem has proved to be of invaluable benefit to the author during this

investigation. A debt of gratitude is owed to Professor L. J. Fila for the many hours which he unselfishly gave to discussing the mathematical, numerical, and physical aspects of every phase of the investigation. These sessions were of immeasurable benefit to the author. I also wish to thank Dr. Jerald Parker; first, for making possible my graduate study at Oklahoma State University, and second, for reading the thesis manuscript and offering valuable suggestions. Thanks are also due Dr. R. B. Deal for serving on my graduate committee.

Appreciation is expressed to Mr. Leonard V. McCommon for the professional manner in which he prepared the figures and graphs. To my parents, I express my inadequate thanks for the formal education which they made possible.

Last, but most important of all, I wish to express my eternal gratitude to my wife, Myrna, without whose forbearance, love, and encouragement this work could never have been accomplished. It is to her that this dissertation is dedicated.

TABLE OF CONTENTS

LIST OF TABLES

LIST OF FIGURES

LIST OF PLATES

NOMENCLATURE

$A(x,y,t)$	blurring term coefficient
A_1	defined on page 62
$B(x,y,t)$	blurring term coefficient
c	local acoustic velocity
c_o	constant of proportionality
C	Crocco number
e	fluid energy
f	defined on page 35
F^x	defined on page 35
F^y	defined on page 35
h	diagonal of finite difference net
h_1	finite difference net spacing in x-direction
h_2	finite difference net spacing in y-direction
k	coefficient of thermal conductivity
K	time parameter defined on page 40
K_1	time parameter defined on page 39
K_2	time parameter defined on page 39
ℓ	mesh number in y-direction
ℓ_i	characteristic length for pressure perturbation in in the i-direction
M	Mach number
	upper bound of perturbation

m	mesh point number in the x-direction
n	time plane number
N_{Re}	Reynolds number
N_{Pr}	Prandtl number
p	static pressure
p_o	stagnation pressure
q	heat conduction term
R	$\frac{u_a}{2\sigma^2}$
	gas constant
	reference length in Appendix C
s	distance
T	temperature
t	time
u	x component of velocity
U	specific internal energy
v	y component of velocity
W	jet width
w	velocity modulus $(u^2 + v^2)^{\frac{1}{2}}$
x,y	cartesian coordinates
y_*	position at which $\frac{u}{u_c} = 0.5$ occurs
Z	quantity defined on page 61
α	blurring term defined on page 39
β	blurring term defined on page 39
γ	ratio of specific heats

$\delta\varphi^{\circ}_{o,o}$	initial value of perturbation
ϵ	virtual kinematic viscosity
ϵ_i	exchange coefficient for pressure perturbations
ζ	defined on page 25
η^*	defined on page 22
η	time parameter defined on page 86
θ_1	defined on page 61
θ_2	defined on page 61
μ	coefficient of viscosity
ξ	defined on page 57
ρ	density
σ_x	normal Reynolds stress
σ_y	normal Reynolds stress
σ	jet spreading rate parameter
$\overline{\sigma}$	local Courant number
$\overline{\sigma}_o$	maximum allowable Courant number
τ	time increment
τ_{ij}	tangential Reynolds stresses
	in Appendix B, laminar shearing stresses
Φ	blurring term in difference form
φ	general perturbation variable
χ	finite difference net angle (Figure 4)
ψ	normal force defined in Appendix B
ψ_1	term defined on page 57
ψ_2	term defined on page 57

ω	damping term due to blurring technique
Ω	defined on page 59

Superscripts

-	time average
	in Appendix C, nondimensional values
'	fluctuating component
*	dimensional quantity
n	time plane number

Subscripts

i,j	denotes direction
N	normal direction
T	tangential direction
R	reference value
m	x net point location
ℓ	y net point location
c	centerline
a	adjacent field
1	conditions in jet
2	conditions in cavity
3	initial slip line conditions
4	conditions in shock tube

CHAPTER I

INTRODUCTION

In recent months a great deal of interest has been expressed concerning the phenomenon which occurs when a ballistic vehicle encounters a blast wave. This interest has resulted in extensive analytical and experimental research programs at various institutions and government agencies. To date, no complete analysis has been given which will adequately predict the aerodynamic and structural effects which result when a wave of arbitrary strength passes over a body at any prescribed flight condition. This is not unexpected, however, because the general blast intercept problem is composed of several aspects, each of which is an extremely complex problem. Figure 1 has been suggested by Wolff (1)[1] as depicting qualitatively the various stages in the progression of a shock wave as it passes axially over a conical body. Figure 1a shows the configuration before intercept has taken place. The figure portrays the body as moving at supersonic speed, but this does not necessarily have to be the case. For instance, both Wolff and Jackomis (2) considered the situation which occurs when a wave passes over a body at rest.

Figure 1b shows the shock front interacting with both the original conical wave and the body. This is the phase of the blast intercept

---

[1]Numbers in parentheses refer to references in the Bibliography.

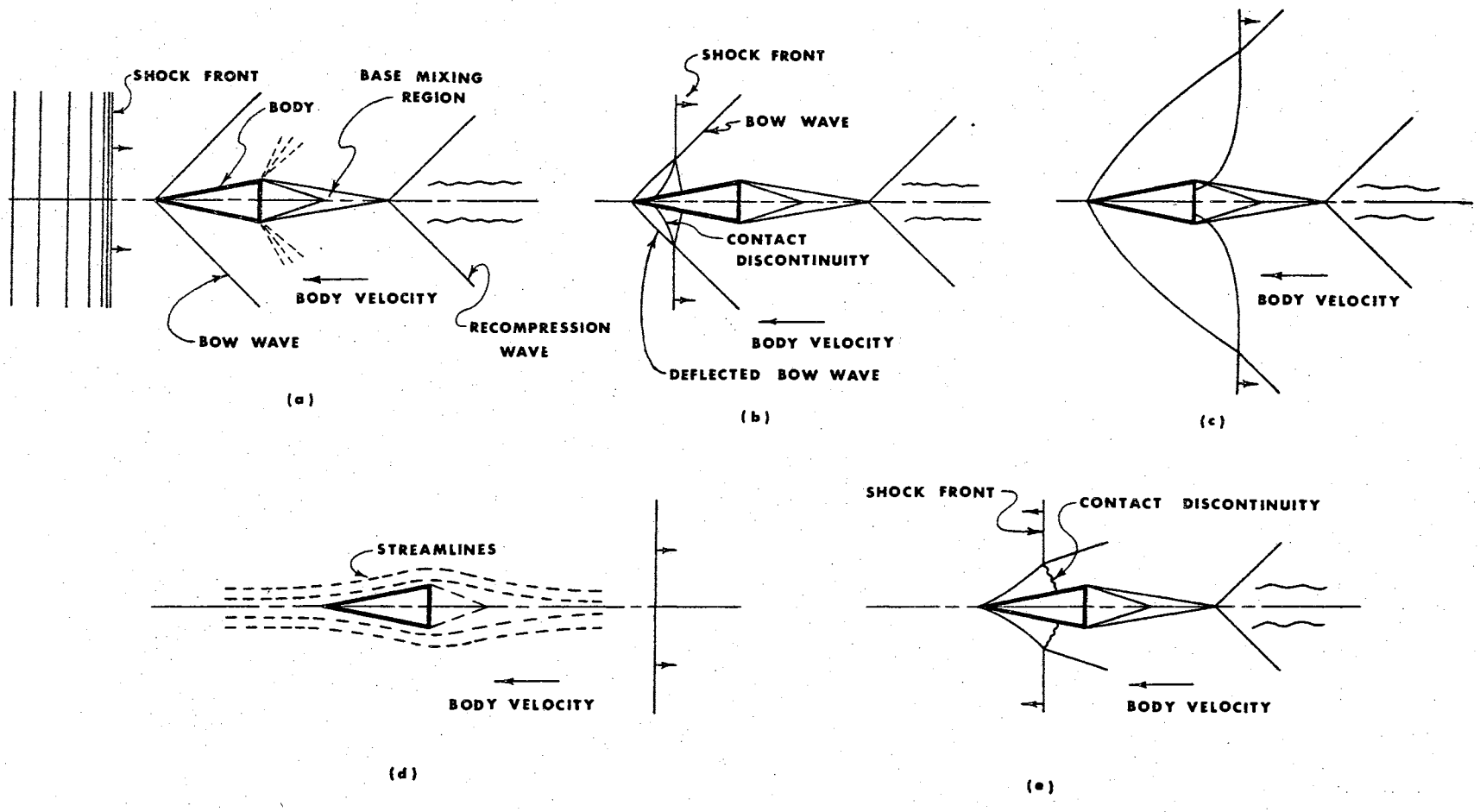

Figure 1. Progression of a Blast Wave over a Ballistic Vehicle.

problem which has heretofore received the most attention (3). Analytical and experimental investigations have been made in order to provide more understanding of both the shock-on-shock interaction and the interaction of the wave with the body.

Figure 1c shows the wave passing through the base mixing region and Figure 1d portrays the phase which occurs when the wave has completely passed over the body. The figure indicates that the flow field over the body is subsonic, but this does not necessarily have to be the case. Figure 1e shows the final phase of the problem; the exit of the body from the blast field. This aspect of the problem has until recently received very little attention. However, the solution of the exiting problem is currently under study at Oklahoma State University.

Figure 1c depicts the phase of the blast intercept problem which has provided the basis for the present investigation. Until now, no analysis has been developed which will account for the interaction of a moving shock wave with a turbulent mixing region. The analyses of the problems depicted by Figures 1b, 1d, and 1e involve only the inviscid hydrodynamic equations. However, the shock-mixing region interaction problem necessitates a complete mathematical description of the turbulent mixing process. Heretofore, whenever a jet mixing analysis has been undertaken, several of the terms in the governing mathematical expression could be omitted because of their insignificant contributions to the overall mixing process. Therefore, no completely general mathematical description of the turbulent mixing process has ever been given. When considering the shock wave-mixing region interaction, however, these

convenient simplifications cannot be tolerated because one no longer knows which, if any, of the terms will be negligible. Furthermore, since the usual methods for studying shock diffraction problems involve numerical procedures, the equations which describe the turbulent mixing process must be in such a form that they, too, can be solved by a numerical technique. Therefore the primary objective of this investigation is to devise a method whereby the phenomenon associated with the interaction of a moving shock wave with a turbulent mixing region can be studied. In order to do this, a series of secondary objectives must be accomplished. These are as follows:

1. to derive the complete set of governing equations which describe the turbulent mixing process;
2. to select a method which has been shown to be capable of predicting the propagation of a moving shock wave; and then to apply this method to the governing equations in order to determine if it is capable of describing realistically a turbulent mixing region; then, if a turbulent mixing region can be established,
3. to introduce a moving shock wave into the flow field in order to determine whether or not any undue numerical difficulties arise as a result of the shock wave-mixing region interaction.

Since the development of the method is of paramount importance, only the two-dimensional case has been considered. However, the theory can be extended directly to the case of axial symmetry.

The analytical investigation which follows can be divided into three parts, which correspond to the secondary objectives previously stated:

1. the derivation of the governing equations and the promulgation of the numerical method,
2. the establishment of a jet mixing region by the numerical method proposed,
3. the passage of a shock wave over the established mixing region.

For all the problems computed during the course of this investigation, the jet Mach number was taken to be two. Two cases of a shock wave interacting with the mixing region were considered. In the first case the shock wave pressure ratio was 4.0, and in the second case, 12.0. In both cases the shock wave was considered to move perpendicular to the jet flow direction. For both of the cases considered, qualitative experimental verification has been obtained.

The numerical solutions from this analysis were obtained with the aid of several computers; namely, the CDC[1] 1604, IBM[2] 1410, and IBM 7094.

---

[1]Control Data Corporation.

[2]International Business Machines.

CHAPTER II

LITERATURE REVIEW

A detailed discussion of the literature applicable to this study could well be given in two parts. The first would deal with the numerical methods currently available for obtaining the solution to problems involving shock dynamics. The second part would deal with the problems associated with shock waves interacting with jet mixing regions. Though the second of these two categories would not be too lengthy, the first could easily constitute an entire textbook. It is for this reason that a detailed discussion of the methods of shock dynamics will not be given here. The interested reader is referred to the works by Tyler and Walker (4), (5) for a discussion of these methods. The remainder of this chapter will be restricted to a discussion of the literature which pertains to shock waves interacting with viscous shearing regions.

A great deal of work has been performed in the analyses of turbulent jet mixing and base flow problems. Unfortunately, none of this work has been concerned with the establishment of a mixing region as a result of solving the hydrodynamic equations numerically. The fact has been pointed out previously that such an analysis is necessary for the present study.

Investigations concerning the interaction of a shock wave and a turbulent boundary layer and the interaction of a shock wave with the

exhaust of a jet engine have proved to be of some help in the present analysis. Charczenko and Hennessey (6) investigated the effect of exhausting a retrorocket from the nose of a blunt body into a supersonic free-stream. Though the authors were primarily interested in the effectiveness of such a device as a means of reducing the pressure drag on a supersonic blunt body, they did provide several informative schlieren photographs showing the interaction of the supersonic jet with the detached bow wave.

Romeo and Sterrett (7) investigated a similar problem. Their main interest was in determining experimentally the effect of a forward facing jet on the bow shock wave in a Mach 6 free-stream. Jet Mach numbers were varied from 1 to 10.3 and the ratio of jet total pressure to free-stream total pressure was varied from 0.03 to 2.5. The ratio of body diameter to jet-exit diameter was varied from 1.12 to 55.6. Though the quantitative information obtained was of little value to the present investigation, the qualitative information obtained has provided some interesting insights into the phenomena which occur when a shock wave interacts with a jet mixing region. The results show that the jet could affect the bow wave in two different ways. The first way, referred to as the strong shock case, was to move the shock further away from the body without significantly altering its shape. This effect was attributed to an apparent increase in the size of the body as seen by the free-stream flow. The second way in which the jet could affect the bow wave was referred to as the weak shock case. When this condition occurred, the bow wave was displaced a considerable distance from the body and its shape was significantly altered.

The parameters determining the occurrence of a particular shock case were found to be the ratio of stagnation pressures, the exit Mach number, and the ratio of body diameter to jet exit diameter. The first two parameters seemed to produce more pronounced effects than did the diameter ratio.

In applying these results to the present investigation, it would appear reasonable to conclude that the shock-mixing region interaction will be strongly dependent upon the ratio of stagnation pressure across the shock as well as dependent upon some characteristic Mach number. The stagnation pressure ratio effect was indicated by Tyler (4), however the Mach number influence was not suggested.

Assuming steady state conditions, Moeckel (8) has devised a method for computing the changes in shock wave shape as a result of an oblique shock wave impinging upon a region of nonuniform flow properties. Under the assumptions of the analysis, this method will predict very nicely the shape of a shock wave as it passes through a jet or wake region of known profile. The applicability of such a method to the problem of a moving shock wave intercepting a viscous mixing region is, however, questionable for two reasons. First, Moeckel made the assumption that in the vicinity of the interaction, viscous effects are negligible. For the problem of interest, with turbulent separated flow regions, this assumption is inadmissable. Second, for a flow field whose properties are varying with time, the wake or jet profile is not necessarily known a priori.

In order to demonstrate the method, Moeckel calculated as a sample problem the trace of an oblique shock wave passing through a wake flow

region. The free-stream Mach number was taken to be 3.0 and the shock angle before impingement upon the wake region was 34.0 degrees. The results of the calculations are shown in Figure 2. For the reasons discussed above, in view of the requirements of the current investigation, one should attempt to glean only qualitative information from Moeckel's results. In so doing the important observation to be made from Figure 2 is that the shock angle increases as the Mach number decreases. This result should not be too surprising, however, if one assumes that the pressure and flow direction downstream of the shock wave are both approximately uniform.

Whitham (9) has put forth a unique method for solving problems similar to those investigated by Moeckel. Whitham's method is more general, however, because it is capable of handling unsteady cases.

The essential steps in obtaining a solution with Whitham's method are fairly simple. The relevant hydrodynamic equations are first written in characteristic form. The differential relation which must be satisfied by the flow quantities along a characteristic are then applied to the flow quantities just behind the shock wave. The differential relation, in conjunction with the shock relations, allows the motion of the shock wave to be determined.

As with Moeckel, Whitham assumed that when a shock wave intercepts a mixing region, the viscous forces do not influence the interaction. This fact, along with the inherent assumption that the flow behind the shock wave must always be supersonic, limits the value of Whitham's method.

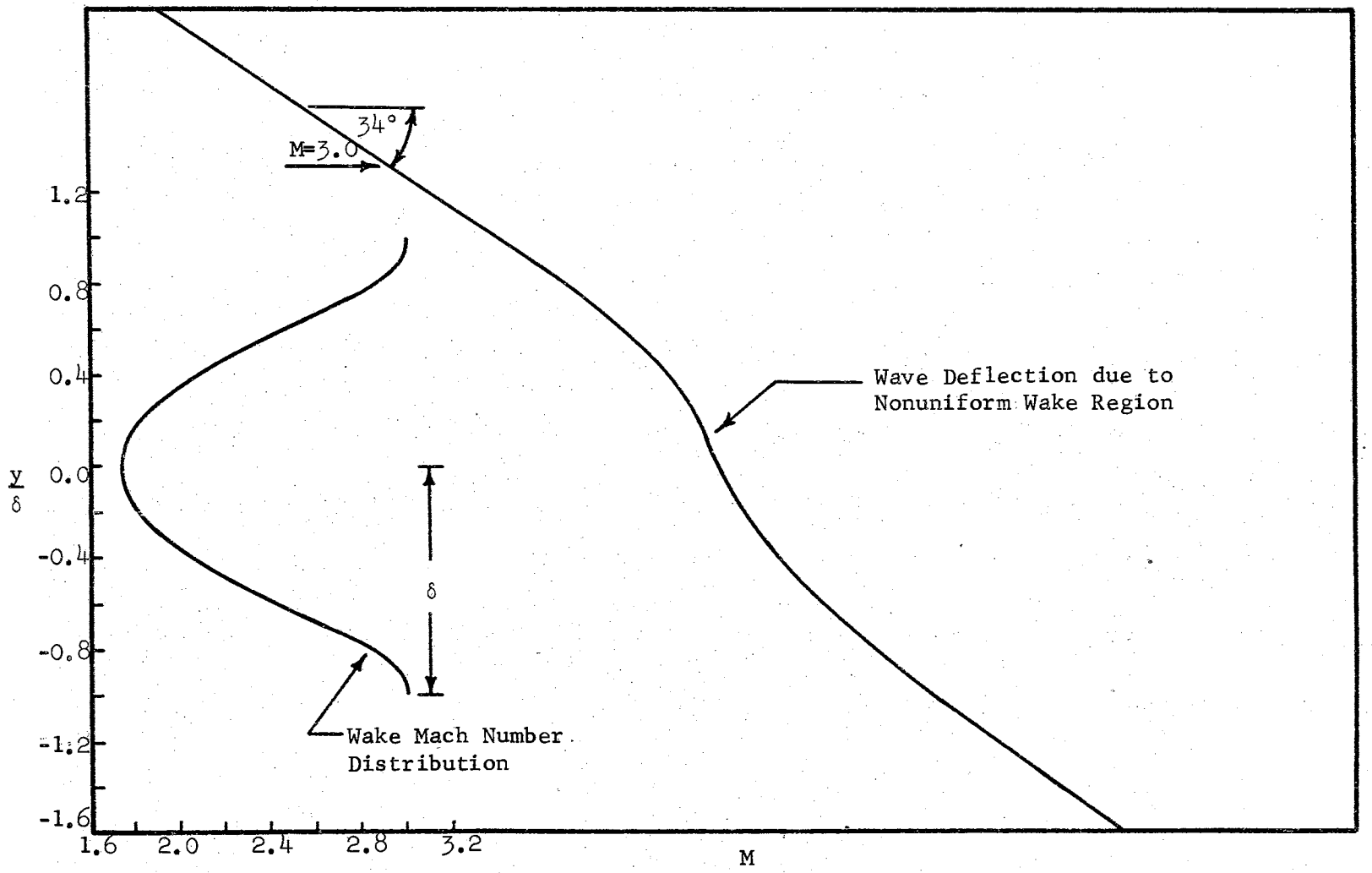

Figure 2. Oblique Shock Wave Impinging on Nonuniform Flow Region (8).

Riley (10) has investigated the interaction of a shock wave with a mixing region by applying Fourier analysis to the linearized equations of motion. As with the other investigators, he did not consider the effect of the viscous forces in the interaction phenomenon.

Dosanjh (11), (12), (13) has made extensive experimental investigations into the effects of propagating a shock wave in the axial direction over an axi-symmetric jet. His studies have been conducted primarily in order to obtain information concerning the noise level which is produced as a result of a shock wave interacting with a turbulent flow field. This information is of course highly desirable in the design of noise suppressors for jet aircraft. Dosanjh's results agree with the weak shock case reported by Romeo and Sterrett (7). He found that as the wave moved into the free jet a "bulge" was produced in the wave which closely resembled the velocity profile of the jet.

Zumwalt and Tang (14) have made a detailed study of a shock wave passing over a conical ballistic vehicle. In their analysis it was assumed that the base flow region was instantaneously subjected to an adiabatic compression. By applying a quasi-steady analysis, the subsequent base pressure decay was computed and found to agree quite well with experiment. No provision was made, however, for the actual wave-mixing region interaction which is the problem of interest in this study.

As was noted previously, none of the work which has heretofore been performed has dealt specifically with providing a method for studying the transient shock-mixing region interaction. However, most of the references which have been mentioned have provided some insight into the interaction phenomenon.

CHAPTER III

DERIVATION OF GOVERNING EQUATIONS

The hydrodynamic equations for the flow of a compressible, viscous, heat conducting fluid have been derived in Appendix B. The equations are presented in the "divergence free" or conservation form discussed by Tyler (4). In Appendix C the molecular transport terms in the hydrodynamic equations have been shown to be negligible for large values of the Reynolds number. As mentioned previously, this investigation is concerned first with establishing numerically a turbulent mixing region, and second with the interaction of a moving shock wave with the mixing region. For this analysis, then, the equations obtained in Appendix C must be altered so as to include the turbulence effects present in a turbulent mixing region. The two-dimensional conservation equations, to which the turbulent transport effects will be added are, from Appendix C:

Continuity,

$$\frac{\partial \rho}{\partial t} + \frac{\partial(\rho u)}{\partial x} + \frac{\partial(\rho v)}{\partial y} = 0 \quad ; \tag{3-1}$$

x-Momentum,

$$\frac{\partial(\rho u)}{\partial t} + \frac{\partial(p + \rho u^2)}{\partial x} + \frac{\partial(\rho uv)}{\partial y} = 0 \quad ; \tag{3-2}$$

y-Momentum,

$$\frac{\partial(\rho v)}{\partial t} + \frac{\partial(\rho uv)}{\partial x} + \frac{\partial(p + \rho v^2)}{\partial y} = 0 \quad ; \qquad (3\text{-}3)$$

Energy,

$$\frac{\partial e}{\partial t} + \frac{\partial(e + p)u}{\partial x} + \frac{\partial(e + p)v}{\partial y} = 0 \quad ; \qquad (3\text{-}4)$$

where ρ - local fluid density,

u - horizontal velocity component,

v - vertical velocity component,

p - local fluid pressure,

$e = \frac{p}{\gamma - 1} + \frac{\rho(u^2 + v^2)}{2}$ (fluid energy),

t - time,

x, y - space coordinates.

For the turbulence analysis, the dependent variables in the conservation equations (3-1) - (3-4) are assumed to represent instantaneous values at a point. Each instantaneous value will be defined, in the usual manner, as the sum of a temporal mean and a fluctuating component.

$$u = \bar{u} + u' \quad ; \quad v = \bar{v} + v' \quad ; \quad p = \bar{p} + p' \quad ;$$

$$\rho u = \overline{(\rho u)} + (\rho u)' \quad ; \quad \rho v = \overline{(\rho v)} + (\rho v)' \quad ;$$

$$\rho = \bar{\rho} + \rho' \quad ; \quad e = \bar{e} + e' \quad . \qquad (3\text{-}5)$$

The bar denotes the time average and the prime denotes the fluctuating component. The representation of (ρu) and (ρv) as fluid properties in equations (3-5) was suggested by Van Driest (15) as a means of reducing the complexity of the derivation. The fluid energy, e, has also been represented in this manner. The requirements which must be met when using this type of representation are given in Appendix D.

The permissible operations which may be performed on time average quantities may be summarized as (16)

$$\overline{\bar{f}} = \bar{f} \quad , \qquad \overline{f+g} = \bar{f} + \bar{g} \quad , \qquad \overline{\bar{f} \cdot g} = \bar{f} \cdot \bar{g} \quad ,$$

$$\overline{\frac{\partial f}{\partial s}} = \frac{\partial \bar{f}}{\partial s} \quad , \qquad \overline{\int f ds} = \int \bar{f} ds \quad . \tag{3-6}$$

In considering the operations which may be performed on the fluctuating components, one should note that the time average of a fluctuating component is zero. However, the time average of the product of two fluctuating components is not necessarily zero.

$$\overline{f'} = 0 \quad , \qquad \overline{f'g'} \neq 0 \quad . \tag{3-7}$$

The equations describing the general, two-dimensional turbulent mixing process will be derived from equations (3-1) - (3-4) by applying the following rule to each of the individual equations:

1. The instantaneous values of the dependent variables are replaced by the sum of their temporal mean and fluctuating components.
2. The time average of the entire equation is developed and simplifications made according to equations (3-6) and (3-7).

Continuity Equation

If the expressions for the instantaneous values of ρ, ρu, and ρv are substituted into equation (3-1), the resulting expression is

$$\frac{\partial(\overline{\rho} + \rho')}{\partial t} + \frac{\partial[\overline{\rho u} + (\rho u)']}{\partial x} + \frac{\partial[\overline{\rho v} + (\rho v)']}{\partial y} = 0 \quad . \tag{3-8}$$

Taking the time average of equation (3-8) and utilizing equations (3-6) and (3-7), one obtains the continuity equation in terms of time average values.

$$\frac{\partial \overline{\rho}}{\partial t} + \frac{\partial \overline{(\rho u)}}{\partial x} + \frac{\partial \overline{(\rho v)}}{\partial y} = 0 \quad . \tag{3-9}$$

x Component of Momentum

Upon replacing the dependent variables in equation (3-2) with the sum of their time average and fluctuating components, one obtains

$$\frac{\partial[\overline{\rho u} + (\rho u)']}{\partial t} + \frac{\partial}{\partial x}\left\{ \overline{p} + p' + [\overline{\rho u} + (\rho u)'](\overline{u} + u') \right\} +$$

$$+ \frac{\partial}{\partial y}\left\{ [\overline{\rho v} + (\rho v)'](\overline{u} + u') \right\} = 0 \quad . \tag{3-10}$$

If the time average of equation (3-10) is taken, and use is made of equations (3-6) and (3-7), equation (3-11) will be obtained.

$$\frac{\partial \overline{(\rho u)}}{\partial t} + \frac{\partial}{\partial x}[\overline{p} + \overline{\rho u}\,\overline{u} + \overline{(\rho u)'u'}] + \frac{\partial}{\partial y}[\overline{\rho u}\,\overline{v} + \overline{(\rho v)'u'}] = 0 \quad . \tag{3-11}$$

y Component of Momentum

The expression for the conservation of momentum in the y-direction in terms of time averages and fluctuating components may be obtained in the same manner as was equation (3-11). Therefore, the desired equation for momentum in the y-direction is

$$\frac{\partial(\overline{\rho v})}{\partial t} + \frac{\partial}{\partial x}\left[\overline{\rho}\,\overline{u}\,\overline{v} + \overline{(\rho u)'v'}\right] + \frac{\partial}{\partial y}\left[\overline{p} + \overline{\rho}\,\overline{v}\,\overline{v} + \overline{(\rho v)'v'}\right] = 0 \quad . (3\text{-}12)$$

Energy Equation

The method for obtaining the turbulent energy equation is of course the same as that used to obtain equations (3-10) and (3-11). However, since several important simplifying assumptions are made in the course of the analysis, a detailed discussion of the derivation will be presented.

If the instantaneous values of the dependent variables in equation (3-4) are replaced by the sum of their temporal mean and fluctuating components, the result is

$$\frac{\partial(\overline{e} + e')}{\partial t} + \frac{\partial}{\partial x}\left[(\overline{e} + e')(\overline{u} + u') + (\overline{p} + p')(\overline{u} + u')\right] +$$

$$+ \frac{\partial}{\partial y}\left[(\overline{e} + e')(\overline{v} + v') + (\overline{p} + p')(\overline{v} + v')\right] = 0. \quad (3\text{-}13)$$

By taking the time average of equation (3-13) and simplifying according to equations (3-6) and (3-7), one will obtain

$$\frac{\partial \bar{e}}{\partial t} + \frac{\partial}{\partial x}\left[\bar{e}\bar{u} + \overline{e'u'} + \bar{p}\bar{u} + \overline{p'u'}\right] +$$

$$+ \frac{\partial}{\partial y}\left[\bar{e}\bar{v} + \overline{e'v'} + \bar{p}\bar{v} + \overline{p'v'}\right] = 0 \quad . \qquad (3\text{-}14)$$

In order to determine which quantities, if any, may be neglected in equation (3-14), it will be necessary to substitute the expression for e' obtained in Appendix D.

The expression for e' is

$$e' = \frac{p'}{\gamma - 1} + \frac{1}{2}\left[\overline{\rho u}u' + (\rho u)'\bar{u} + (\rho u)'u' - \overline{(\rho u)'u'} + \right.$$

$$\left. + \overline{\rho v}v' + (\rho v)'\bar{v} + (\rho v)'v' - \overline{(\rho v)'v'}\right] \quad . \qquad (3\text{-}15)$$

From equation (3-14) it is noted that the quantities $\overline{e'u'}$ and $\overline{e'v'}$ are required. These expressions may be obtained by multiplying equation (3-15) by the velocity fluctuation, forming the time average, and then simplifying according to equations (3-6) and (3-7). The desired equations are

$$\overline{e'u'} = \frac{\overline{p'u'}}{\gamma - 1} + \frac{1}{2}\left[\overline{\rho u}\overline{u'^2} + \bar{u}\overline{(\rho u)'u'} + \overline{(\rho u)'u'^2} + \right.$$

$$\left. + \overline{\rho v}\;\overline{v'u'} + \bar{v}\overline{(\rho v)'u'} + \overline{(\rho v)'v'u'}\right] \quad , \qquad (3\text{-}16)$$

and

$$\overline{e'v'} = \frac{\overline{p'v'}}{\gamma-1} + \frac{1}{2}\left[\overline{\rho u}\ \overline{u'v'} + \bar{u}\overline{(\rho u)'v'} + \overline{(\rho u)'u'v'} + \right.$$

$$\left. + \overline{\rho v}\ \overline{v'^2} + \bar{v}\overline{(\rho v)'v'} + \overline{(\rho v)'v'^2}\right] . \qquad (3\text{-}17)$$

If equations (3-16) and (3-17) are substituted into equation (3-14), the resulting expression is

$$\frac{\partial \bar{e}}{\partial t} + \frac{\partial}{\partial x}\left\{ \bar{e}\bar{u} + \bar{p}\bar{u} + \overline{p'u'} + \frac{\overline{p'u'}}{\gamma-1} + \frac{1}{2}\left[\overline{\rho u}\ \overline{u'^2} + \bar{u}\overline{(\rho u)'u'} + \right.\right.$$

$$\left.\left. + \overline{(\rho u)'u'^2} + \overline{\rho v}\ \overline{u'v'} + \bar{v}\overline{(\rho v)'u'} + \overline{(\rho v)'v'u'}\right] \right\} +$$

$$+ \frac{\partial}{\partial y}\left\{ \bar{e}\bar{v} + \bar{p}\bar{v} + \overline{p'v'} + \frac{\overline{p'v'}}{\gamma-1} + \frac{1}{2}\left[\overline{\rho u}\ \overline{u'v'} + \bar{u}\overline{(\rho u)'v'} + \right.\right.$$

$$\left.\left. + \overline{(\rho u)'u'v'} + \overline{\rho v}\ \overline{v'^2} + \bar{v}\overline{(\rho v)'v'} + \overline{(\rho v)'v'^2}\right] \right\} = 0 , \qquad (3\text{-}18)$$

where

$$\bar{e} = \frac{\bar{p}}{\gamma-1} + \frac{\overline{\rho u}\ \bar{u} + \overline{(\rho u)'u'} + \overline{\rho v}\ \bar{v} + \overline{(\rho v)'v'}}{2} . \qquad (3\text{-}19)$$

The products $\overline{eu}$ and $\overline{ev}$ appear in equation (3-18); therefore, if $\bar{e}$ is multiplied by $\bar{u}$ in equation (3-19), the terms $\overline{\rho u}\ \overline{u^2}$ and $\overline{\rho v}\ \bar{v}\ \bar{u}$ will appear in equation (3-18). The assumption is now made that the product of time average velocities is much larger than the product of fluctuating components. This may be stated in the form of an inequality which pertains directly to equation (3-18).

$$(\overline{\rho u}\ \overline{u^2} + \overline{\rho v}\ \bar{u}\ \bar{v}) \gg \frac{1}{2}(\overline{\rho u}\ \overline{u'^2} + \overline{\rho v}\ \overline{v'u'})$$

$$(\overline{\rho u}\ \bar{u}\ \bar{v} + \overline{\rho v}\ \overline{v^2}) \gg \frac{1}{2}(\overline{\rho u}\ \overline{u'v'} + \overline{\rho v}\ \overline{v'^2}) \qquad (3\text{-}20)$$

Therefore, the terms which appear on the right hand side of inequality (3-20) may be removed from equation (3-18) since they are negligibly small compared to the terms on the left hand side of the inequality.

According to Van Driest (15), terms which contain only the product of three fluctuating components, "third order" terms, are negligibly small compared to terms containing the product of time average values and two fluctuating components. Therefore, from equation (3-18) the terms $\overline{(\rho u)'u'^2}$, $\overline{(\rho v)'v'u'}$, $\overline{(\rho u)'u'v'}$, and $\overline{(\rho v)'v'^2}$ are assumed to be small compared to the other terms in the equation.

By considering the terms which may be neglected according to inequality (3-20), and the negligible third order terms just discussed, the energy equation may be written in a more simplified form as

$$\frac{\partial \bar{e}}{\partial t} + \frac{\partial}{\partial x}\left\{ \bar{e}\bar{u} + \bar{p}\bar{u} + \frac{\gamma}{\gamma-1}\overline{p'u'} + \frac{1}{2}[\bar{u}\overline{(\rho u)'u'} + \bar{v}\overline{(\rho v)'u'}] \right\} +$$

$$+ \frac{\partial}{\partial y}\left\{ \bar{e}\bar{v} + \bar{p}\bar{v} + \frac{\gamma}{\gamma-1}\overline{p'v'} + \frac{1}{2}[\bar{u}\overline{(\rho u)'v'} + \bar{v}\overline{(\rho v)'v'}] \right\} = 0 , \qquad (3\text{-}21)$$

where $\bar{e}$ is given by equation (3-19).

Turbulent Reynolds Stresses

The products of the momentum and velocity fluctuation terms appearing in equations (3-11), (3-12), and (3-21) may be interpreted as representing the rate of transfer of momentum across a surface due to turbulent fluctuations. Schlichting (16) has shown that these fluctuations act as additional stresses on the surfaces of an elemental volume of fluid. These terms have thus come to be called apparent stresses or turbulent Reynolds stresses. Taken together, they form a complete stress tensor of turbulent flow. For the turbulent stresses obtained in the preceeding equations, the matrix which defines the turbulent stress tensor is

$$\begin{pmatrix} \sigma_x & \tau_{xy} \\ \tau_{yx} & \sigma_y \end{pmatrix} = - \begin{pmatrix} \overline{(\rho u)'u'} & \overline{(\rho u)'v'} \\ \overline{(\rho v)'u'} & \overline{(\rho v)'v'} \end{pmatrix}, \qquad (3\text{-}22)$$

where σ_x denotes the normal stress in the x-direction and σ_y that in the y-direction. The subscripts for the shearing stresses have the usual meaning: the first subscript indicates the axis to which the stress is perpendicular, the second denotes the direction in which it acts.

Representation of Turbulent Reynolds Stresses and Pressure Fluctuation Terms

In order to obtain a solution to the system of partial differential equations which have been derived, it is necessary to express the turbulent shear stress terms and the pressure fluctuation terms $\overline{p'u'}$,

$\overline{p'v'}$, as functions of the variables which describe any given problem. As is the case with most turbulence analyses, such functional relationships can only be obtained with the use of semi-empirical theories. Unfortunately, no general empirical method for expressing the turbulent stress terms has been devised. The particular theory utilized in any given situation is therefore determined by the hydrodynamic problem under consideration.

For jet mixing, or free turbulence, problems similar to those of interest in the present investigation, a theory proposed by L. Prandtl (17) is usually used. Prandtl's theory makes use of the assumption that the physical dimensions of lumps of fluid moving in the transverse direction during the mixing process are about the same size as the width of the mixing zone. Therefore, by utilizing the suggestion by Boussinesq (18) that the turbulent shear stress terms can be expressed as

$$\tau_{ij} = \rho\epsilon \frac{\partial \bar{u}_i}{\partial x_i} \quad , \tag{3-23}$$

Prandtl's theory will lead to an expression for the virtual kinematic viscosity, ϵ, of the form

$$\epsilon \propto u_a x \quad , \tag{3-24}$$

where u_a is the velocity of the uniform flow adjacent to the mixing region and x is the distance from the point where mixing begins. Equation (3-24) when written as an equality is

$$\epsilon = c_o u_a x \quad . \tag{3-25}$$

The constant of proportionality, c_o, may be expressed as a function of an experimentally determined constant known as the jet spreading rate parameter. For any theoretical analysis, this parameter is a function

of the particular velocity profile which has been assumed. For the much-used error function profile, the jet spreading rate parameter is expressed as

$$\sigma = \eta^* \frac{x}{y} \quad , \tag{3-26}$$

where η^* is related to the constant of proportionality, c_o, and the velocity profile according to equation (3-27),

$$\frac{u}{u_a} = \frac{1}{2}[1 + \text{erf } \eta^*] \tag{3-27}$$

$$\eta^* = \frac{1}{\sqrt{2c_o}} \frac{y}{x} = \sigma \frac{y}{x} \quad . \tag{3-27}$$

Equation (3-27) has been derived by Korst (19) assuming fully developed turbulence and no boundary layer at the point where flow separation occurs.

Figure 3 shows the variation of jet spreading rate parameter with the square of the Crocco number. The data for Figure 3 was obtained from experiments conducted at Sandia Corporation (20) and Oklahoma State University (21). Zumwalt and Tang (14) have suggested as functional relationships for the spreading rate parameter the expressions

$$\sigma \cong 47.1 C_a^2 \quad \text{for} \quad C_a^2 > .23 \quad (M_a > 1.23)$$

$$\sigma = 11.0 \quad \text{for} \quad C_a^2 < .23 \quad (M_a < 1.23), \tag{3-28}$$

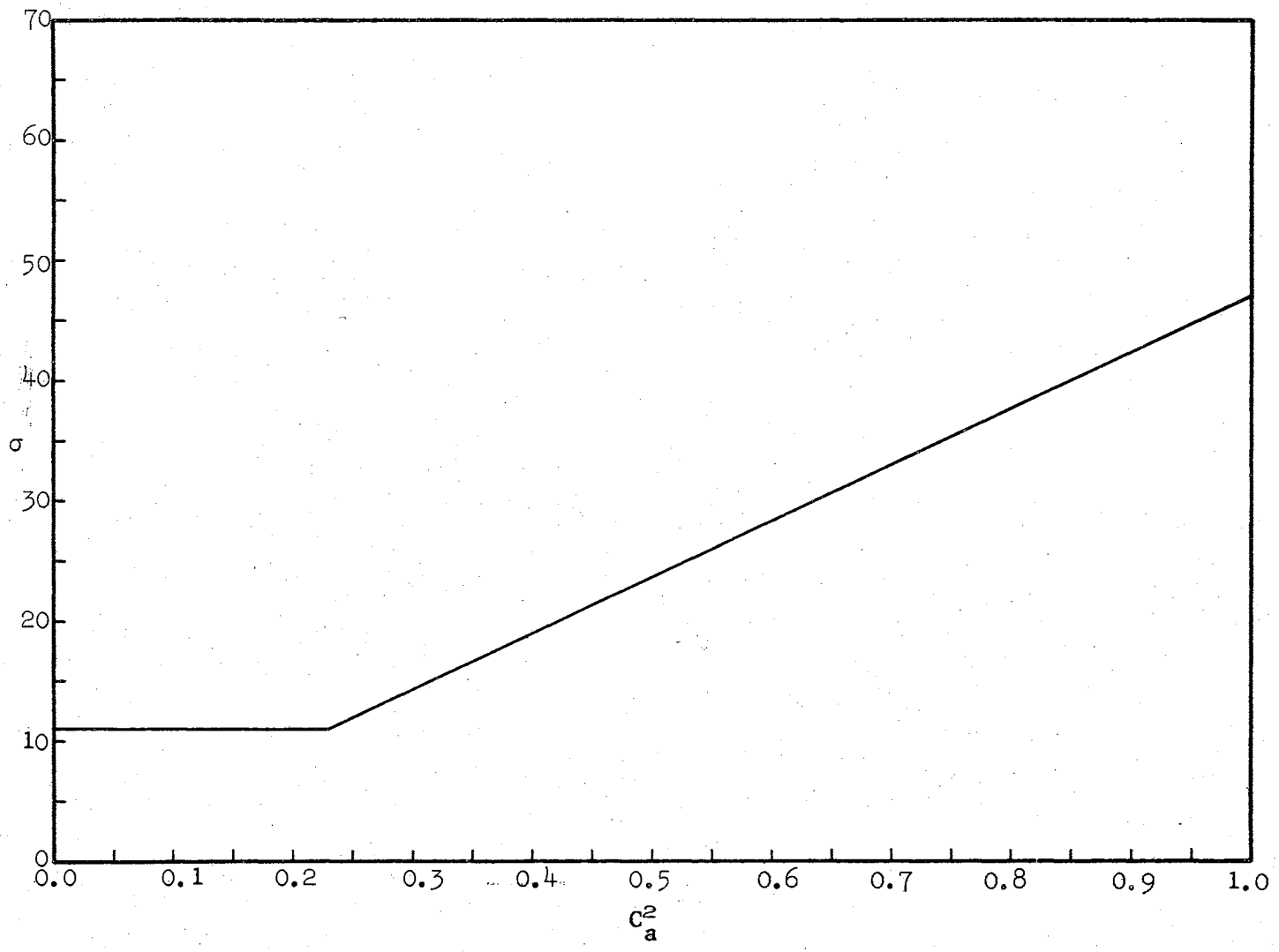

Figure 3. Variation of Jet Spreading Parameter with Crocco Number.

where

$$C_a^2 = \frac{M_a^2}{\frac{2}{\gamma-1} + M_a^2} .$$

Equation (3-28) is valid for values of the Mach number less than five and has been used in this investigation whenever a numerical value of the jet spreading rate parameter has been required.

If equation (3-27) is solved for c_o, and the resulting expression substituted into equation (3-25), the equation for the virtual kinematic viscosity is found to be

$$\varepsilon = \frac{u_a}{2\sigma^2} x . \tag{3-29}$$

By substituting equation (3-29) into equation (3-23), one finds the equation expressing the turbulent shear stresses in terms of known parameters to be

$$\tau_{ij} = \frac{u_a}{2\sigma^2} \rho x \frac{\partial \bar{u}_i}{\partial x_j} . \tag{3-30}$$

In matrix notation, equation (3-30) may be combined with equation (3-22) and expressed as

$$\begin{pmatrix} \sigma_x & \tau_{xy} \\ \tau_{yx} & \sigma_y \end{pmatrix} = - \begin{pmatrix} \overline{(\rho u)'u'} & \overline{(\rho u)'v'} \\ \overline{(\rho v)'u'} & \overline{(\rho v)'v'} \end{pmatrix} = \zeta \begin{pmatrix} \frac{\partial \bar{u}}{\partial x} & \frac{\partial \bar{v}}{\partial x} \\ \frac{\partial \bar{u}}{\partial y} & \frac{\partial \bar{v}}{\partial y} \end{pmatrix} , \tag{3-31}$$

where $\zeta = \frac{u_a}{2\sigma^2}\rho x$.

The occurrence of pressure perturbations in the energy equation (3-21) is somewhat different from most turbulence analyses. The assumption is usually made that the turbulent flow under investigation occurs at constant pressure. If this condition is not assumed, then either sufficient information is usually available to dictate the spatial variations in pressure or it is assumed that the perturbations in pressure are small compared to other turbulence quantities. Even for problems of free turbulence, similar to those of interest here, the assumption of constant pressure is rightfully made. However, when the passage of a shock wave over the mixing region is to be considered, then the constant pressure assumption may be invalid and account should be made of the perturbation terms.

For the purposes of this study, the assumption is made that significant pressure perturbations occur only as a result of subjecting an established mixing region to a moving shock wave. In addition, an analogy has been drawn between the turbulent transport phenomenon and the pressure perturbations. Thus, if the term $\overline{p'u_i'}$, where u_i' denotes either of the two fluctuating velocity components, is assumed to represent a "pressure transport" term, then in analogy with the other turbulent transport processes, one should be able to write an expression of the form

$$\overline{p'u_i'} = -\epsilon'_i \frac{\partial \bar{p}}{\partial x_i} , \qquad (3\text{-}32)$$

where ϵ_i' is an exchange coefficient for the pressure perturbation in the i-direction. For the analagous "mixing length" associated with ϵ_i', it seems proper under the assumption previously mentioned to choose a length which is of the same order of magnitude as a shock wave thickness. For a finite difference net, similar to that to be discussed later, this length would represent one or two mesh widths. From equation (3-32) it may be seen that a velocity term will be required in the final expression for ϵ_i'. This is not unexpected since any pressure disturbance has associated with it a speed of propagation. In one direction this speed is, relative to a fixed observer, $(|u_i| + c)$, where c is the local accoustic velocity. The expression for ϵ_i' is therefore

$$\epsilon_i' = \ell_i(|u_i| + c) , \tag{3-33}$$

and from equation (3-32) the resulting equation for the pressure perturbations is

$$\overline{p'u_i'} = - \ell_i(|u_i| + c)\frac{\partial \bar{p}}{\partial x_i} . \tag{3-34}$$

Summary of Governing Equations

If equations (3-31) and (3-34) are substituted into the equations of momentum and energy, the final form of the governing equations will be obtained. These equations are presented here for convenience.

Continuity,

$$\frac{\partial \bar{\rho}}{\partial t} + \frac{\partial \overline{(\rho u)}}{\partial x} + \frac{\partial \overline{(\rho v)}}{\partial y} = 0 \quad ; \tag{3-9}$$

x-Momentum,

$$\frac{\partial \overline{(\rho u)}}{\partial t} + \frac{\partial}{\partial x}\left[\bar{p} + \overline{\rho u}\,\bar{u} - \zeta\frac{\partial \bar{u}}{\partial x}\right] + \frac{\partial}{\partial y}\left[\overline{\rho u}\,\bar{v} - \zeta\frac{\partial \bar{u}}{\partial y}\right] = 0 \quad ; \tag{3-35}$$

y-Momentum,

$$\frac{\partial \overline{(\rho v)}}{\partial t} + \frac{\partial}{\partial x}\left[\overline{\rho u}\,\bar{v} - \zeta\frac{\partial \bar{v}}{\partial x}\right] + \frac{\partial}{\partial y}\left[\bar{p} + \overline{\rho v}\,\bar{v} - \zeta\frac{\partial \bar{v}}{\partial y}\right] = 0 \quad ; \tag{3-36}$$

Energy,

$$\frac{\partial \bar{e}}{\partial t} + \frac{\partial}{\partial x}\left[(\bar{e} + \bar{p})\bar{u} - \frac{\gamma}{\gamma-1}\ell_x(|\bar{u}| + c)\frac{\partial \bar{p}}{\partial x} - \frac{\zeta}{2}\left(\bar{u}\frac{\partial \bar{u}}{\partial x} + \bar{v}\frac{\partial \bar{u}}{\partial y}\right)\right] +$$

$$+ \frac{\partial}{\partial y}\left[(\bar{e} + \bar{p})\bar{v} - \frac{\gamma}{\gamma-1}\ell_y(|\bar{v}| + c)\frac{\partial \bar{p}}{\partial y} - \frac{\zeta}{2}\left(\bar{u}\frac{\partial \bar{v}}{\partial x} + \bar{v}\frac{\partial \bar{v}}{\partial y}\right)\right] = 0; \tag{3-37}$$

where $\bar{e} = \dfrac{\bar{p}}{\gamma-1} + \dfrac{\overline{\rho u}\,\bar{u} + \overline{\rho v}\,\bar{v} - \zeta\left(\frac{\partial \bar{u}}{\partial x} + \frac{\partial \bar{v}}{\partial y}\right)}{2}$

and $\zeta = \dfrac{u_a}{2\sigma^2}\rho x$.

Equations (3-9), (3-35), (3-36), and (3-37) are in the form of the general conservation equation

$$\frac{\partial f}{\partial t} + \frac{\partial F^x}{\partial x} + \frac{\partial F^y}{\partial y} = 0 \ , \tag{3-38}$$

where f, F^x, and F^y are four-component first order tensors which may be written as

$$f = \begin{bmatrix} \bar{\rho} \\ \overline{\rho u} \\ \overline{\rho v} \\ \bar{e} \end{bmatrix} ;$$

$$F^x = \begin{bmatrix} \overline{\rho u} \\ \bar{p} + \overline{\rho u}\,\bar{u} - \zeta \dfrac{\partial \bar{u}}{\partial x} \\ \overline{\rho u}\,\bar{v} - \zeta \dfrac{\partial \bar{v}}{\partial x} \\ (\bar{e} + \bar{p})\bar{u} - \dfrac{\gamma}{\gamma-1} \ell_x (|\bar{u}| + c) \dfrac{\partial \bar{p}}{\partial x} - \dfrac{\zeta}{2}\left(\bar{u} \dfrac{\partial \bar{u}}{\partial x} + \bar{v} \dfrac{\partial \bar{u}}{\partial y}\right) \end{bmatrix} ; \qquad (3\text{-}39)$$

$$F^y = \begin{bmatrix} \overline{\rho v} \\ \overline{\rho u}\,\bar{v} - \zeta \dfrac{\partial \bar{u}}{\partial y} \\ \bar{p} + \overline{\rho v}\,\bar{v} - \zeta \dfrac{\partial \bar{v}}{\partial y} \\ (\bar{e} + \bar{p})\bar{v} - \dfrac{\gamma}{\gamma-1} \ell_y (|\bar{v}| + c) \dfrac{\partial \bar{p}}{\partial y} - \dfrac{\zeta}{2}\left(\bar{u} \dfrac{\partial \bar{v}}{\partial x} + \bar{v} \dfrac{\partial \bar{v}}{\partial y}\right) \end{bmatrix} .$$

The notations of equations (3-38) and (3-39) will prove useful when considering both the finite difference approximations of the governing equations and the stability analysis of the finite difference equations.

Equations (3-39) have been derived using the following assumptions:

1. The gas under consideration is perfect and satisfies the equation of state, $p = \rho RT$.

2. The flow of the gas is two-dimensional and compressible.
3. Molecular transport is negligible compared to turbulent transport.
4. The product of time average velocities is much larger than the product of fluctuating components.
5. Third order fluctuation terms are small.
6. Boussinesq's turbulent shear stress approximation is valid.
7. The turbulent mixing length is dependent only upon x, but is the same in all directions.
8. Pressure perturbations occur by a process which is analogous to the turbulent transport of mass and momentum.

Within the limitations of the above assumptions equations (3-39) should describe any physically realistic situation. The equations will not apply to the case of turbulent boundary layer flow for two reasons: First, there has been no provision made for the laminar sublayer region and second, the exchange coefficients for boundary layer flows are usually different from those used for free turbulence flows. Therefore the analysis is restricted to free turbulence cases where the Reynolds number is sufficiently high so as to insure negligible contributions from laminar effects. Also, equations (3-39) are valid under certain temperature restrictions. The more obvious reason for this is that no provision has been made for real gas phenomenon. However, a second reason, which is of equal importance, has been noted by Abramovich (22). He points out that at temperatures of the order of 5000° K the terms which reflect the influence of viscosity and molecular thermal conductivity are not negligibly small, but are in fact more significant than the turbulent viscosity and thermal conductivity. When this is the

case, one must also take into account the radiant heat which will become a significant factor in the energy equation.

Boundary and Initial Conditions

Equations (3-38) and (3-39) constitute a system of four partial differential equations whose solutions are to be represented in two space dimensions and in time. Irrespective of whether an analytical or a numerical solution is sought, sufficient information must be given both initially and during the course of the solution to insure that the mathematical model always approximates the physical model. These predetermined pieces of information are known respectively as the initial and boundary conditions.

The initial conditions seldom afford any appreciable difficulties and are usually unique for each particular problem. The boundary conditions, on the other hand, are usually assumed to be the same for all problems described by equations (3-38) and (3-39); namely, free turbulence problems. Difficulties can be encountered whenever the boundary conditions fail to describe adequately the conditions which actually occur at a boundary.

Difficulties can also be encountered if too few or too many boundary conditions are dictated. Problems in the first situation are classified as under determined because there is not a sufficient number of boundary conditions to yield a solution. Problems characterized by the second situation are classified as over determined since there are too many boundary conditions to yield a unique solution.

For plane flows two types of boundaries are likely to occur. The first is a solid wall or plane of symmetry and the second is the boundary of the flow field, hereafter referred to as the flow plane. Whenever a finite difference solution is employed the flow plane corresponds to the boundary of the finite difference net. Therefore whenever a numerical method is used for the solution of equations (3-39), the boundary conditions for both types of boundaries must be stated.

Since equation (3-38) involves four dependent variables, and three of these, u, v, and p are present in second order terms, the number of boundary conditions required is seven. In the next chapter it will be necessary to add additional second order terms in all four of the dependent variables; therefore ρ will now be assumed to occur in a second order term thus indicating that a total of eight boundary conditions are required. However, when a wall boundary is considered, the condition of no flow through the wall deletes the necessity of computing the momentum equation which would otherwise give the velocity component normal to the wall. This condition eliminates the necessity of dictating an additional boundary condition for the normal velocity; thus reducing to seven the number of boundary conditions which must be prescribed.

The boundary conditions at a wall or plane of symmetry for problems which can be described by equations (3-39) will be assumed to be

$$u_N = 0 ; \quad \frac{\partial u_T}{\partial N} = 0 ; \quad \frac{\partial p}{\partial N} = 0 ; \quad \frac{\partial \rho}{\partial N} = 0 ;$$

$$\frac{\partial^2 u_T}{\partial N^2} = 0 ; \quad \frac{\partial^2 p}{\partial N^2} = 0 ; \quad \frac{\partial^2 \rho}{\partial N^2} = 0 , \tag{3-40}$$

where subscript N denotes the direction normal to the boundary and T denotes the direction tangential to the boundary.

In Chapter IV equations (3-39) will be approximated with finite difference equations. As indicated previously the question inevitably arises as to how the points on a flow plane boundary should be treated. The technique which is employed to handle these points is merely to dictate the variation of the dependent variables p, ρ, u, and v with time. Thus, for net boundary points four boundary conditions are required and can be expressed as

$$\begin{aligned} u &= f_1(t) \quad ; \\ v &= f_2(t) \quad ; \\ p &= f_3(t) \quad ; \\ \rho &= f_4(t) \quad . \end{aligned} \tag{3-41}$$

Since equations (3-39) are not actually solved at the flow plane, equations (3-41) are sufficient to describe the conditions at net boundary points.

CHAPTER IV

DERIVATION OF FINITE DIFFERENCE EQUATIONS

As has been indicated previously, the equations derived in the preceeding chapter will be solved numerically by means of the method of finite differences. A great deal of effort has been put forth in the past several years to provide numerical methods whereby solutions to complicated flow problems may be obtained. These efforts have been concerned mainly with problems which deal with shock wave reflection and diffraction. From these investigations the realization has slowly emerged that the classical methods of finite difference analysis are not sufficient to handle problems which involve the occurrence of large, local variations in the dependent variables. Thus, in order to handle problems associated with shock wave phenomenon, new methods have been required which would allow computations to proceed through regions where surfaces of discontinuity exist. The basis of these new methods was provided by J. von Neumann (23) who suggested that the inviscid equations of flow be altered so that surfaces of discontinuity would be "blurred" into regions where all the flow variables would be continuous, but rapidly changing. This method has been termed the method of artificial viscosity because it makes use of mechanisms similar to that of viscosity to accomplish the blurring process. Since the time of von Neumann's work, most of the significant theories dealing

with discontinuous solutions have relied, to some extent, on the blurring technique. The present investigation is no exception. Here a method developed by G. B. Rusanov (24) has been employed. A detailed discussion of Rusanov's method has been given by Tyler (4). However, the derivation of the finite difference equations will be presented here since they are instrumental in obtaining a numerical solution to the equations derived in Chapter III. Since the work of Rusanov and of Tyler dealt entirely with inviscid equations, only the principles of the method can be utilized in the present study. This also applies to the stability analysis to be performed in the next chapter.

A method promulgated by Lax (25) was also considered for the numerical solution of equations (3-38) and (3-39). The disadvantage of Lax's method was that the blurring method used resulted in constant blurring coefficients. This is opposed to Rusanov's more general method which allows the blurring coefficients to be explicitly dependent upon space and time and implicitly dependent upon the properties at a point. Lax's constant blurring coefficient has a tendency to blur all gradients equally irrespective of the magnitude of the gradient. This is depicted in the numerical results as an extensive diffusion of the original strong gradients. It was found in the early stages of this investigation that for a particular problem (See Figures 8 and 9) an initial shock wave thickness of two mesh widths would diffuse to about fourteen mesh widths using Lax's method, whereas it would diffuse to only about five mesh widths using Rusanov's method. It is for these reasons that Rusanov's method was chosen over the more popular method developed by Lax.

The general first order, non-linear, partial differential equation for which a solution is desired is

$$\frac{\partial f}{\partial t} + \frac{\partial F^x}{\partial x} + \frac{\partial F^y}{\partial y} = 0 , \qquad (4\text{-}1)$$

where the expressions for f, F^x, and F^y are given in equation (3-39). However, as mentioned previously, problems involving discontinuities in the flow variables cannot be solved by difference techniques without the addition of certain blurring terms. Therefore equation (4-1) is not the equation from which a solution will be sought. The addition of the blurring terms to equation (4-1) results in the expression (4), (24),

$$\frac{\partial f}{\partial t} + \frac{\partial F^x}{\partial x} + \frac{\partial F^y}{\partial y} = \frac{\partial}{\partial x}\left[A(x,y,t)\frac{\partial f}{\partial x}\right] + \frac{\partial}{\partial y}\left[B(x,y,t)\frac{\partial f}{\partial y}\right] , \qquad (4\text{-}2)$$

where A(x,y,t) and B(x,y,t) are the so-called artificial viscosity terms whose functional values are obtained from stability analysis.

The only criteria which must be observed in the selection of the blurring terms are those given by von Neumann (23) in his original paper.

1. The blurring terms must be such that the equations representing the physical conservation laws must possess solutions without discontinuities.
2. The thickness of shock layers must be everywhere of the same order as the interval lengths Δx and Δy used in the numerical calculations.

3. The effect of the blurring terms must be negligible outside the shock layers.

4. The Rankine-Hugoniot equations must hold across shock layers.

The differencing scheme to be applied to equation (4-2) will use forward differences for time derivatives, and centered differences for space derivatives and turbulence derivative terms. Utilizing a scheme such as this allows the computations to proceed forward in time. Thus the value of f at one instant is evaluated explicitly from the values of f, F^x and F^y at the preceeding time.

The finite difference net to be used is shown in Figure 4. The increments in the independent variables (Δx, Δy, Δt) are denoted in the differencing scheme as (h_1, h_2, τ). The angle χ is the angle between h_1 and h where

$$h = [h_1^2 + h_2^2]^{\frac{1}{2}} . \qquad (4\text{-}3)$$

At some point in the difference net, a quantity q with co-ordinates (mh_1, ℓh_2, $n\tau$) will be denoted by $q^n_{m,\ell}$. For purposes of discussion n will be referred to either as the nth time layer or as the nth time plane.

Before writing the finite difference approximation of equation (4-2) it should be noted that the form of the difference equation will vary depending upon the placement of the net point in the flow field. Thus, the difference equation for points lying entirely within the field of flow, field points, will not be the same as the difference

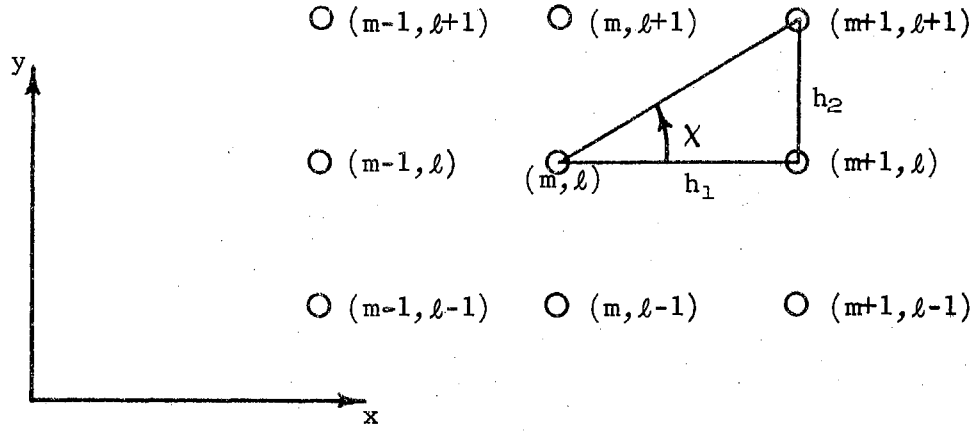

Figure 4. Finite Difference Net Notation.

equations describing points lying either on walls or on planes of symmetry; i.e., boundary points. The reason for this difference in representation is that the boundary conditions (3-40) must be satisfied whenever the mesh points lie on boundaries. Thus, the required number of finite difference approximations to equation (4-2) depends upon the flow field configuration of each particular problem.

Difference Equations for Field Points

Utilizing the differencing techniques and the difference net definitions previously discussed, the difference approximations of the derivatives in equation (4-2) may be written as

$$\frac{\partial f}{\partial t} \rightarrow \frac{f^{n+1}_{m,\ell} - f^{n}_{m,\ell}}{\tau}$$

$$\frac{\partial F^x}{\partial x} \rightarrow \frac{\left[F^x_{m+1,\ell} - F^x_{m-1,\ell}\right]^n}{2h_1}$$

$$\frac{\partial F^y}{\partial y} \rightarrow \frac{\left[F^y_{m,\ell+1} - F^y_{m,\ell-1}\right]^n}{2h_2} \qquad (4\text{-}4)$$

$$\frac{\partial}{\partial x}\left[A\frac{\partial f}{\partial x}\right] \rightarrow \frac{1}{h_1}\left[A_{m+\frac{1}{2},\ell}\left(\frac{\partial f}{\partial x}\right)_{m+\frac{1}{2},\ell} - A_{m-\frac{1}{2},\ell}\left(\frac{\partial f}{\partial x}\right)_{m-\frac{1}{2},\ell}\right]^n$$

$$\rightarrow \frac{1}{h_1^2}\left[A_{m+\frac{1}{2},\ell}\left(f_{m+1,\ell} - f_{m,\ell}\right) - A_{m-\frac{1}{2},\ell}\left(f_{m,\ell} - f_{m-1,\ell}\right)\right]^n,$$

and

$$\frac{\partial}{\partial y}\left[B\frac{\partial f}{\partial y}\right] \rightarrow \frac{1}{h_2^2}\left[B_{m,\ell+\frac{1}{2}}\left(f_{m,\ell+1} - f_{m,\ell}\right) - B_{m,\ell-\frac{1}{2}}\left(f_{m,\ell} - f_{m,\ell-1}\right)\right]^n.$$

The difference approximations for the individual derivatives (4-4) can now be used to write the complete finite difference approximation to equation (4-2).

$$f^{n+1}_{m,\ell} = f^{n}_{m,\ell} - \frac{\tau}{2h_1}\left[F^{x}_{m+1,\ell} - F^{x}_{m-1,\ell} \right]^{n} - \frac{\tau}{2h_2}\left[F^{y}_{m,\ell+1} - F^{y}_{m,\ell-1} \right]^{n} +$$

$$+ \frac{\tau}{h_1^2}\left[A_{m+\frac{1}{2},\ell}\,(f_{m+1,\ell} - f_{m,\ell}) - A_{m-\frac{1}{2},\ell}\,(f_{m,\ell} - f_{m-1,\ell}) \right]^{n} +$$

$$+ \frac{\tau}{h_2^2}\left[B_{m,\ell+\frac{1}{2}}\,(f_{m,\ell+1} - f_{m,\ell}) - B_{m,\ell-\frac{1}{2}}\,(f_{m,\ell} - f_{m,\ell-1}) \right]^{n}. \qquad (4\text{-}5)$$

Equation (4-5) may be simplified somewhat by letting

$$A^{n}_{m,\ell} = \frac{h_1^2}{2\tau}\,\alpha^{n}_{m,\ell}$$

and (4-6)

$$B^{n}_{m,\ell} = \frac{h_2^2}{2\tau}\,\beta^{n}_{m,\ell}\,.$$

Also, if the new parameters K_1 and K_2 are defined as

$$K_1 = \frac{\tau}{h_1}$$

$$K_2 = \frac{\tau}{h_2} \qquad (4\text{-}7)$$

then in analogy with equation (4-3) a new parameter K can be defined such that

$$K = [K_1^2 + K_2^2]^{\frac{1}{2}} = \frac{[h_1^2 + h_2^2]^{\frac{1}{2}}}{h_1 h_2} \tau , \tag{4-8}$$

and

$$K_1 = K \sin \chi , \qquad K_2 = K \cos \chi . \tag{4-9}$$

Upon substituting equations (4-6) and (4-7) into equation (4-5), one obtains

$$f_{m,\ell}^{n+1} = f_{m,\ell}^{n} - \frac{K_1}{2} \left[F_{m+1,\ell}^{x} - F_{m-1,\ell}^{x} \right]^{n} - \frac{K_2}{2} \left[F_{m,\ell+1}^{y} - F_{m,\ell-1}^{y} \right]^{n} +$$

$$+ \frac{1}{2} \left[\alpha_{m+\frac{1}{2},\ell} \left(f_{m+1,\ell} - f_{m,\ell} \right) - \alpha_{m-\frac{1}{2},\ell} \left(f_{m,\ell} - f_{m-1,\ell} \right) \right]^{n} +$$

$$+ \frac{1}{2} \left[\beta_{m,\ell+\frac{1}{2}} \left(f_{m,\ell+1} - f_{m,\ell} \right) - \beta_{m,\ell-\frac{1}{2}} \left(f_{m,\ell} - f_{m,\ell-1} \right) \right]^{n} . \tag{4-10}$$

In order to simplify the notation in equation (4-10), the terms which have come about as a result of the blurring technique will be represented as

$$\begin{aligned}
\Phi_{m+\frac{1}{2},\ell}^{x} &= \alpha_{m+\frac{1}{2},\ell}^{n} \left(f_{m+1,\ell} - f_{m,\ell} \right)^{n} \\
\Phi_{m-\frac{1}{2},\ell}^{x} &= \alpha_{m-\frac{1}{2},\ell}^{n} \left(f_{m,\ell} - f_{m-1,\ell} \right)^{n} , \\
\Phi_{m,\ell+\frac{1}{2}}^{y} &= \beta_{m,\ell+\frac{1}{2}}^{n} \left(f_{m,\ell+1} - f_{m,\ell} \right)^{n} , \\
\Phi_{m,\ell-\frac{1}{2}}^{y} &= \beta_{m,\ell-\frac{1}{2}}^{n} \left(f_{m,\ell} - f_{m,\ell-1} \right)^{n} .
\end{aligned} \tag{4-11}$$

In view of equation (4-11) then, equation (4-10) may be written as

$$f^{n+1}_{m,\ell} = f^{n}_{m,\ell} - \frac{K_1}{2}\left[F^{x}_{m+1,\ell} - F^{x}_{m-1,\ell} \right]^{n} - \frac{K_2}{2}\left[F^{y}_{m,\ell+1} - F^{y}_{m,\ell-1} \right]^{n} +$$

$$+ \frac{1}{2}\left[\Phi^{x}_{m+\frac{1}{2},\ell} - \Phi^{x}_{m-\frac{1}{2},\ell} + \Phi^{y}_{m,\ell+\frac{1}{2}} - \Phi^{y}_{m,\ell-\frac{1}{2}} \right]^{n} . \qquad (4\text{-}12)$$

Rusanov (24) sought expressions for $\alpha^{n}_{m,\ell}$ and $\beta^{n}_{m,\ell}$ from linear stability analysis and found them to be

$$\begin{aligned} \alpha^{n}_{m,\ell} &= \omega K\,(w + c)^{n}_{m,\ell} \sin^2 \chi \\ \beta^{n}_{m,\ell} &= \omega K\,(w + c)^{n}_{m,\ell} \cos^2 \chi , \end{aligned} \qquad (4\text{-}13)$$

where ω is a damping parameter which is also obtained from stability considerations and

$$w = \left[u^2 + v^2 \right]^{\frac{1}{2}} . \qquad (4\text{-}14)$$

The stability criteria which equation (4-12) must satisfy at all points in the $(mh_1, \ell h_2, n\tau)$ space is, according to Rusanov,

$$K^2 \left[(w + c)^{n}_{m,\ell}\right]^2 \leq \omega K\,(w + c)^{n}_{m,\ell} \leq 1 . \qquad (4\text{-}15)$$

The quantity $K\,(w + c)^{n}_{m,\ell}$ which occurs in equation (4-15) is the Courant number at the particular point under consideration, and is written as

$$\bar{\sigma}^{n}_{m,\ell} = K\,(w + c)^{n}_{m,\ell} . \qquad (4\text{-}16)$$

Equation (4-16) in conjunction with the maximum allowable value of the Courant number, $\bar{\sigma}_o^n$, determines the time increment between any two successive time steps according to the relation

$$K = \frac{\bar{\sigma}_o^n}{(w + c)_{max}} . \tag{4-17}$$

The damping factor ω must be chosen such that the inequality

$$\bar{\sigma}_o^n \leq \omega \leq \frac{1}{\bar{\sigma}_o^n} . \tag{4-18}$$

is satisfied.

Because the hydrodynamic equations describing the jet mixing process are significantly different from the inviscid equations used by Rusanov, an analysis was made to find the stability requirements for equation (3-39). Thus, the mechanics of the derivation of (4-15) are omitted here, but may be seen in the following chapter as a special case of the stability analysis of equation (4-2).

Difference Equations for Boundary Points

As was noted earlier, the finite difference equations for field points are not the same as the difference equations for points lying on walls or on planes of symmetry. Therefore, in order to be able to calculate boundary points, the difference equation (4-12) must be altered such that the boundary conditions (3-40) are at least approximately satisfied. There are actually three ways by which one can take

into account the presence of a boundary when a finite difference method is being employed.

The first method consists of forcefully imposing the boundary conditions which ideally must exist at the boundary in question (equations (3-40)). Thus, if a point on a wall parallel to the x-axis is under consideration (see Figure 5), then one possible set of boundary conditions which could be applied are

$$v = \frac{\partial u}{\partial y} = \frac{\partial^2 u}{\partial y^2} = \frac{\partial p}{\partial y} = \frac{\partial^2 p}{\partial y^2} = \frac{\partial \rho}{\partial y} = \frac{\partial^2 \rho}{\partial y^2} = 0 , \qquad (4\text{-}19)$$

or in finite difference form the first derivatives are

$$\frac{p_{m,\ell+1} - p_{m,\ell}}{h_2} = 0 ,$$

$$\frac{\rho_{m,\ell+1} - \rho_{m,\ell}}{h_2} = 0 , \qquad (4\text{-}20)$$

$$\frac{u_{m,\ell+1} - u_{m,\ell}}{h_2} = 0 .$$

from which the obvious result is

$$p_{m,\ell} = p_{m,\ell+1} ,$$

$$\rho_{m,\ell} = \rho_{m,\ell+1} , \qquad (4\text{-}21)$$

$$u_{m,\ell} = u_{m,\ell+1} .$$

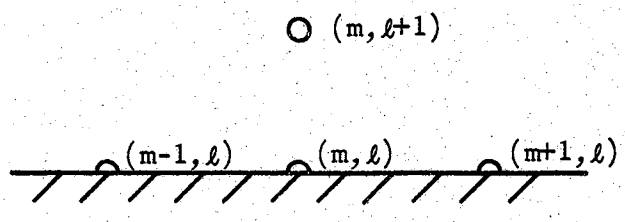

Figure 5. Net Point on a Wall Parallel to x-Axis.

Similar expressions would result if one considered a point lying on a wall parallel to the y-axis, or a point on an axis of symmetry. There is a pronounced disadvantage to this method of treating a boundary point. Whenever one is considering, for instance, an oblique shock wave impinging on a wall, or perhaps a general problem in shock dynamics, the gradients in equation (4-19) are not necessarily zero. Thus, the strict usage of equations (4-19) and (4-21), without due regard for the physical problem under consideration, could feasibly lead to erroneous results.

A second method of treating boundary points is to apply either forward or backward differences to the appropriate space derivatives in equation (4-2). The choice of the particular kind of difference approximation employed, forward or backward, would depend upon the placement of the boundary with respect to the coordinate axes. For a boundary such as that shown in Figure 5, the space derivative $\frac{\partial F^y}{\partial y}$ would be approximated by the expression

$$\frac{F^y_{m,\ell+1} - F^y_{m,\ell}}{h_2} .$$

It is interesting to note that for the inviscid equations employed by Rusanov (24), Tyler (4), and Jackomis (2), the value of $F^y_{m,\ell}$ on a horizontal boundary is always zero, except in the y-momentum equation which is not calculated.

The advantage of the forward, or backward, difference method for establishing boundary difference approximations is that the derivatives

in equation (4-19) are not necessarily forced to a zero value. The reason for this may be seen by considering a simple example. For a wall parallel to the x-axis the F^y term in the inviscid, x-momentum equation is

$$F^y = \rho uv, \tag{4-22}$$

where

$$v\big|_{wall} = 0. \tag{4-23}$$

The derivative $\left.\frac{\partial F^y}{\partial y}\right|_w$ is

$$\left.\frac{\partial F^y}{\partial y}\right|_w = \rho_w u_w \left.\frac{\partial v}{\partial y}\right|_w + \rho_w v_w \left.\frac{\partial u}{\partial y}\right|_w + u_w v_w \left.\frac{\partial \rho}{\partial y}\right|_w , \tag{4-24}$$

and the forward difference approximation of the derivative is

$$\left.\frac{\partial F^y}{\partial y}\right|_w \rightarrow \frac{(\rho uv)_{m,\ell+1} - (\rho uv)_w}{h_2} , \tag{4-25}$$

but since $v\big|_w = 0$

$$\left.\frac{\partial F^y}{\partial y}\right|_w \rightarrow \frac{(\rho uv)_{m,\ell+1}}{h_2} . \tag{4-26}$$

Therefore, because of the boundary condition $v\big|_w = 0$ it has not been necessary to evaluate the derivatives which appear in equation (4-24), thus allowing them to assume whatever value is necessary in the computations. The forward difference method of obtaining boundary difference equations is not entirely suitable for the case of equations (3-39). The reason for this is that the condition of no flow normal to a wall is not sufficient to completely relax the requirements of the wall

derivatives as was the case in the example. Hence, the need becomes obvious for a third and more general method of handling the boundary difference equations.

The third method is based upon a reflection technique which recently has been discussed by Burstein (26). By this technique points which are adjacent to plane walls are assumed to be imaged by virtual points which actually lie within the wall. Thus, for a wall such as that shown in Figure 6, the variables at the field point $(m,\ell+1)$ would be related to the variables at the virtual point $(m,\ell-1)$ by the expressions

$$\begin{aligned} \rho_{m,\ell+1} &= \rho_{m,\ell-1} , \\ u_{m,\ell+1} &= u_{m,\ell-1} , \\ v_{m,\ell+1} &= -v_{m,\ell-1} , \\ p_{m,\ell+1} &= p_{m,\ell-1} . \end{aligned} \tag{4-27}$$

The advantage of such a representation is that it allows boundary points to be treated by centered differences in much the same way as field points. Thus, for a wall parallel to the x-axis the difference approximation is (see equation (4-12))

$$f^{n+1}_{m,\ell} = f^{n}_{m,\ell} - \frac{K_1}{2}\left[F^{x}_{m+1,\ell} - F^{x}_{m-1,\ell} \right]^{n} - \frac{K_2}{2}\left[F^{y}_{m,\ell+1} - F^{y}_{m,\ell-1} \right]^{n} + \\ + \frac{1}{2}\left[\Phi^{x}_{m+\frac{1}{2},\ell} - \Phi^{x}_{m-\frac{1}{2},\ell} \right]^{n} , \tag{4-28}$$

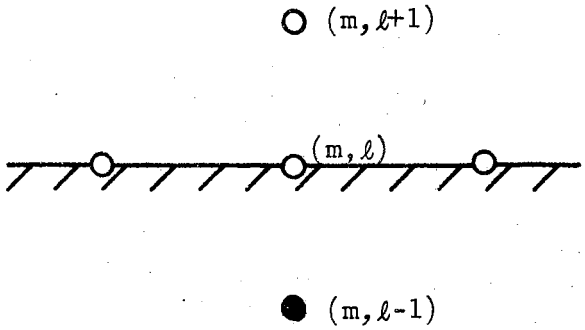

Figure 6. Image Point Principle for Wall Point.

where the $F^{y}_{m,\ell+1}$ and $F^{y}_{m,\ell-1}$ terms are handled according to equation (4-27). The blurring terms which act in a direction normal to the wall have been omitted from equation (4-28) by utilizing the boundary conditions (3-40). This has been done so as to reduce the amount of artificial dissipation normal to the wall. For the analogous situation of a net point lying on a wall parallel to the y-axis the image point principle yields

$$\begin{aligned} \rho_{m+1,\ell} &= \rho_{m-1,\ell} \,, \\ u_{m+1,\ell} &= -u_{m-1,\ell} \,, \\ v_{m+1,\ell} &= v_{m-1,\ell} \,, \\ p_{m+1,\ell} &= p_{m-1,\ell} \,, \end{aligned} \tag{4-29}$$

with the difference approximation being

$$f^{n+1}_{m,\ell} = f^{n}_{m,\ell} - \frac{K_1}{2}\left[F^{x}_{m+1,\ell} - F^{x}_{m-1,\ell} \right]^{n} - \frac{K_2}{2}\left[F^{y}_{m,\ell+1} - F^{y}_{m,\ell-1} \right]^{n} + \frac{1}{2}\left[\Phi^{y}_{m,\ell+\frac{1}{2}} - \Phi^{y}_{m,\ell-\frac{1}{2}} \right]^{n} . \tag{4-30}$$

In view of the requirements of the present study, the obvious advantage of the image point method for treating boundary points is that it completely deletes the necessity of dictating a priori the values of derivatives at a surface. As was true when the inviscid equations were considered in the forward difference method, the image

point technique allows the derivatives at a surface to assume whatever realistic value may be necessary in the computations. Thus by this method the boundary conditions are not imposed in such a manner that they negate the possibility of certain phenomenon occurring in the vicinity of a wall. This should not be taken to mean, however, that the conditions imposed on the surface derivatives are completely relaxed; the very nature of the image point technique requires that conditions (3-40) be at least approximately satisfied.

Unfortunately, the image point method is not devoid of limitations. For the case of two boundaries intersecting as shown in Figure 7 the reflection technique requires that the point interior to the walls be the virtual point (m_1-1,ℓ_1) as well as the virtual point (m_2,ℓ_2-1). Thus the interior point must be the image of both the point (m_1+1,ℓ_1) and the point (m_2,ℓ_2+1). This obviously implies that either the conditions at (m_1+1,ℓ_1) and (m_2,ℓ_2+1) are the same or that the virtual point is double valued. For most problems of interest the first choice is not realistic and the second choice is even less desirable since it is physically impossible. This problem is manifested in the numerical computations as an expansion region with pressures which are unrealistically low. This is due to the fact that a particle at the corner of the two boundaries is required to change flow direction in a radial length of zero. In order for this to occur the particle must be subjected to an infinite acceleration, thus requiring the pressure at the point directly below the corner to approach zero.

The problem can be alleviated if, at locations where image points must be double valued, the boundary conditions (3-40) are strictly

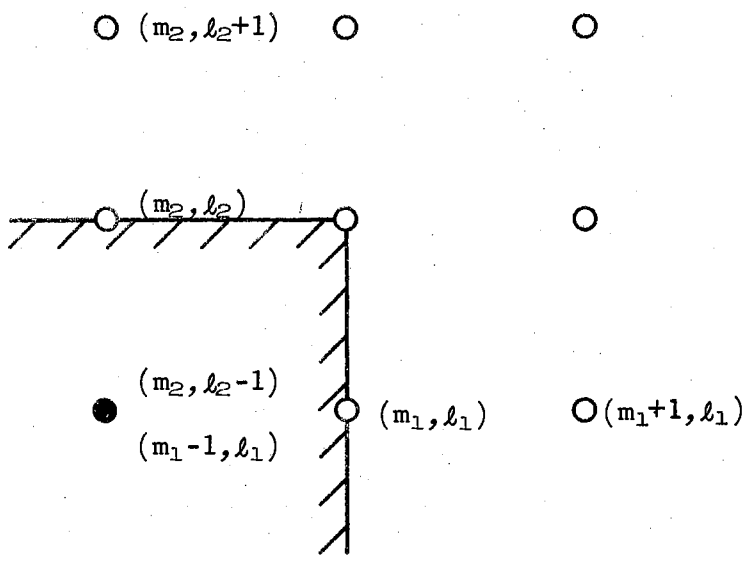

Figure 7. Double Valued Image Point.

enforced. In so doing a fluid particle is not required to change directions instantaneously and the phenomenon of flow separation is allowed to transpire in much the same way as in nature.

A simple problem which considered a moving shock wave passing over a two-dimensional step was computed using the inviscid equations of Rusanov. These are the equations which would be obtained if all the turbulence terms were to be dropped from equation (3-39). The purpose of the problem was to check the computer program which was to be used later for jet mixing analysis. Samples of the results are shown in Figures 8 and 9. The wave started from its initial position with a Mach number of 1.89. The uniform pressure in front of the wave had an initial value of unity and that behind the wave had an initial value of four. The first figure shows lines of constant pressure at fifty time planes and the second figure shows the same lines at one hundred time planes. The approximate shock position at each time is denoted by the dashed line. The agreement between this problem and a similar problem computed by Tyler (4) was found to be quite good.

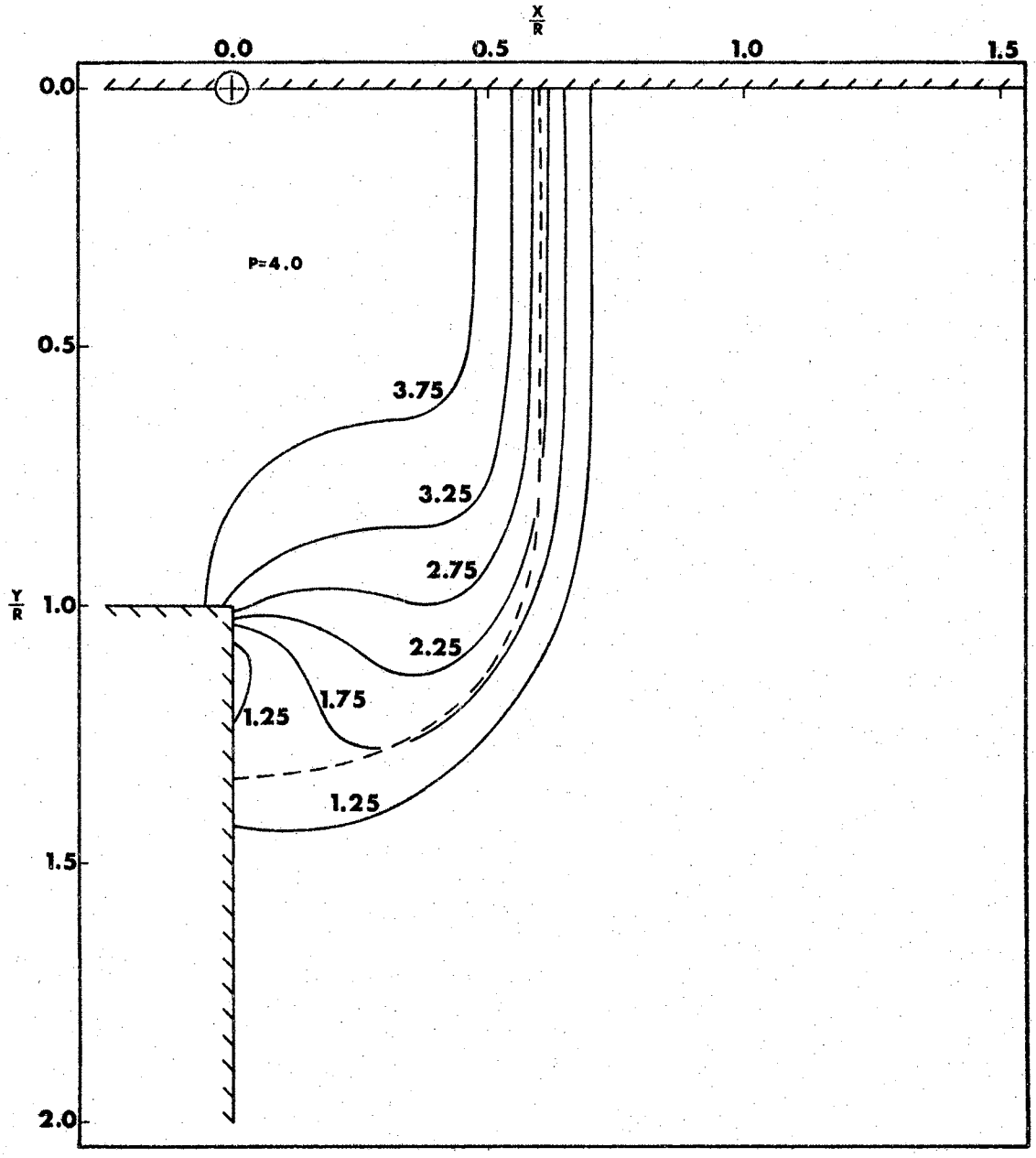

Figure 8. Constant Pressure Lines at Time Plane 50 for two Dimensional Example Problem.

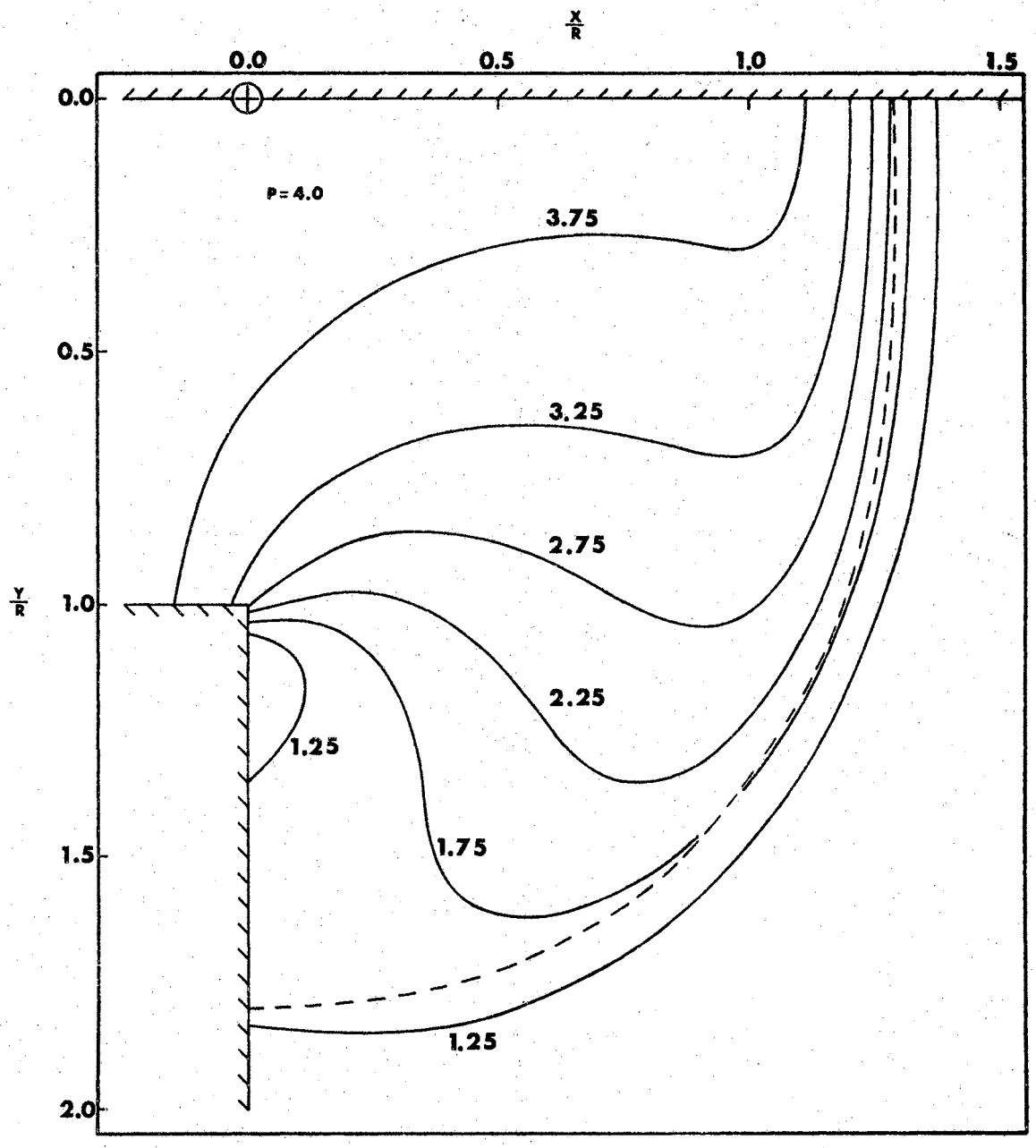

Figure 9. Constant Pressure Lines at Time Plane 100 for two Dimensional Example Problem.

CHAPTER V

STABILITY ANALYSIS OF THE FINITE DIFFERENCE EQUATIONS

Equation (3-39) is a system of second order non-linear partial differential equations which are to be approximated by a finite difference technique. As with any finite difference method, it is necessary to determine the conditions which must be met in order to assure that a perturbation will not increase without bound with increasing time. Richtmyer (27) has stated that even for a first order non-linear system, there exists no rigorous analysis whereby these stability criteria can be determined. Therefore one is restricted to the use of linear theories for the determination of the stability requirements of non-linear systems. The usual method for obtaining these requirements is to perturb the dependent variables in the difference equation; and then to replace the perturbed quantities with a Fourier series representation (23). The necessary conditions for the convergence of the series are then assumed to represent the stability criteria of the difference equations. This technique, which has been called the von Neumann method, will be used to determine the stability requirements for the difference equation (4-12). In addition to the assumption that a linear analysis will provide the stability requirements for the non-linear system (3-39), a second assumption made is that the stability criteria will be the same no matter which three equations of expression (3-39)

are perturbed. In this analysis the continuity and two momentum equations are perturbed. It is therefore assumed that the resulting stability condition is identical to that which would have been obtained if the energy equation and two others had been perturbed.

The perturbation analysis is accomplished by first allowing the dependent variables ρ, u, v, and p to change slightly. The effect of the variation on equation (4-12) is then investigated. Rather than determine the effect of perturbing each of the four dependent variables, however, a general perturbation variable φ will be introduced. Therefore a change in $\varphi_{m,\ell}^{n+1}$ will cause a resultant change in $f_{m,\ell}^{n+1}$ of

$$df_{m,\ell}^{n+1} = \frac{df}{d\varphi}\,\delta\varphi_{m,\ell}^{n+1} = \frac{df}{d\varphi}\,\delta\varphi_{m,\ell}^{n} - \frac{K_1}{2}\,\frac{dF^x}{d\varphi}\left(\delta\varphi_{m+1,\ell} - \delta\varphi_{m-1,\ell}\right)^n -$$

$$- \frac{K_2}{2}\,\frac{dF^y}{d\varphi}\left(\delta\varphi_{m,\ell+1} - \delta\varphi_{m,\ell-1}\right)^n + \frac{1}{2}\,\alpha\frac{df}{d\varphi}\left(\delta\varphi_{m+1,\ell} - 2\delta\varphi_{m,\ell} + \delta\varphi_{m-1,\ell}\right)^n +$$

$$+ \frac{1}{2}\,\beta\frac{df}{d\varphi}\left(\delta\varphi_{m,\ell+1} - 2\delta\varphi_{m,\ell} + \delta\varphi_{m,\ell-1}\right)^n , \qquad (5\text{-}1)$$

where the subscripts have been omitted from the terms whose functional values are independent of position. For example,

$$\frac{dF^x_{m+1,\ell}}{d\varphi_{m+1,\ell}} = \frac{dF^x_{m,\ell}}{d\varphi_{m,\ell}} = \frac{dF^x_{m+d,\ell}}{d\varphi_{m+e,\ell}} = \frac{dF^x}{d\varphi} , \qquad (5\text{-}2)$$

where d and e are integers with arbitrary values.

The next step in the stability analysis is to express the perturbation term $\delta\varphi$ as a product of its initial value and its wave components.

In equation form this may be written as

$$\delta\varphi^{n}_{m,\ell} = \xi^{n} e^{i(m\psi_1+\ell\psi_2)} \delta\varphi^{\circ}_{\circ,\circ} \quad , \tag{5-3}$$

where $\delta\varphi^{\circ}_{\circ,\circ}$ is the initial perturbation value, ψ_1 and ψ_2 are real numbers to be determined and ξ is the term whose value dictates whether or not stability may be realized under the influence of $\delta\varphi^{\circ}_{\circ,\circ}$.

For the purposes of this investigation, equation (4-12) is said to be stable if, for all values of m, ℓ, and n, there exists some number M such that

$$\delta\varphi^{n}_{m,\ell} < M. \tag{5-4}$$

This merely means that if the system under consideration is subjected to a perturbation, then at all points in space and time the perturbation must be bounded. In order for this condition to be realized the series ξ^{n} in equation (5-3) must be convergent, thus requiring that

$$| \xi | \leq 1. \tag{5-5}$$

In the strict sense, inequality (5-5) is not convergent if the equality is realized. However, for stability purposes the principle objective is to insure that a perturbation does not increase without bound. Therefore if

$$| \xi | = 1 ,$$

expression (5-4) is satisfied and stability is theoretically assured. Thus, for the purposes of stability analysis, the strict definition of

convergence can be relaxed such that (5-5) is a necessary condition for the convergence of the series ξ^n.

In order to obtain the conditions which will satisfy expression (5-5), it is necessary to substitute equation (5-3) into equation (5-1) and solve for ξ. The substitution is straightforward and the resulting expression is

$$(\xi-1)\frac{df}{d\varphi} + iK_1 \sin\psi_1 \frac{dF^x}{d\varphi} + iK_2 \sin\psi_2 \frac{dF^y}{d\varphi} +$$

$$+ 2\left(\alpha \sin^2\frac{\psi_1}{2} + \beta \sin^2\frac{\psi_2}{2}\right)\frac{df}{d\varphi} = 0 \quad . \tag{5-6}$$

Equation (5-6) is the expression from which the values of ξ which satisfy inequality (5-5) will be obtained. The expressions for f, F^x, and F^y to be used in the analysis are

$$f = \begin{bmatrix} \rho \\ \rho u \\ \rho v \end{bmatrix}, \qquad F^x = \begin{bmatrix} \rho u \\ p + \rho u^2 - \zeta \frac{\partial u}{\partial x} \\ \rho uv - \zeta \frac{\partial v}{\partial x} \end{bmatrix},$$

$$F^y = \begin{bmatrix} \rho v \\ \rho uv - \zeta \frac{\partial u}{\partial y} \\ p + \rho v^2 - \zeta \frac{\partial v}{\partial y} \end{bmatrix}, \tag{5-7}$$

where $\zeta = \frac{u_a}{2\sigma^2}\rho x = R\rho x$.

The independent variable in equation (5-6) is φ. The differential of φ may therefore be expressed as

$$d\varphi \cong \delta\varphi \,. \tag{5-8}$$

In view of equation (5-8) one can write equation (5-6) in differential form as

$$(\xi - 1)\, df + iK_1 \sin\psi_1\, dF^x + iK_2 \sin\psi_2\, dF^y +$$

$$+ 2\left(\alpha \sin^2\frac{\psi_1}{2} + \beta \sin^2\frac{\psi_2}{2}\right) df = 0. \tag{5-9}$$

If the substitutions

$$\zeta\frac{\partial u}{\partial x} = \Omega_{ux}\,, \qquad \zeta\frac{\partial v}{\partial x} = \Omega_{vx}$$

$$\zeta\frac{\partial u}{\partial y} = \Omega_{uy}\,, \qquad \zeta\frac{\partial v}{\partial y} = \Omega_{vy} \tag{5-10}$$

are made, the differentials in equation (5-9) may be expressed as

$$df = \begin{bmatrix} d\rho \\ \rho du + u d\rho \\ \rho dv + v d\rho \end{bmatrix}, \qquad dF^x = \begin{bmatrix} \rho du + u d\rho \\ dp + u^2 d\rho + 2\rho u du - d\Omega_{ux} \\ \rho v du + \rho u dv + uv d\rho - d\Omega_{vx} \end{bmatrix},$$

and

$$dF^y = \begin{bmatrix} \rho dv + v d\rho \\ \rho v du + \rho u dv + uv d\rho - d\Omega_{uy} \\ dp + v^2 d\rho + 2\rho v dv - d\Omega_{vy} \end{bmatrix} , \tag{5-11}$$

where

$$\begin{aligned} d\Omega_{ux} &= R\rho \frac{\partial u}{\partial x} dx + Rx \frac{\partial u}{\partial x} d\rho + R\rho x d\left(\frac{\partial u}{\partial x}\right) \\ d\Omega_{vx} &= R\rho \frac{\partial v}{\partial x} dx + Rx \frac{\partial v}{\partial x} d\rho + R\rho x d\left(\frac{\partial v}{\partial x}\right) \\ d\Omega_{uy} &= R\rho \frac{\partial u}{\partial y} dx + Rx \frac{\partial u}{\partial y} d\rho + R\rho x d\left(\frac{\partial u}{\partial y}\right) \\ d\Omega_{vy} &= R\rho \frac{\partial v}{\partial y} dx + Rx \frac{\partial v}{\partial y} d\rho + R\rho x d\left(\frac{\partial v}{\partial y}\right) . \end{aligned} \tag{5-12}$$

In writing equations (5-12) the assumption has been made that u_a and σ are constant. For most turbulent mixing problems this assumption is justifiable on the grounds that pressure changes in the adjacent stream are small. For the case of the mixing region-shock interaction phenomenon, however, the changes in the adjacent stream velocity will depend, to a large extent, upon the shock wave pressure ratio. Therefore for those cases which consider large shock wave pressure ratios the assumption of constant u_a is violated. The violation of this assumption is manifested in the same manner as is the violation of the linearity assumption; namely, in an overestimation of the stability criteria for the difference equations.

Equation (5-9) represents a system of three simultaneous equations where the expressions for the differentials are obtained from equations (5-11). If the first of equations (5-11) is substituted into (5-9) and simplified, the result is

$$\frac{dv}{d\rho} = \frac{-i\theta_1 \rho \frac{du}{d\rho} - Z}{i\theta_2 \rho} \tag{5-13}$$

where

$$\theta_1 = K_1 \sin \psi_1$$

$$\theta_2 = K_2 \sin \psi_2$$

and

$$Z = \xi - 1 + 2 \left(\alpha \sin^2 \frac{\psi_1}{2} + \beta \sin^2 \frac{\psi_2}{2} \right) + i\theta_1 u + i\theta_2 v.$$

Similarly if the second equation in (5-11) is substituted into (5-9), the result is

$$\frac{du}{d\rho} = \frac{i\theta_1 \frac{d\Omega_{ux}}{d\rho} + i\theta_2 \frac{d\Omega_{uy}}{d\rho} - i\theta_1 c^2}{Z\rho} \tag{5-14}$$

where $c^2 = \frac{dp}{d\rho}$ is the local sonic velocity squared. When the last equation in (5-11) is substituted into (5-9), use is made of equations (5-14) and (5-13) to yield, after minor simplifications

$$Z^2 + c^2 \left(\theta_1^2 + \theta_2^2 \right) - \theta_1\theta_2 \left(\frac{d\Omega_{uy}}{d\rho} + \frac{d\Omega_{vx}}{d\rho} \right) -$$

$$- \theta_1^2 \frac{d\Omega_{ux}}{d\rho} - \theta_2^2 \frac{d\Omega_{vy}}{d\rho} = 0 \quad . \tag{5-15}$$

In order to reduce the magnitude of the expressions somewhat, the substitutions

$$A_1 = \frac{d\Omega_{uy}}{d\rho} \quad , \qquad A_2 = \frac{d\Omega_{vx}}{d\rho} \quad , \qquad A_3 = \frac{d\Omega_{ux}}{d\rho} \quad ,$$

$$A_4 = \frac{d\Omega_{vy}}{d\rho} \quad , \qquad A_5 = A_1 + A_2$$

are made. Then if equation (5-15) is solved for Z, the result is

$$Z = \pm \left[\theta_1\theta_2 A_5 + \theta_1^2 A_3 + \theta_2^2 A_4 - c^2 \left(\theta_1^2 + \theta_2^2 \right) \right]^{\frac{1}{2}} \quad . \tag{5-16}$$

Now, if the expressions for Z, θ_1, and θ_2 are substituted into (5-16), the resulting expression can be solved for ξ to yield

$$\xi = 1 - 2 \left(\alpha \sin^2 \frac{\psi_1}{2} + \beta \sin^2 \frac{\psi_2}{2} \right) - i \left(K_1 u \sin \psi_1 + K_2 v \sin \psi_2 \right) \pm$$

$$\pm \left[K_1K_2 \sin \psi_1 \sin \psi_2 A_5 + K_1^2 \sin^2 \psi_1 A_3 + K_2^2 \sin^2 \psi_2 A_4 - \right.$$

$$\left. - c^2 \left(K_1^2 \sin^2 \psi_1 + K_2^2 \sin^2 \psi_2 \right) \right]^{\frac{1}{2}} \quad . \tag{5-17}$$

Equation (5-17) is the functional relation for ξ from which stability criteria will be established according to expression (5-5). Unfortunately, no simple solution of (5-5) can be obtained because of the

complexity of (5-17). Therefore, the procedure to be followed will be to evaluate ξ as the angles ψ_1 and ψ_2 assume large and small values. First, for values of ψ_1 and ψ_2 which are large,

$$\psi_1 = \psi_2 = \pi , \tag{5-18}$$

equation (5-17) will reduce to

$$\xi = 1 - 2(\alpha + \beta) . \tag{5-19}$$

Then, applying inequality (5-5) to equation (5-19) results in

$$| 1 - 2(\alpha + \beta) | \leq 1 ,$$

from which one can obtain

$$0 \leq \alpha + \beta \leq 1 . \tag{5-20}$$

For values of ψ_1 and ψ_2 which are very small

$$\psi_1 \cong \sin \psi_1$$

and (5-21)

$$\psi_2 \cong \sin \psi_2 .$$

These approximations for the small angles allow equation (5-17) to be expressed as

$$\xi_s = 1 - \frac{1}{2}(\alpha\psi_1^2 + \beta\psi_2^2) - i(K_1 u\psi_1 + K_2 v\psi_2) \pm$$

$$\pm [K_1K_2\psi_1\psi_2A_5 + K_1^2\psi_1^2A_4 + K_2^2\psi_2^2A_4 - c^2(K_1^2\psi_1^2 + K_2^2\psi_2^2)]^{\frac{1}{2}} . \tag{5-22}$$

From equation (5-22) it can be seen that there are two cases which must be considered when evaluating $|\xi_s|$. The first case is the condition where

$$\mathcal{R}(\xi_s) = 1 - \frac{1}{2}(\alpha\psi_1^2 + \beta\psi_2^2) \pm T$$

and (5-23)

$$I(\xi_s) = -(K_1 u\psi_1 + K_2 v\psi_2) ,$$

and the second case is for

$$\mathcal{R}(\xi_s) = 1 - \frac{1}{2}(\alpha\psi_1^2 + \beta\psi_2^2)$$

and (5-24)

$$I(\xi_s) = -(K_1 u\psi_1 + K_2 v\psi_2) \pm T$$

where

$$T = [K_1K_2\psi_1\psi_2A_5 + K_1^2\psi_1^2A_3 + K_2^2\psi_2^2A_4 - c^2(K_1^2\psi_1^2 + K_2^2\psi_2^2)]^{\frac{1}{2}} > 0 .$$

From order of magnitude arguments which will be presented later, it has been found that the conditions which correspond to equations (5-23) are not likely to occur. Therefore, considering equations (5-24), one can find the expression for the modulus of ξ_s to be

$$|\xi_s| = \left\{ 1 - \alpha\psi_1^2 - \beta\psi_2^2 + [K_1 u\psi_1 + K_2 v\psi_2 \left\{c^2(K_1^2\psi_1^2 + K_2^2\psi_2^2) - \right.\right.$$
$$\left.\left. - K_1K_2\psi_1\psi_2A_5 - K_1^2\psi_1^2A_3 - K_2^2\psi_2^2A_4 \right\}^{\frac{1}{2}}]^2 \right\}^{\frac{1}{2}} . \qquad (5\text{-}25)$$

Inequality (5-5) can be expressed as

$$1 - |\xi_s|^2 \geq 0 , \tag{5-26}$$

which provides help in reducing (5-25) to a useful form. If the operations indicated in (5-26) are performed on equation (5-25) the result is

$$\alpha\psi_1^2 + \beta\psi_2^2 \geq \left\{K_1 u\psi_1 + K_2 v\psi_2 + [c^2(K_1^2\psi_1^2 + K_2^2\psi_2^2) - K_1K_2\psi_1\psi_2A_5 - K_1^2\psi_1^2A_3 - K_2^2\psi_2^2A_4]^{\frac{1}{2}}\right\}^2 . \tag{5-27}$$

If the substitutions

$$\cos\theta = \frac{K_1\psi_1}{[K_1^2\psi_1^2 + K_2^2\psi_2^2]^{\frac{1}{2}}} , \quad \sin\theta = \frac{K_2\psi_2}{[K_1^2\psi_1^2 + K_2^2\psi_2^2]^{\frac{1}{2}}} \tag{5-28}$$

are made, inequality (5-27) can be simplified to

$$\frac{\alpha\cos^2\theta}{K_1^2} + \frac{\beta\sin^2\theta}{K_2^2} \geq \left\{u\cos\theta + v\sin\theta + [c^2 - A_5\cos\theta\sin\theta - A_3\cos^2\theta - A_4\sin^2\theta]^{\frac{1}{2}}\right\}^2 . \tag{5-29}$$

The next step in the analysis is to show, with order of magnitude arguments, that

$$c^2 > A_5\cos\theta\sin\theta + A_3\cos^2\theta + A_4\sin^2\theta . \tag{5-30}$$

If such is the case then the inequality

$$\frac{\alpha\cos^2\theta}{K_1^2} + \frac{\beta\sin^2\theta}{k_2^2} \geq [u\cos\theta + v\sin\theta + c]^2 , \tag{5-31}$$

insures that inequality (5-29) will be satisfied. This amounts to eliminating the turbulence effects from the stability criteria. Only one of the coefficients, A_4, will be used because the order of magnitude arguments will apply equally to A_3 and A_5. Therefore, from equation (5-12) and the definition for A_4,

$$A_4 = \frac{d\Omega_{vy}}{d\rho} = \frac{u_a}{2\sigma^2}\left[\rho\frac{\partial v}{\partial y}\frac{dx}{d\rho} + x\frac{\partial v}{\partial y} + \rho x\frac{d\left(\frac{\partial v}{\partial y}\right)}{d\rho}\right]. \qquad (5\text{-}32)$$

The greatest possible values of the terms in equation (5-32) occur when one-dimensional flow through a stationary normal shock wave is considered. Therefore if x and y are replaced with a general space variable s, and if the thermodynamic and kinematic properties are non-dimensionalized according to the method discussed in Appendix F, then equation (5-32) can be written as

$$A_4 = \frac{d\Omega_{vy}}{d\rho} = \frac{u_a}{2\sigma^2}\left[\rho\frac{\partial u}{\partial s}\frac{\partial s}{\partial \rho} + s\frac{\partial u}{\partial s} + \rho s\frac{d\left(\frac{\partial u}{\partial s}\right)}{d\rho}\right]. \qquad (5\text{-}33)$$

The orders of magnitude for the various terms in equation (5-33) are, for problems of interest in this study;

$$\begin{aligned} u_a &= O[10^0] \\ \sigma &= O[10^1] \Rightarrow \sigma^2 = O[10^2] \\ \rho &= O[10^0] \\ \frac{\partial u}{\partial s}\frac{\partial s}{\partial \rho} &= O[10^0] \end{aligned} \qquad (5\text{-}34)$$

$$s = O[10^1]$$

$$\frac{\partial u}{\partial s} = O[10^0] \qquad (5\text{-}34)$$

$$\frac{d\left(\frac{\partial u}{\partial s}\right)}{d\rho} = O[10^0] \, .$$

Therefore the order of A_4 is

$$O[A_4] = \frac{O[10^0]}{O[10^2]} \left[O[10^0]O[10^0] + O[10^1]O[10^0] + O[10^0]O[10^1]O[10^0] \right]$$

$$= O[10^{-1}] \, . \qquad (5\text{-}35)$$

The order of magnitude of the non-dimensional accoustic velocity is

$$c = O[\sqrt{\gamma}] \, ,$$

or

$$c^2 = O[\gamma] = O[10^0] \, . \qquad (5\text{-}36)$$

Upon comparing expressions (5-35) and (5-36) it can be seen that

$$A_4 < c^2$$

Therefore since inequality (5-31) is satisfied, inequality (5-29) will also be satisfied. Inequality (5-31) is identical to the inequality obtained by Rusanov (24) from the inviscid hydrodynamic equations.

Expression (5-31) must be true for all values of the expression on the right side of the inequality. Therefore, in order to insure that the inequality is always satisfied, it is sufficient to dictate

that

$$\frac{\alpha \cos^2 \theta}{K_1^2} + \frac{\beta \sin^2 \theta}{K_2^2} \geq [(u \cos \theta + v \sin \theta + c)^2]_{max} . \quad (5\text{-}37)$$

It is a simple matter to show that the terms on the right side of (5-37) attain a maximum whenever

$$\theta = \tan^{-1} \frac{v}{u} , \quad (5\text{-}38)$$

from which one can obtain

$$\cos \theta = \frac{u}{w} , \qquad \sin \theta = \frac{v}{w} . \quad (5\text{-}39)$$

If equations (5-39) are substituted into the right side of (5-37), and equations (4-9) for K_1 and K_2 are substituted into the left side, the result is

$$\frac{\alpha \cos^2 \theta}{\sin^2 \chi} + \frac{\beta \sin^2 \theta}{\cos^2 \chi} \geq K^2 [w + c]^2 = \bar{\sigma}^2 , \quad (5\text{-}40)$$

where $\bar{\sigma} = K(w + c)$ is the Courant number.

Inequalities (5-40) and (5-20) furnish values of α and β which will insure the stability of the system of equations (4-2) under the limits of the assumptions in the analysis. Inequality (5-20) can be written as an equality

$$\alpha + \beta = \omega\bar{\sigma} \quad (5\text{-}41)$$

so long as

$$0 \leq \omega\bar{\sigma} \leq 1 . \quad (5\text{-}42)$$

If equation (5-41) is solved for β, and that result substituted into (5-40), the resulting expression is

$$\frac{\alpha \cos^2\theta \cos^2\chi + \omega\bar{\sigma} \sin^2\theta \sin^2\chi - \alpha \sin^2\theta \sin^2\chi}{\sin^2\chi \cos^2\chi} \geq \bar{\sigma}^2. \qquad (5\text{-}43)$$

Any expression for α and β may be chosen as long as inequality (5-42) is satisfied. Therefore if the expression

$$\alpha = \omega\bar{\sigma} \sin^2\chi \qquad (5\text{-}44)$$

is chosen, expression (5-43) will be simplified to

$$\frac{\alpha}{\sin^2\chi} \geq \bar{\sigma}^2 . \qquad (5\text{-}45)$$

In view of expressions (5-44) and (5-45) inequality (5-42) can now be written as

$$\bar{\sigma}^2 \leq \omega\bar{\sigma} \leq 1 ,$$

or

$$K^2(w + c)^2 \leq \omega K(w + c) \leq 1 . \qquad (5\text{-}46)$$

From equation (5-41) the β term which corresponds to equation (5-44) is

$$\beta = \omega\bar{\sigma} \cos^2\chi . \qquad (5\text{-}47)$$

Inequalities (5-40) and (5-20) have thus been combined into the one equality (5-46), wherein the definitions of α and β, equations (5-44) and (5-47), have been used.

Expression (5-46) therefore represents the stability criteria for the difference equations (4-12). The damping parameter, ω, is an arbitrary quantity which must satisfy the inequality

$$\bar{\sigma} \leq \omega \leq \frac{1}{\bar{\sigma}} . \tag{5-48}$$

For computational purposes, the maximum allowable Courant number, $\bar{\sigma}_o$, is introduced, where

$$\bar{\sigma}_o = K (w + c)_{max} . \tag{5-49}$$

If the inequalities

$$0 \leq \bar{\sigma}_o \leq 1 ,$$

and

$$\bar{\sigma}_o \leq \omega \leq \frac{1}{\bar{\sigma}_o} \tag{5-50}$$

are satisfied, then the conditions (5-46) and (5-48) will be satisfied and the time step K can be evaluated from

$$K = \frac{\bar{\sigma}_o}{(w + c)_{max}} . \tag{5-51}$$

Several assumptions have been utilized in the development of (5-46) and (5-48). As noted previously the most significant of these is that linear perturbation theory provides the stability requirements for the non-linear system (3-39). For the inviscid equations, the effect of this assumption is to overestimate the allowable upper value and to underestimate the allowable lower value of inequality (5-48). However, when the turbulence terms are considered, the allowable lower value of (5-48) is overestimated. Therefore, as might be expected, the turbulence effects

have a tendency to aid the blurring terms and thus to relax the stability criteria. This result has been indicated from the results of numerical experimentation and will be discussed further in Chapter VI.

CHAPTER VI

ESTABLISHMENT OF A MIXING REGION BY THE NUMERICAL SOLUTION OF THE GOVERNING EQUATIONS

The governing equations for this study have been derived in Chapter III. The finite difference technique and the stability criteria for the difference equations have been discussed in Chapters IV and V respectively. Equations (3-38) and (3-39) describe both the two-dimensional, time dependent turbulent mixing process and the two-dimensional, time dependent, mixing region-shock interaction phenomenon. Even though the interaction problem is of paramount interest here, its solution cannot be attempted until a steady, two-dimensional turbulent mixing region has been established from the numerical solution of the governing equations. This chapter is concerned with the establishment of such a steady state mixing region. Chapter VII will be concerned with the passage of a shock wave across the established mixing region.

For the problems which have been considered in this investigation, the use of a digital computer was necessary in order to accomplish the computations required in the numerical method. Appendix E shows the computer logic diagram from which the computer program was written. The logic diagram was drawn for a data processing system with an overall memory size of not less than 32,000 words. For such a system, a finite difference net of approximately 2000 points can be accommodated.

Preliminary Considerations

Before the results of the computations for a typical mixing problem are presented, the results obtained from a series of numerical experiments will be discussed. These computations were conducted in order to obtain information concerning the numerical method which has been presented in the previous chapters. Specifically, the following items needed to be considered:

1. the finite difference mesh size;
2. an economical representation of the initial conditions;
3. the effect of reducing the damping term, ω, below the values indicated in the stability criteria (5-48);
4. the effect of the blurring terms upon the flow properties, and particularly upon the mixing region velocity profiles.

In order to obtain this information a simple problem was postulated. Then, a sufficient number of cases was computed to allow determination of the items above.

The basic configuration which was used is shown in Figure 10. The flow of a Mach 2.0 stream over a plane wall was considered. As indicated in the figure, the flow field is divided into three regions. The non-dimensional properties in region 1 were maintained at the values shown. The method for non-dimensionalizing the properties is discussed in Appendix F. Twenty points were taken in both the positive and negative y-directions, and thirty-five points were taken in the x-direction. In each case the computations were started at time zero and, depending upon the objectives of the particular problem, continued to either fifty or

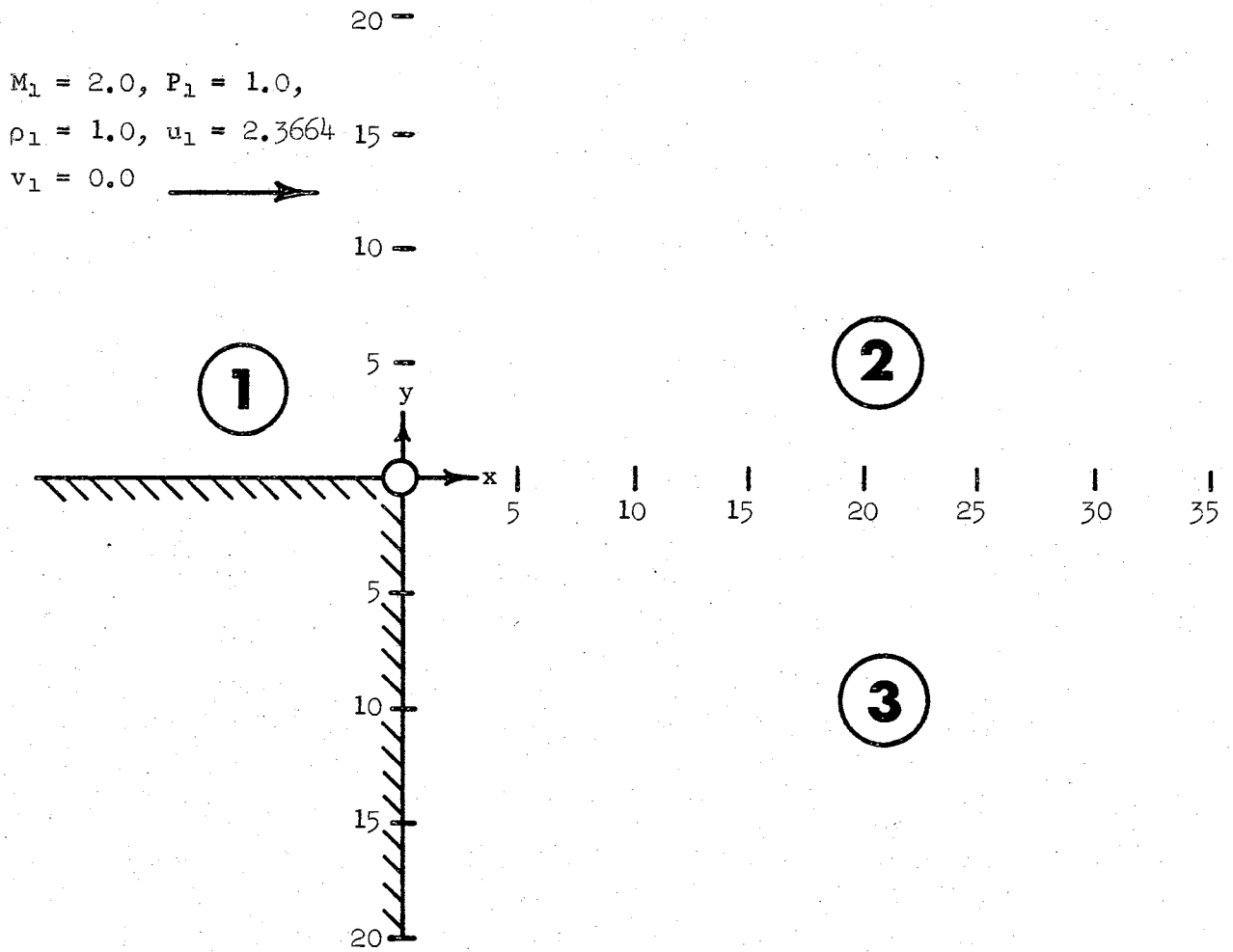

Figure 10. Basic Geometry for Numerical Experiments.

one-hundred time planes. The significant results obtained from these initial numerical experiments will now be presented.

Finite Difference Mesh Size

For an accurate description of most turbulent mixing processes, a large density of mesh points in the y-direction is desirable. Though the density of points in the x-direction need not be as large as that in the y-direction, the total length of mixing region in the x-direction should be quite large compared to the y mesh width. Thus it appears that a square finite difference mesh requires an unrealistically large number of mesh points. This conclusion was substantiated by the numerical experimentation. Further, it was found that for a rectangular mesh spacing with $\frac{h_1}{h_2} = 5$ (See Figure 4), the solution of the difference equations would describe the physical phenomenon very nicely.

Representation of Initial Conditions

From the results of two different cases which were considered, it appears that, within the bounds of reason, the initial description of the flow field has little effect upon the computer time required for a mixing region to develop. Figure 11 shows the two cases which were considered. In the first case, Figure 11a, properties in regions 1 and 2 were initially equal; but regions 2 and 3 were significantly different, being separated by a slip region as shown. In the second case, Figure 11b, a mixing region was used for the initial description of the field.

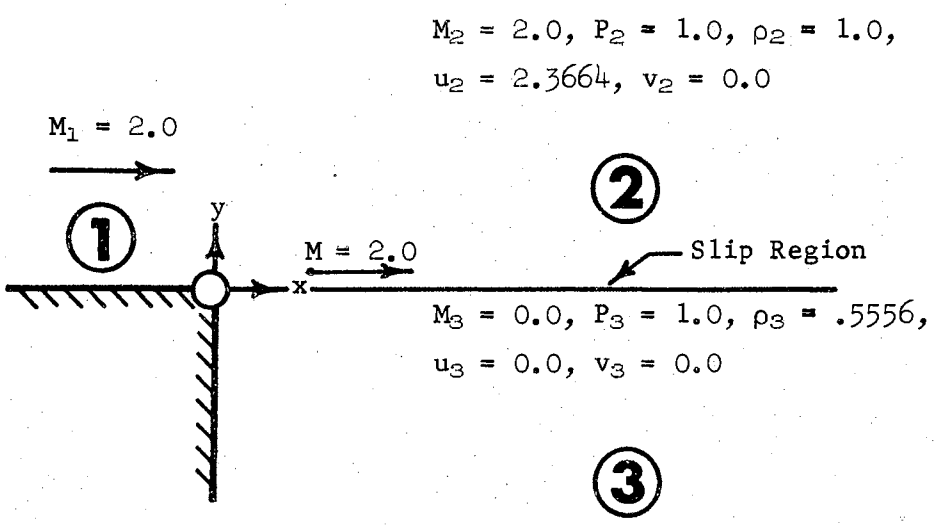

(a) Initial Slip Line at y = 0

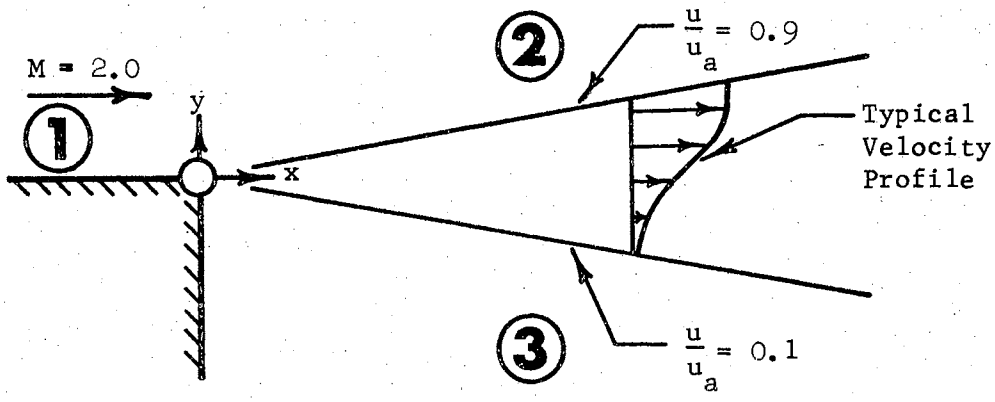

(b) Initial Mixing Region Described

Figure 11. Two Methods for Describing Initial Conditions.

After the calculation of fifty time planes (n = 50), the difference in the results for the two different initial representations was negligible. Therefore, since it is extremely time consuming to represent a fully developed mixing region, it appears that the slip line is the most economical method to initiate the computations.

Effect of Reducing Damping Term Below Values Allowed by Stability Criteria

As was discussed in Chapter V, because of the turbulence terms it seems reasonable to hypothesize that the damping parameter, ω, can be reduced below the values indicated by the inequality

$$\bar{\sigma}_o \leq \omega \leq \frac{1}{\bar{\sigma}_o} . \qquad (6\text{-}1)$$

This hypothesis was verified by a parametric study. For all the computations in this study, only the value of ω was varied from case to case. The value of the maximum allowable Courant number was taken to be 0.5, for which the allowable values of ω would be, according to (6-1),

$$0.5 \leq \omega \leq 2.0 . \qquad (6\text{-}2)$$

The results of the computations are shown in Table I.

TABLE I

RESULTS OF VARYING DAMPING PARAMETER

ω	Stable	Unstable
0.0		*
0.05	*	
0.10	*	
0.50	*	
1.00	*	
1.50	*	
2.00		*

From the results presented in the table it appears that the effect of the turbulence terms is to reduce the allowable value of ω which may be used. For values of ω of 0.0 and 2.0, the computations indicated an unstable condition near $y = 0$ and $x = 30$. These results should only be considered as qualitative, however; because if other values of Mach number or $\bar{\sigma}_o$ had been considered, it seems reasonable to assume that the results could have been different.

Effect of Blurring Terms on Velocity Profiles

In order to have confidence in the results obtained from the numerical method, it is necessary to have a knowledge of the influences that the blurring terms have on the velocity profiles. The parametric study discussed in the preceeding section has provided information concerning these influences. Figure 12 shows the velocity profiles obtained at time plane 50 for three values of the damping term ω. Also shown in the figure are the experimentally verified error function profiles (equation 3-27) at the three x locations. The error function profiles are determined under the assumption of steady state conditions. Even though, at time plane 50, a steady state does not exist, the error function profiles show the solutions which should be approached asymptotically with time. Thus, at time plane 50, a profile which has larger gradients than the error function profile is desired.

One important observation to be made from Figure 12 is that the reduction of the value of ω alters the velocity profiles significantly. The solutions for the lower values of ω exhibit larger velocity gradients

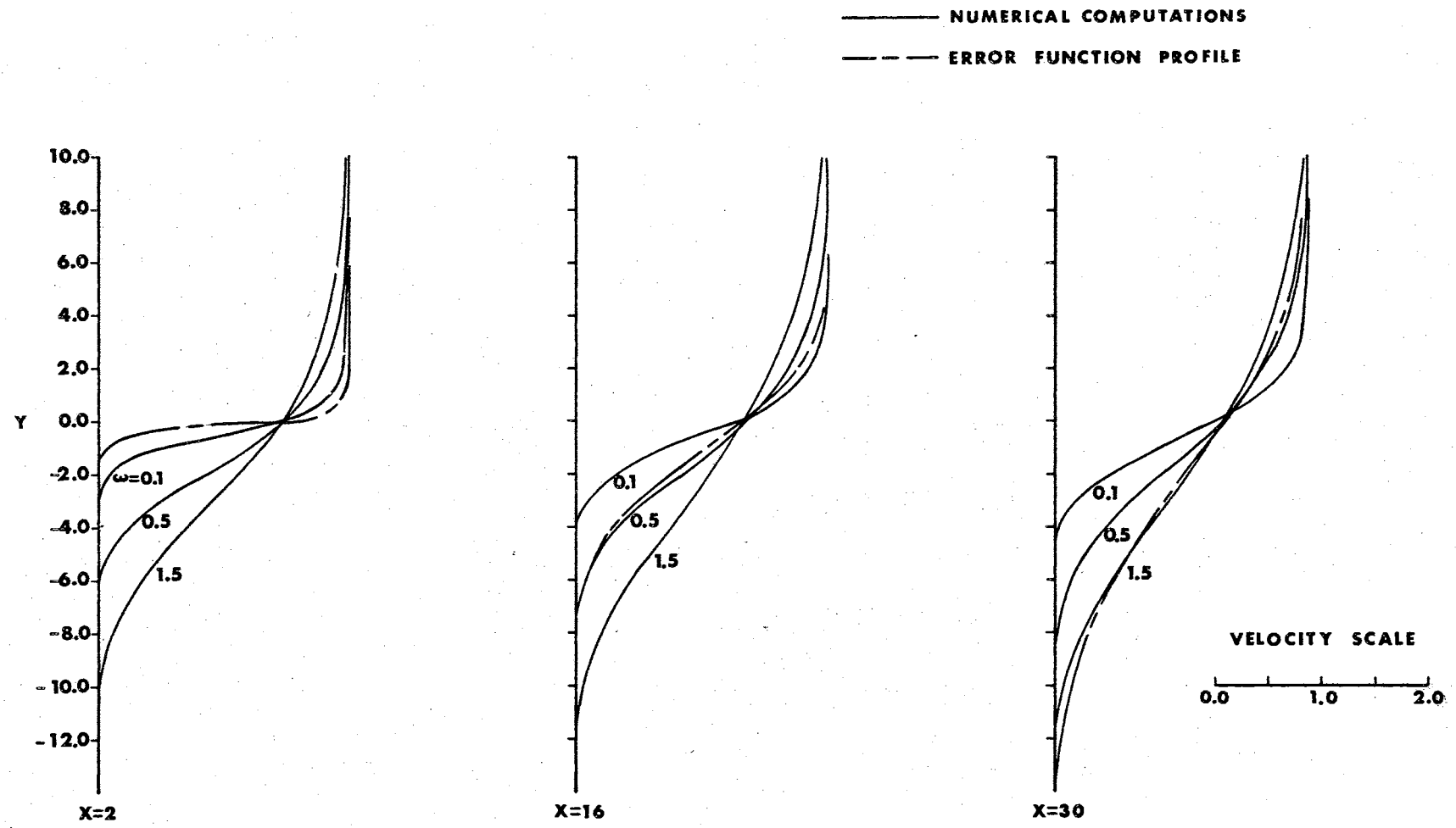

Figure 12. Velocity Profiles after Fifty Time Planes for Three Values of ω.

than do those for the larger values of ω. This is not unexpected, since the objective of the artificial terms is to blur gradients; and ω reflects directly the magnitude of the blurring terms. A second observation to be made from Figure 12 is that, for the lowest value of x, all the velocity profiles have been blurred to the extent that they are beyond that which should be attained as $t \rightarrow \infty$. Similarly, at $x = 16$ values of ω of 1.5 and 0.5 have caused too much blurring, whereas at $x = 30$ only the profile which corresponds to $\omega = 1.5$ has been blurred excessively. From these observations the following conclusions can be drawn: The effect of the blurring terms is to attenuate gradients, the amount of attentuation being a strong function of the magnitude of ω. The blurring of velocity gradients in the vicinity of a backstep ($x = 2$) is extensive, and thus raises a question as to the validity of the solution in these regions. Therefore the blurring terms cause an attenuation in gradients in addition to that caused by the turbulence effects. However, if the magnitude of ω can be maintained at a sufficiently low value, then for x sufficiently large, the turbulence effects will outweigh the effects due to the blurring terms.

For the turbulent mixing problem which will be discussed presently, it was found that the excessive blurring at small values of x could be reduced somehwat by applying additional constraints in the vicinity of the wall. One such constraint consists of dictating that the velocities in the neighborhood of the separation point be zero. Specificially, the velocities at the points (0,-1) and (1,-1) (See Figure 10) are required to maintain a zero value. The presence of this condition allows flow

separation to transpire in much the same manner as in nature. A second constraint, which retards the rate of artificial blurring, consists of assigning triple values to all variables along the $y = 0$ axis. For net points on the $y = 1$ line, the upper values of the variables at $y = 0$ are used in the computations; while for points on the $y = -1$ line, the lower values of the variables at $y = 0$ are used. For points which lie on the $y = 0$ axis, the mid-values of the variables are used. It was found that after computing approximately 50 time planes the triple values were identical, but the amount of artificial blurring had been reduced slightly.

Problem Description and Initial Conditions

For the two-dimensional, turbulent jet mixing problem, a Mach 2 jet issuing into a cavity was considered. Figure 13 shows schematically the configuration which was considered. The cavity was divided into three regions as shown in the figure. The thermodynamic and kinematic properties in region 1 were held constant for all times; and the properties in region 3 were set equal to those in region 1 as an assumed initial representation. The conditions in regions 2 and 3 were then allowed to vary according to the dictates of the computations.

Figure 14 shows the finite difference net which was used. A total of 1470 points are shown; however, because of symmetry, the number of points required for the mixing analysis was 756. Of course all 1470 points are necessary when a shock wave-mixing region interaction problem is considered.

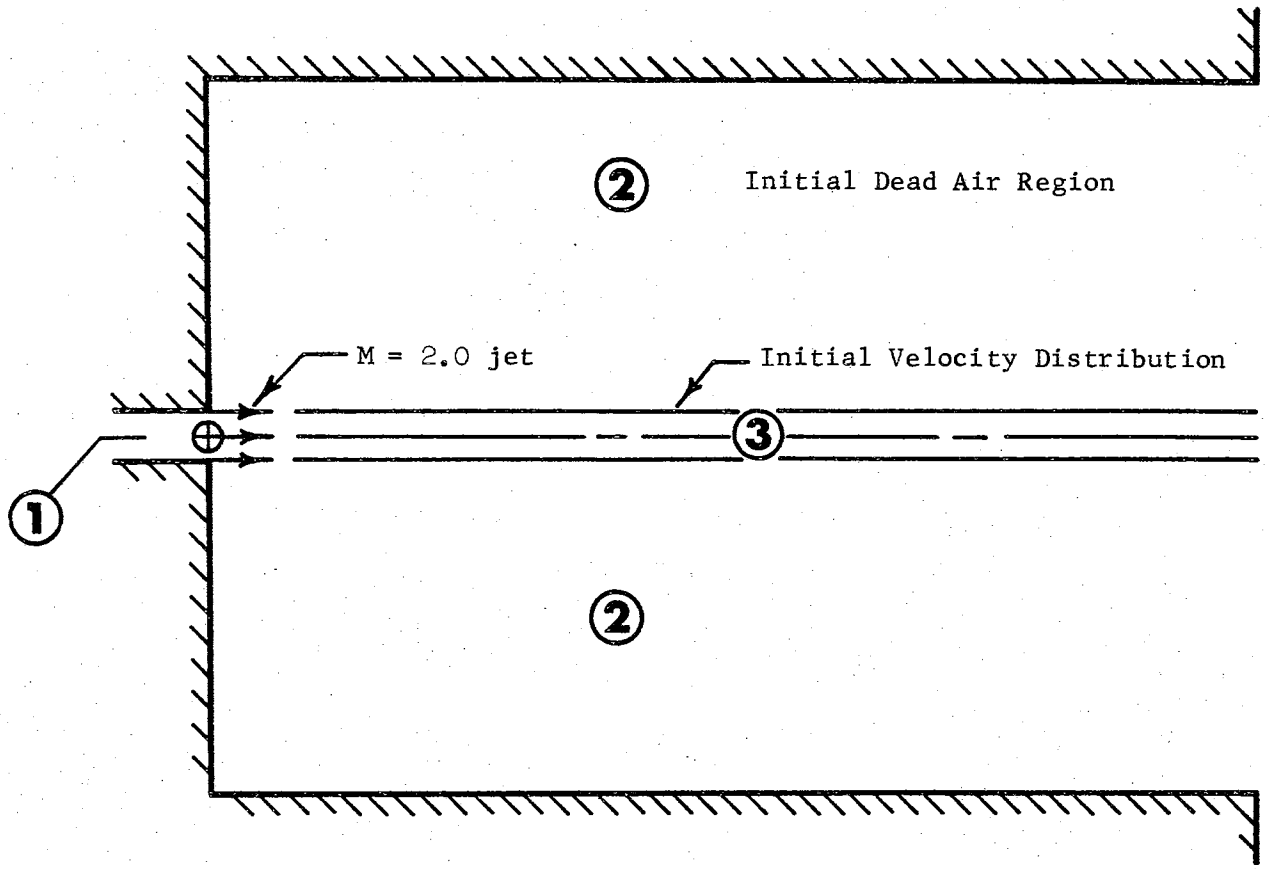

Figure 13. Geometry for Turbulent Mixing Problem.

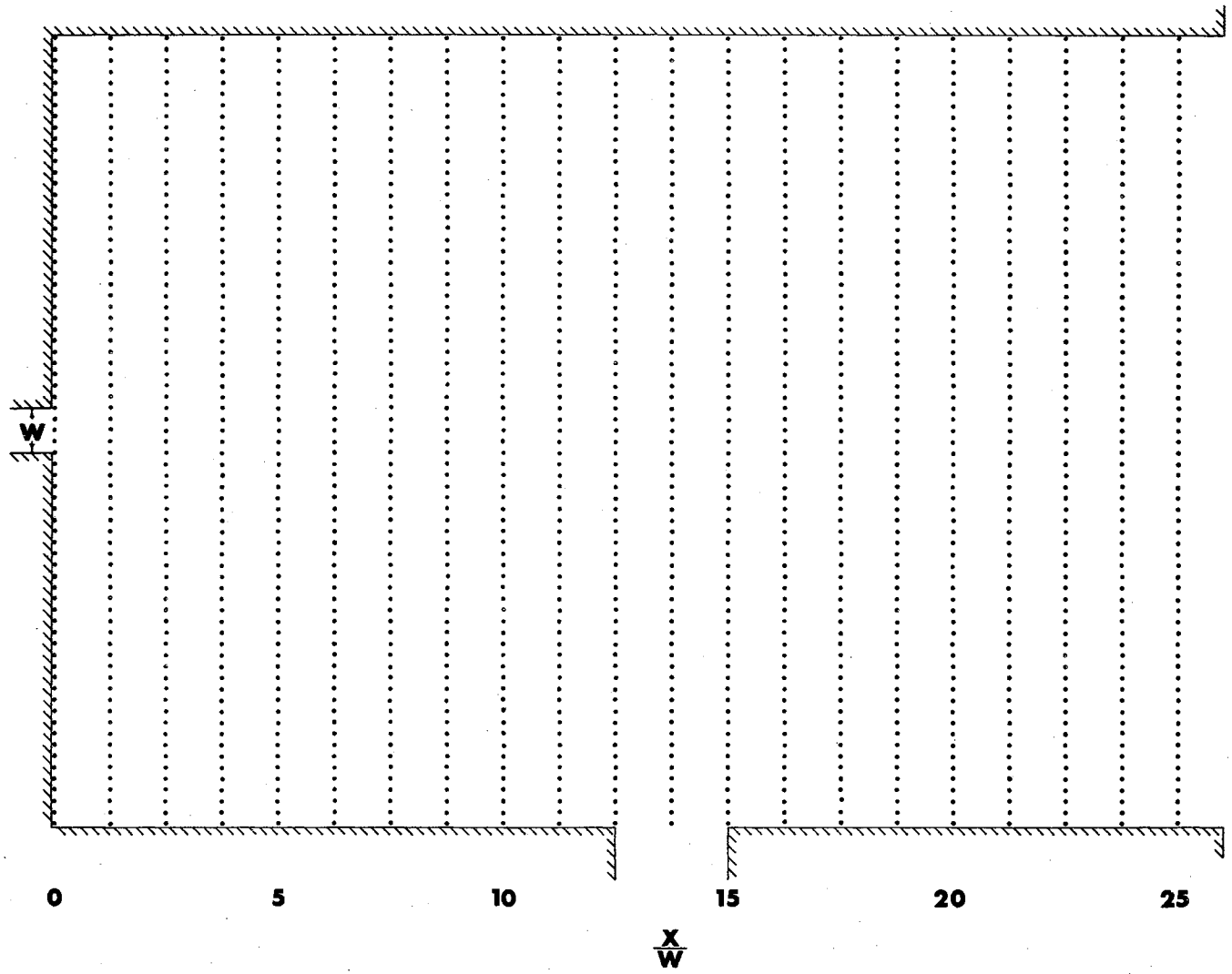

Figure 14. Finite Difference Net for Turbulent Mixing Problem and Shock Wave-Mixing Region Interaction Problem.

Table II presents the initial conditions for the turbulent mixing problem.

TABLE II

INITIAL CONDITIONS FOR TURBULENT MIXING PROBLEM

$\rho_1 = 1.0$	$\rho_2 = .5556$	$\rho_3 = 1.0$
$p_1 = 1.0$	$p_2 = 1.0$	$p_3 = 1.0$
$u_1 = 2.3664$	$u_2 = 0.0$	$u_3 = 2.3664$
$v_1 = 0.0$	$v_2 = 0.0$	$v_3 = 0.0$

$h_1 = 5.0$	$\gamma = 1.4$
$h_2 = 1.0$	$\bar{\sigma}_o = 0.5$
$\chi = 11.3099°$	$\omega = 0.25$

The value shown for the initial density in region 2 was obtained by assuming that the temperature in region 2 was equal to the stagnation temperature in region 1. Then, the equation of state was used to obtain $\rho_2 = 0.5556$.

Before the results of the computations for the turbulent mixing problem are presented, it will be advantageous to discuss the method whereby the non-dimensional computer results can be expressed in terms of physical dimensions.

Method for Dimensionalizing Computer Results

As noted previously, the method for non-dimensionalizing the variables p, ρ, u, and v is discussed in Appendix F. In order to determine the dimensional value which corresponds to one of these

four variables, one merely multiplies the non-dimensional quantity by its reference value; for instance

$$p^* = pp_R \ , \tag{6-3}$$

where the asterisk denotes the dimensional quantity and subscript R denotes the reference value.

The dimensionalization of the independent variable time is somewhat more involved than that of the dependent variables p, ρ, u, and v. The non-dimensional time increment over one time plane is, from equation (4-8)

$$\tau^n = \frac{h_1 h_2}{h} K^n \ , \tag{6-4}$$

where

$$K = \frac{\bar{\sigma}_o}{(w+c)_{max}} \ .$$

The total non-dimensional time is therefore

$$t = \sum^n \tau^n = \frac{h_1 h_2}{h} \sum^n K^n \ ,$$

or

$$t = \frac{h_1 h_2}{h} \sum^n \frac{\bar{\sigma}_o}{(w+c)_{max}} \ . \tag{6-5}$$

By using the definitions of h_1 and h (See Figure 4), equation (6-5) can be expressed as

$$t = h_2 \cos \chi \sum^{n} \frac{\bar{\sigma}_o}{(w+c)_{max}} . \qquad (6\text{-}6)$$

The expression for dimensional time will have the same form as (6-6) and can be written as

$$t^* = h_2^* \cos \chi \sum^{n} \frac{\bar{\sigma}_o}{(w^*+c^*)_{max}} . \qquad (6\text{-}7)$$

The dimensional mesh width h_2^* will be defined as

$$h_2^* = \frac{L}{Q} = \frac{\text{characteristic length in y-direction}}{\text{number of mesh spaces over L}} ;$$

and from Appendix F the dimensional velocities are

$$w^* + c^* = (w + c) \left[\frac{p_R^*}{\rho_R^*} \right]^{\frac{1}{2}} .$$

Equation (6-7) can therefore be expressed as

$$t^* = \frac{L}{Q} \frac{\sqrt{\gamma}}{c^*} \cos \chi \sum^{n} \frac{\bar{\sigma}_o}{(w+c)_{max}} , \qquad (6\text{-}8)$$

where

$$c^* = \left[\gamma \frac{p^*}{\rho^*} \right]^{\frac{1}{2}}$$

In correspondence with the notation adopted by Tyler (4), the time parameter η will be introduced, where

$$\eta = \frac{t^* c^*}{L} . \qquad (6\text{-}9)$$

Thus, equation (6-8) can be written as

$$\eta = \frac{\sqrt{\gamma}\cos\chi}{Q} \sum^{n} K^{n} . \qquad (6\text{-}10)$$

All of the problems which will be considered for the remainder of this investigation will be for the basic configuration shown in Figure 13. For these cases the characteristic length L will be taken to be the height of the backstep. From Figure 14, it can be seen that the number of mesh spaces for this height is 33. Therefore, for

$$\gamma = 1.4$$

and

$$\chi = 11.3099^{\circ} ,$$

equation (6-10) can be expressed as

$$\eta = 0.0351 \sum^{n} K^{n} , \qquad (6\text{-}11)$$

which applies only to the problems considered in this study.

Presentation of Results

As indicated previously, the reason for considering a simple mixing problem was to establish whether or not the numerical method would yield an accurate description of the mixing region. Since, for the shock interaction study, a reasonably steady state mixing region is necessary, one would expect the calculation of a large number of time planes to be required. This expectation was realized. It proved necessary to calculate 1000 time planes before an approximately steady

state condition was obtained. Even then, it would have been desirable to calculate still another 1000 time planes in order to assure that all perturbations had been damped. However, for the purposes of this study, 1000 time planes was sufficient; because, in the interaction study, the perturbations due to a passing shock wave were much larger than any perturbations in the system at time plane 1000.

The computations were performed with an IBM 7094 data processing system. For this system, it was possible to calculate one-hundred time planes of the mixing region problem (approximately one-half the finite difference net in Figure 14) in fifteen minutes.

Figure 15 shows the variation of the time parameter, η, with time plane. The variation is linear because for this problem $(w + c)_{max}$ always occurs in the constant property high velocity jet, region 1. Figure 16 shows the velocity profiles at time plane 800 for various values of $\frac{x}{w}$. For purposes of clarity, only selected values of $\frac{x}{w}$ have been presented. The lines of $\frac{u}{u_c} = 0.5$, where u_c is the local center-line velocity, have been determined and are indicated in the figure. The important observation to be made from Figure 16 is that a reverse flow region has been established in the upper and lower portions of the cavity. This condition agrees quite well with what is known to occur physically. The significant point to be made is that few mixing theories can account for the reverse flow even when only one velocity component is considered; however, the present theory has considered both velocity components and has successfully predicted the reverse flow phenomenon.

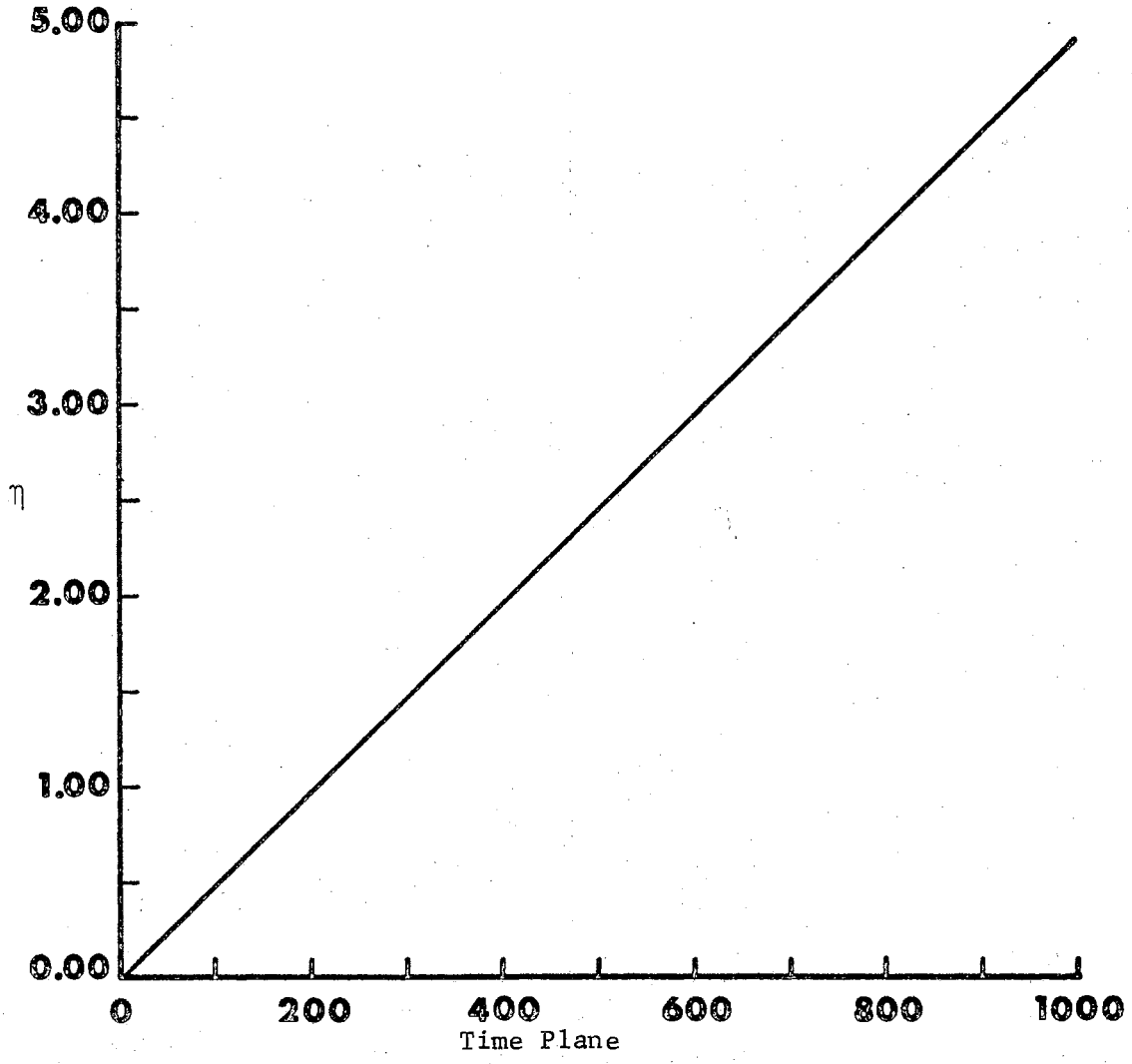

Figure 15. η Versus Time Plane for Turbulent Mixing Problem.

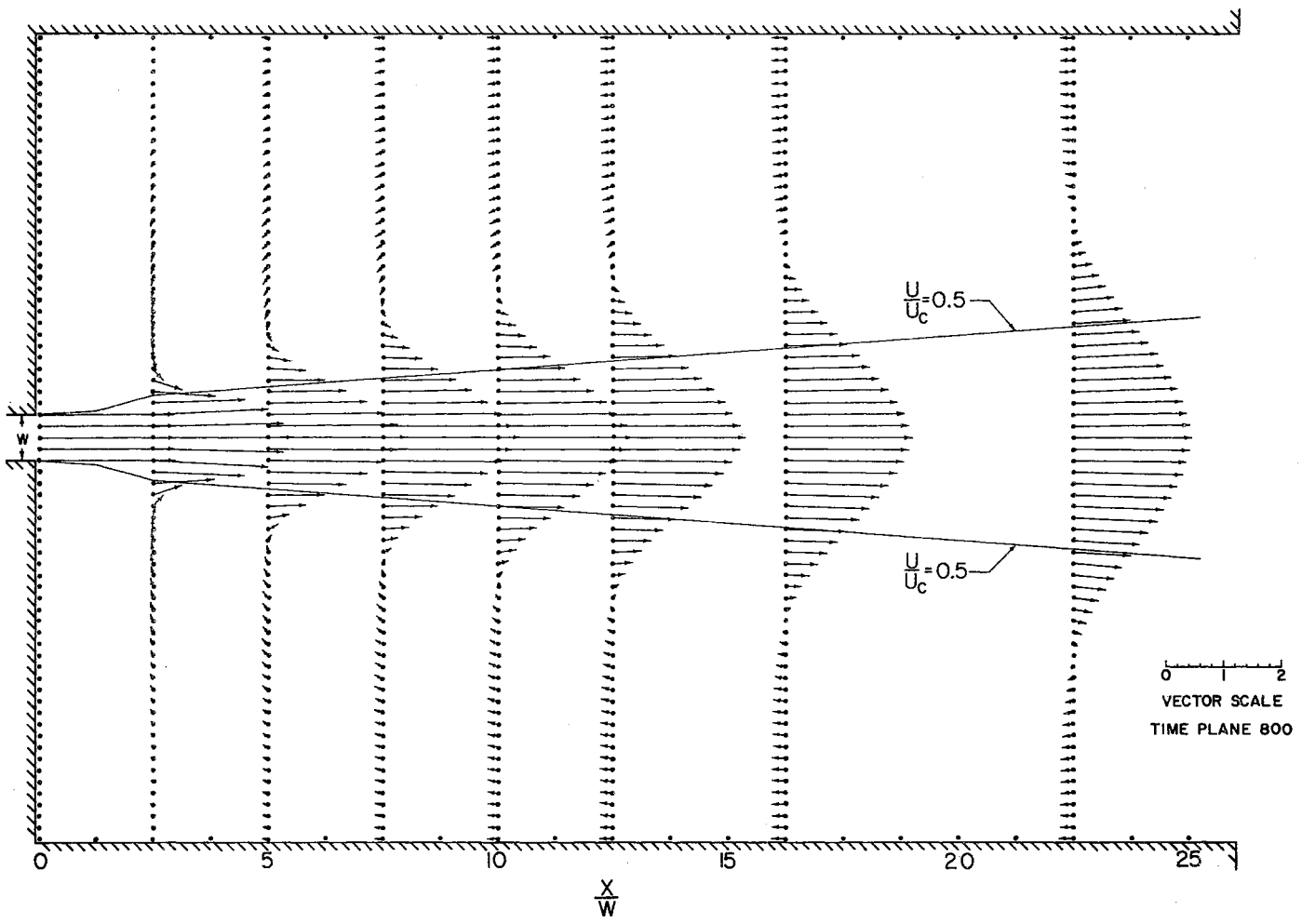

Figure 16. Velocity Vector Field for Turbulent Mixing Problem (n = 3.93).

Figure 17 shows the velocity profiles at time plane 1000. Once again the lines of $\frac{u}{u_c}$ = 0.5 are shown. The profiles at time planes 800 and 1000 are practically identical, differing by only a few per cent. Figure 18 presents the variation with time of $\frac{u}{u_c}$ = 0.5 lines. As one would expect, the lines vary rapidly for early times but seem to be approaching some asymptotic value at later times. Figure 19 is a crossplot of Figure 18 at two values of $\frac{x}{w}$ and verifies that the lines of $\frac{u}{u_c}$ = .5 are indeed approaching some limiting value asymptotically. Furthermore, between time planes 800 and 1000 (η = 3.93 and 4.90), the $\frac{u}{u_c}$ = 0.5 lines change only about 1.5 per cent at $\frac{x}{w}$ = 10 and 1.0 per cent at $\frac{x}{w}$ = 22. Thus, Figure 19 indicates that, for engineering purposes, a steady state has been attained. Further verification of this conclusion is indicated in Figure 20, which depicts the growth of the horizontal components of velocity with time. For the lower values of $\frac{x}{w}$ it appears that the profiles attain their ultimate shape rather quickly. However at the larger value of $\frac{x}{w}$ ($\frac{x}{w}$ = 22.5) the profile is still changing somewhat, the greatest change occurring at the centerline. Though not indicated in Figure 20, the change in centerline velocity from time plane 800 to time plane 1000 is about 3 per cent. Therefore once again, one can conclude that, for all practical purposes, a steady state condition exists after the calculation of 1000 time planes.

Figure 20 also shows a comparison between the horizontal velocity profiles obtained from the present theory, and those which would be predicted for a Gaussian distribution. The Gaussian profile is obtained from the expression

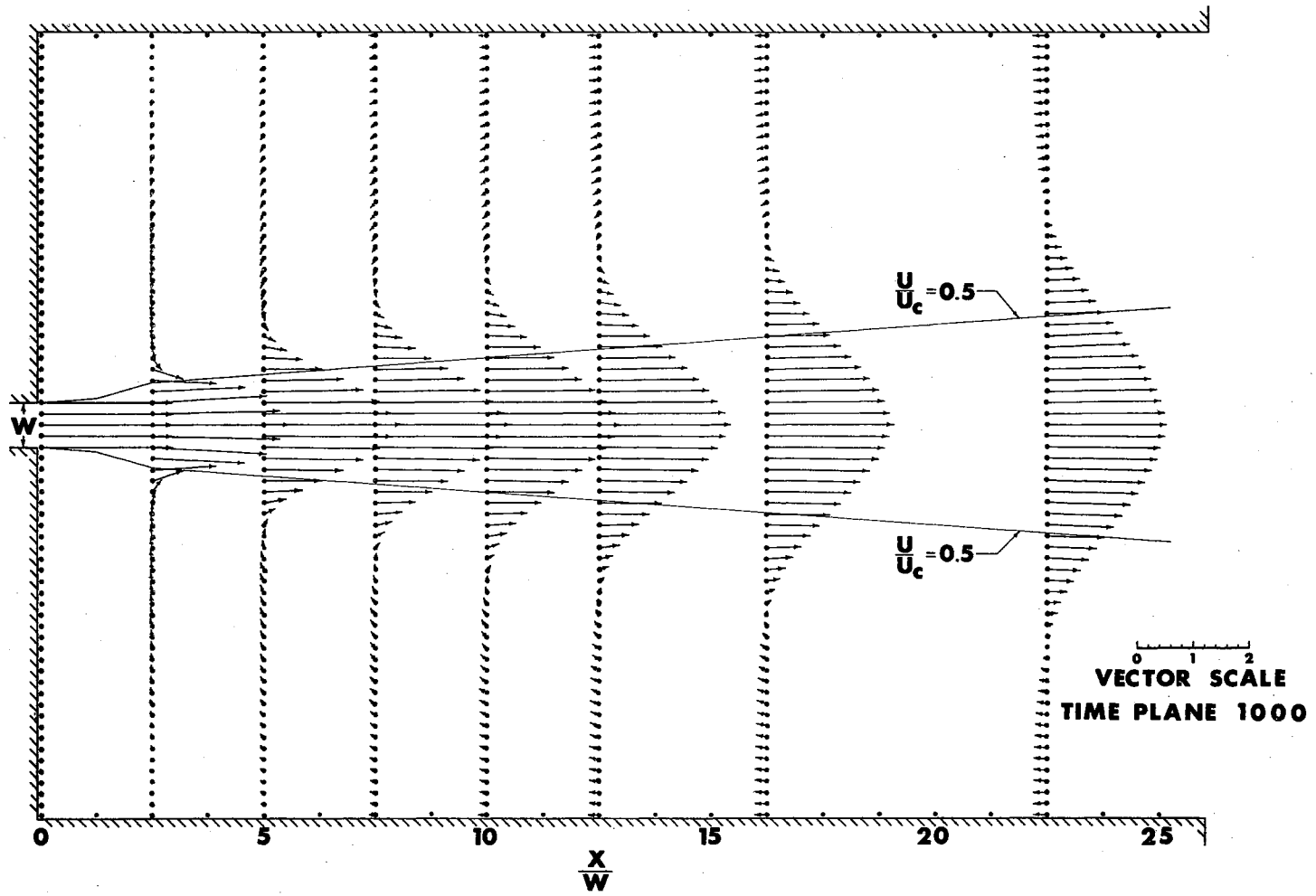

Figure 17. Velocity Vector Field for Turbulent Mixing Problem (n = 4.90).

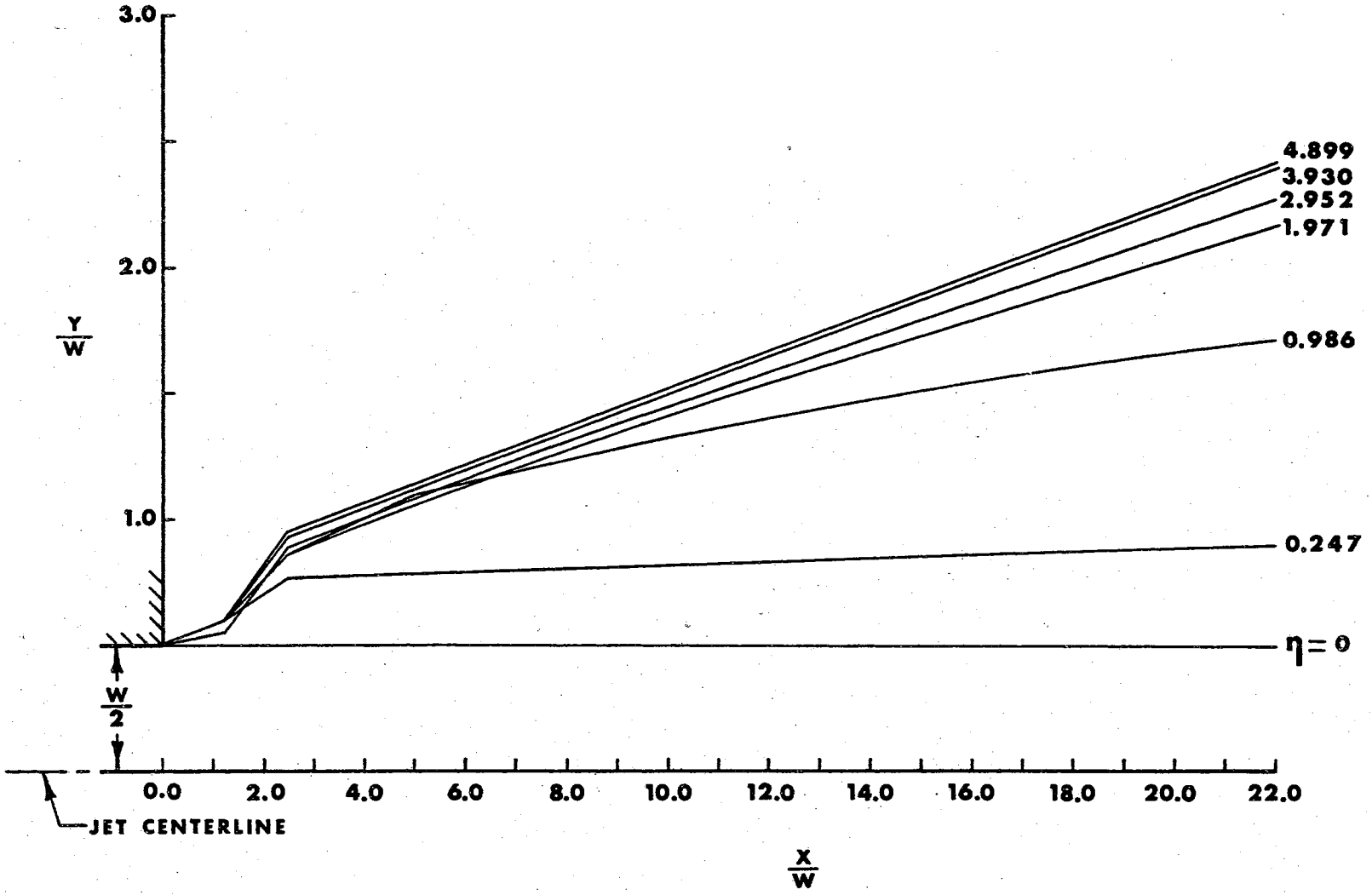

Figure 18. Growth of $\frac{u}{u_c} = 0.5$ Lines with Time.

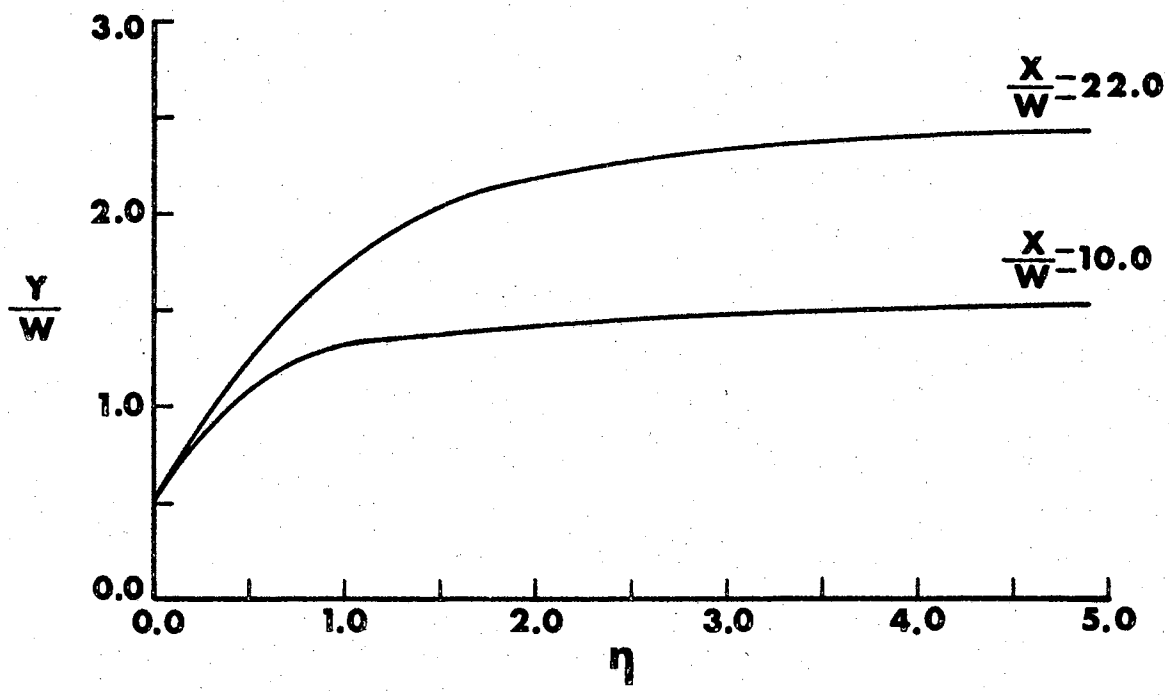

Figure 19. Crossplot of $\frac{u}{u_c} = 0.5$ Lines for Two values of $\frac{x}{w}$.

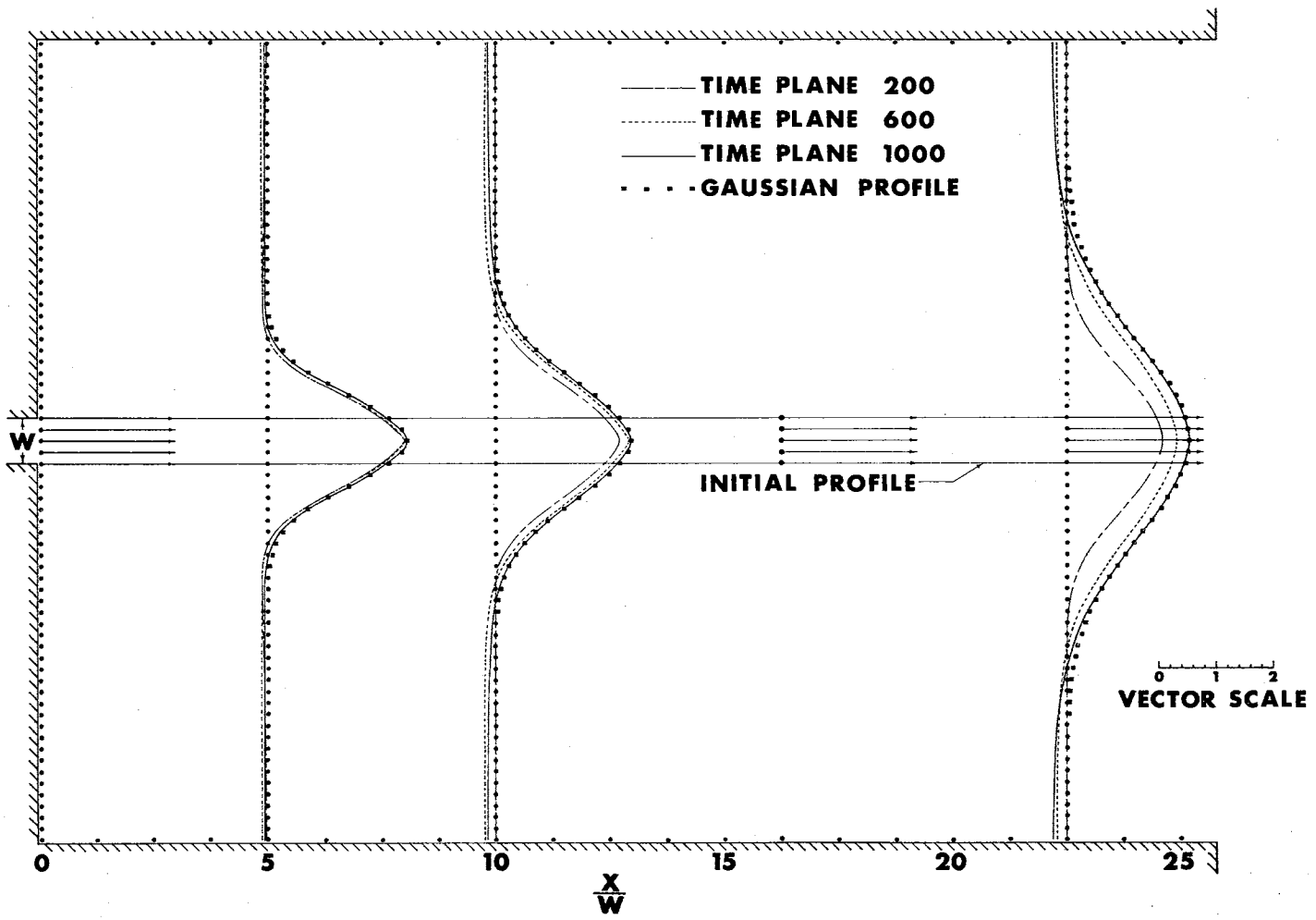

Figure 20. Development of Horizontal Velocity Components with Time.

$$\frac{u}{u_c} = \exp\left[-.693 \left(\frac{y}{y_*} \right)^2 \right], \qquad (6\text{-}12)$$

where y_* is the position where $\frac{u}{u_c} = 0.5$ occurs (28). Equation (6-12) has been shown by Olsen and Miller (28) to compare almost perfectly with experiment except for the low velocity regions. The reason for the failure of the Gaussian profile in the low velocity regions is obvious from equation (6-12); it cannot predict reverse flows and can only approach zero asymptotically. Therefore the second, and possibly most important, observation to be made from Figure 20 is that the present theory predicts profiles which agree well with the experimentally verified Gaussian profiles. The present theory therefore provides a method which is preferable; because it not only accounts for both the horizontal and vertical velocity components, but also because it is capable of predicting the reverse flow phenomenon for confined jets.

Figure 21 shows lines of constant pressure which occur in the cavity at time plane 1000 ($\eta = 4.90$). The pressure map shows, as did the velocity vector plots (Figures 16 and 17), that the jet has not attached to the cavity walls. If this condition had occurred, a reattachment shock would have been indicated and the pressure in the separated flow region would have dropped to approximately 0.35 (14).

From the results which have been presented in this chapter, two very important conclusions can be drawn. First, a reduction in the magnitude of the blurring terms will permit the numerical solution to describe a physically realistic turbulent mixing region. Second, even though large computer times are required, the fact that a steady state

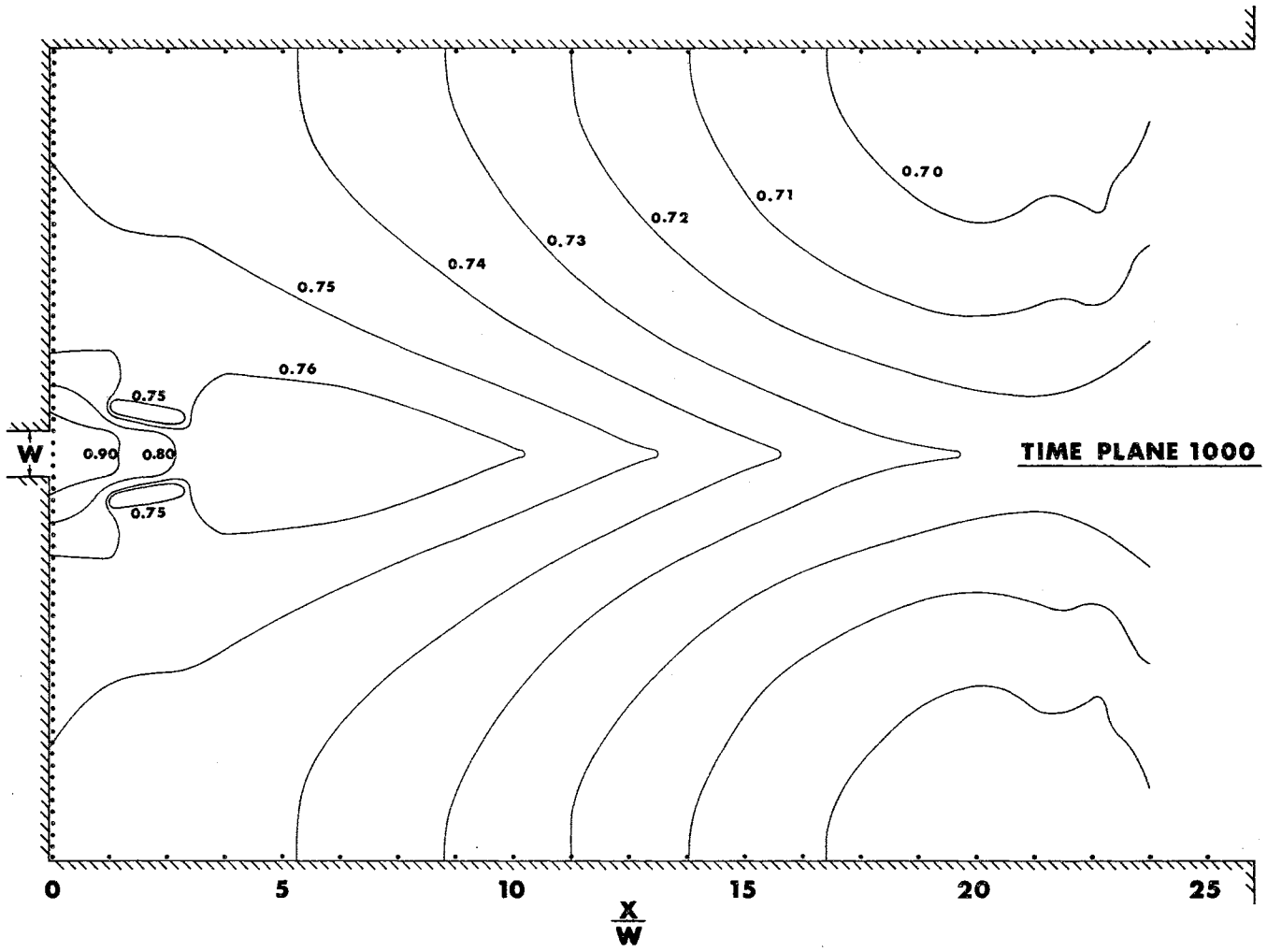

Figure 21. Constant Pressure Lines for Turbulent Mixing Problem (η = 4.90).

mixing region has been described implies that this numerical method holds great promise for the solution of complicated turbulent boundary layer and jet mixing problems which have heretofore evaded rigorous analysis. In fact, there appears to be no reason for suspecting that the method cannot be applied to the laminar hydrodynamic equations, and thus become applicable to laminar boundary layer and jet mixing problems as well.

CHAPTER VII

PASSAGE OF A SHOCK WAVE ACROSS THE TURBULENT MIXING REGION

As indicated in Chapter I the primary objective of this study is to provide an analysis which is capable of predicting the interaction between a moving shock wave and a turbulent mixing region. Jackomis (2) has shown that the artificial viscosity method will produce results which agree with available experimental data for the case of a shock wave passing over a body at rest. This method has been used in the current investigation and is assumed to be adequate for handling the shock propagation aspects of the present problem. The major question which has needed resolution was whether the presence of blurring terms would prohibit the correct description of a steady state mixing region. The results which were presented in Chapter VI have enabled this question to be answered. There it was noted that if the magnitude of the blurring terms can be restricted to sufficiently small values, then the numerical solution can describe a mixing region which shows excellent agreement with a theory which has been verified experimentally.

Thus, the final step in this analysis is to introduce a moving shock wave into the steady state flow field which was presented in Chapter VI, and then to trace its progression as it moves across the mixing region. Figure 22 shows the configuration and nomenclature for the problems to be considered, and Figure 14 shows the finite difference

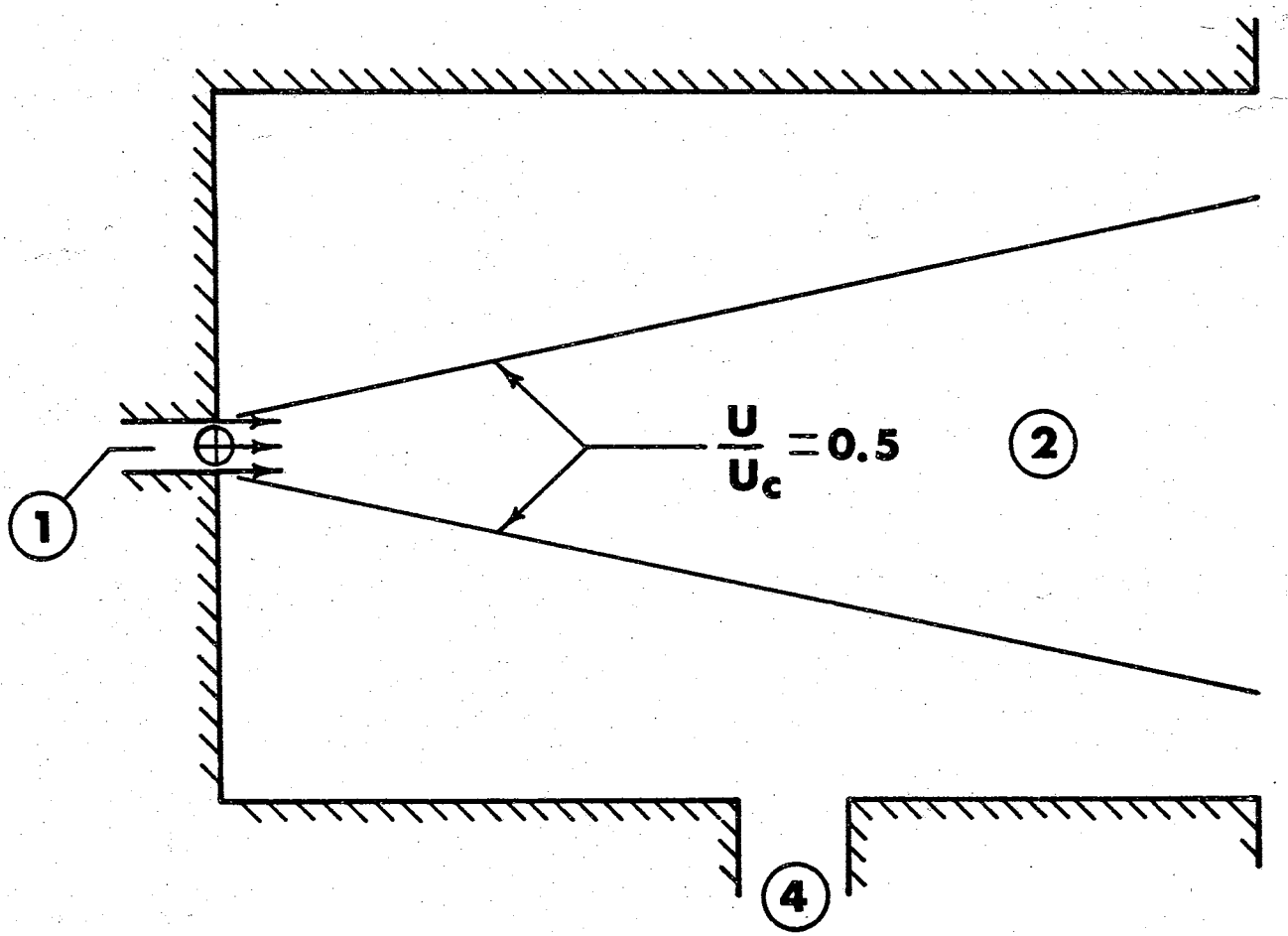

Figure 22. Geometry for Shock-Mixing Region Interaction.

net. A shock tube has been placed in the side of the cavity which was considered in Chapter VI. The shock tube will be denoted as region 4 and the invariant portion of the Mach 2 jet as region 1. Region 2 is the entire flow field which, as indicated earlier, was obtained after the calculation of 1000 time planes.

For the shock wave-mixing region interaction study two primary cases have been considered. The first case, hereafter referred to as the weak shock case, corresponds to the stagnation pressure ratio $\frac{p_{o4}}{p_{o1}} = 0.615$; and the second case, the strong shock case, corresponds to the stagnation pressure ratio $\frac{p_{o4}}{p_{o1}} = 3.53$. These two cases were chosen because it has been indicated (4) (7) that the interaction of two fluid streams is strongly dependent upon the ratio of their stagnation pressures.

In addition to the two shock-mixing region interaction cases, two other problems were computed. These correspond to the weak and strong shock cases, but are without the free jet. The purpose of these computations was to allow the comparison of shock wave profiles both with and without the presence of the mixing region; thus allowing the effects of the mixing region on the shock wave to be studied.

Initial Conditions

Table III shows the initial conditions for both the weak shock and the strong shock cases. For each case the initial shock wave was described over two mesh widths by the method suggested by Tyler (4).

TABLE III

INITIAL CONDITIONS FOR SHOCK WAVE-MIXING REGION INTERACTION CASES

Properties	Weak Shock Case	Strong Shock Case
p_1	1.00	1.00
ρ_1	1.00	1.00
u_1	2.3664	2.3664
v_1	0.0	0.0
p_{o1}	7.83	7.83
p_2	Properties Describing Steady State Mixing Region	
ρ_2		
u_2		
v_2		
p_4	2.84	8.54
ρ_4	1.103	1.790
u_4	0.0	0.0
v_4	1.709	3.649
p_{o4}	4.82	27.6
h_1	5.0	5.0
h_2	1.0	1.0
χ	11.3099°	11.3099°
γ	1.4	1.4
$\bar{\sigma}_o$	0.5	0.3
ω	0.5	1.50

Table IV shows the initial conditions for the weak shock and strong shock cases without the mixing region. The values of pressure and density in region 2 were obtained by taking the average of the pressures and densities over the entire field of the mixing region computations at time plane 1000.

TABLE IV

INITIAL CONDITIONS FOR SHOCK WAVE PROPAGATING INTO STILL MEDIUM

Properties	Weak Shock Case	Strong Shock Case
p_1	1.00	1.00.
ρ_1	1.00	1.00
u_1	0.0	0.0
v_1	0.0	0.0
p_2	0.725	0.725
ρ_2	0.45	0.45
u_2	0.0	0.0
v_2	0.0	0.0
p_4	2.84	8.54
ρ_4	1.103	1.790
u_4	0.0	0.0
v_4	1.709	3.649
h_1	5.0	5.0
h_2	1.0	1.0
χ	11.3099°	11.3099°
γ	1.4	1.4
$\bar{\sigma}_o$	0.5	0.3
ω	0.5	1.50

Presentation of Results

For this phase of the investigation time plane zero will correspond to time plane 1000 of the mixing region computations. Figure 23 shows the variation of the time parameter η with time plane for the weak shock condition. The graph is applicable to the cases both with and without the jet. Figure 24 shows a similar graph for the strong shock condition.

The major portion of the results of the computations for this chapter, Figures 34 through 56, are presented in graphical form in Appendix A. For both shock wave cases, velocity vector plots and graphs of constant pressure lines are presented for various stages in the progression of a wave across the mixing region. Approximate shock wave positions have been indicated by dashed lines on the pressure maps and velocity vector plots. These wave positions have been determined by taking the midpoint of the steepest pressure gradient in a concentrated pressure rise region.

Figure 25 shows, for the weak shock case, the position of the wave at various time planes as it progresses across the cavity. The shock wave positions without the jet are indicated by the solid lines. Figure 26 shows the wave positions for the strong shock case. Two interesting observations can be made from these two figures. First, for both the weak and the strong shock cases, the wave is definitely retarded when it encounters the mixing region; the amount of retardation being greater in regions where the wave advances in a direction opposite to that of the oncoming jet. Second, for the weak shock case the wave profile is significantly altered; whereas for the strong shock case, the profile

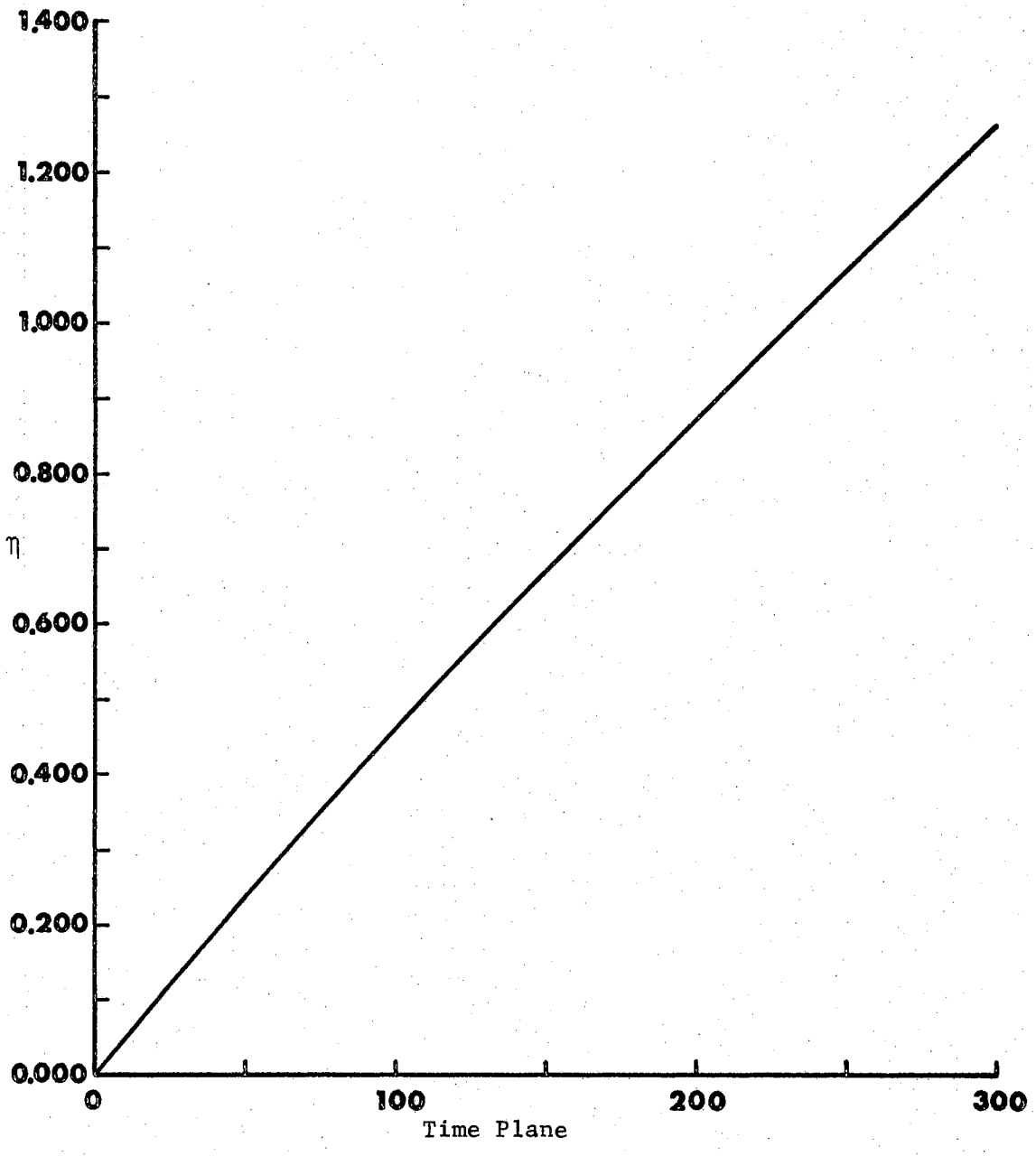

Figure 23. η Versus Time Plane for Weak Shock Case--with and without Jet.

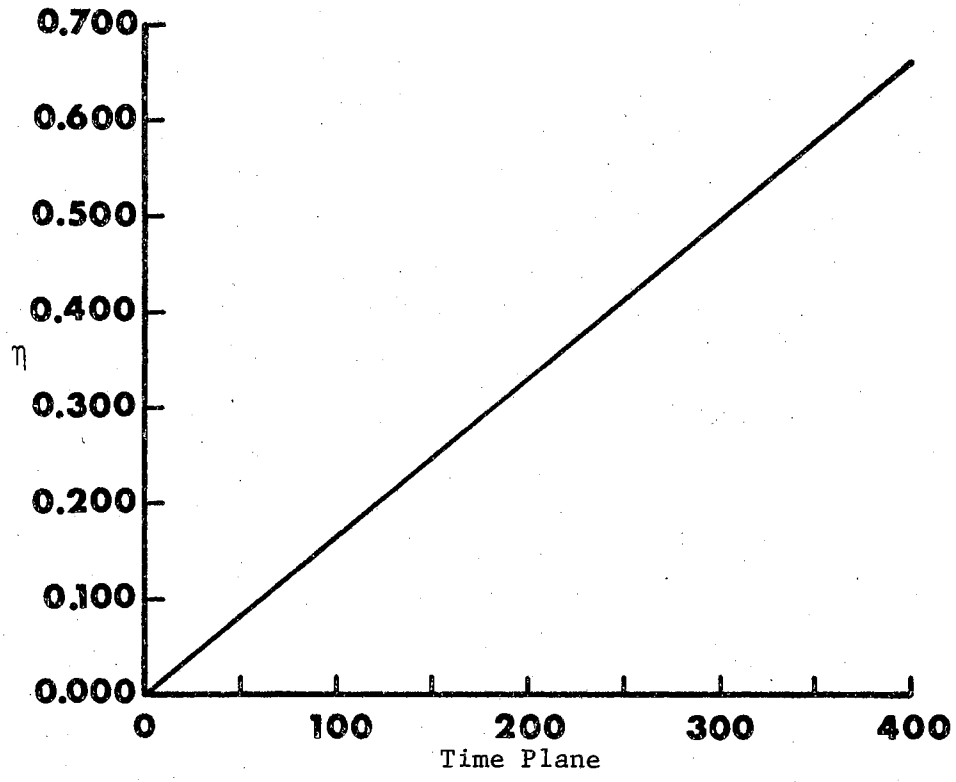

Figure 24. η Versus Time Plane for Strong Shock Case--with and without Jet.

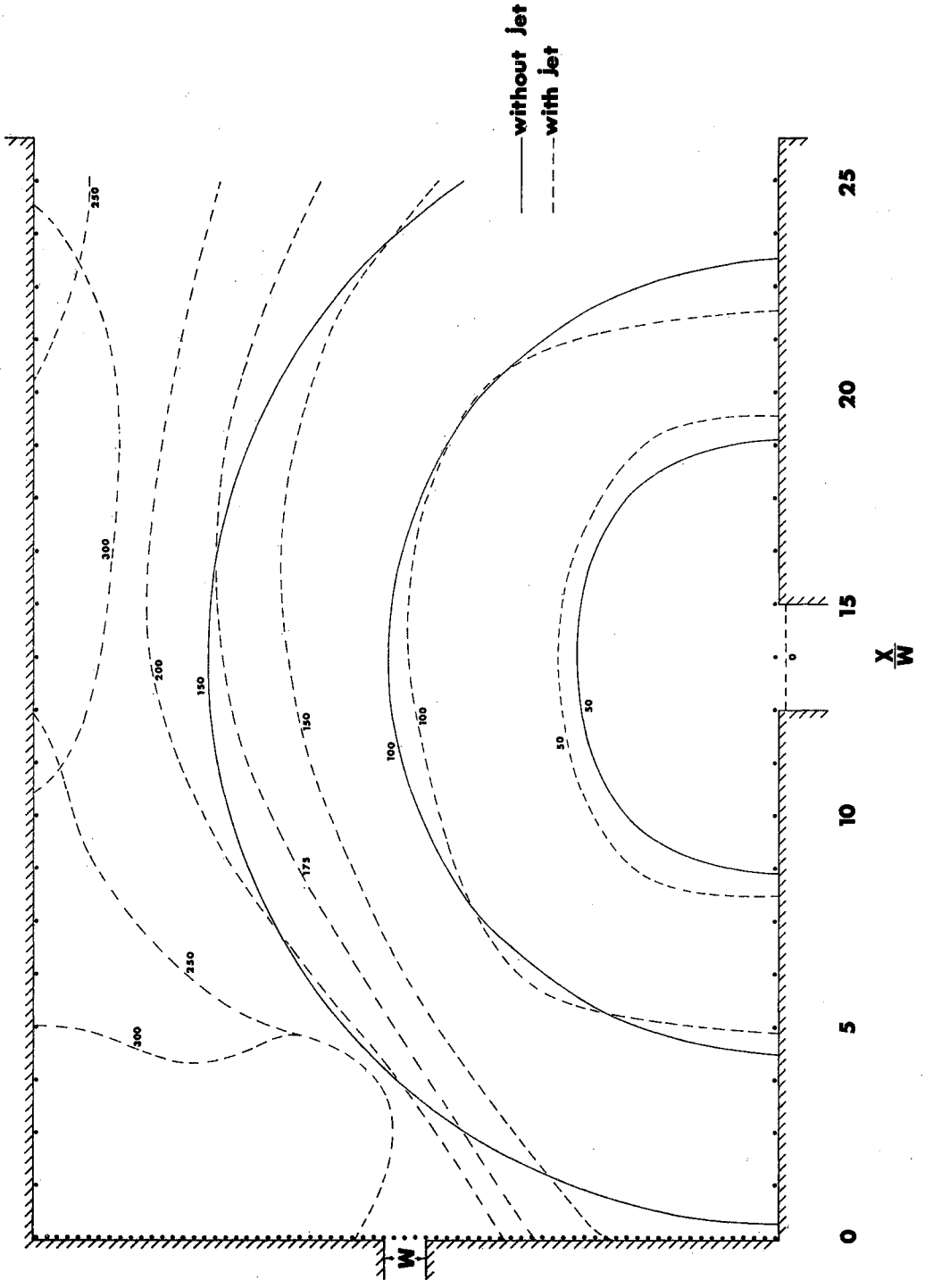

Figure 25. Wave Position with Time for Weak Shock Case.

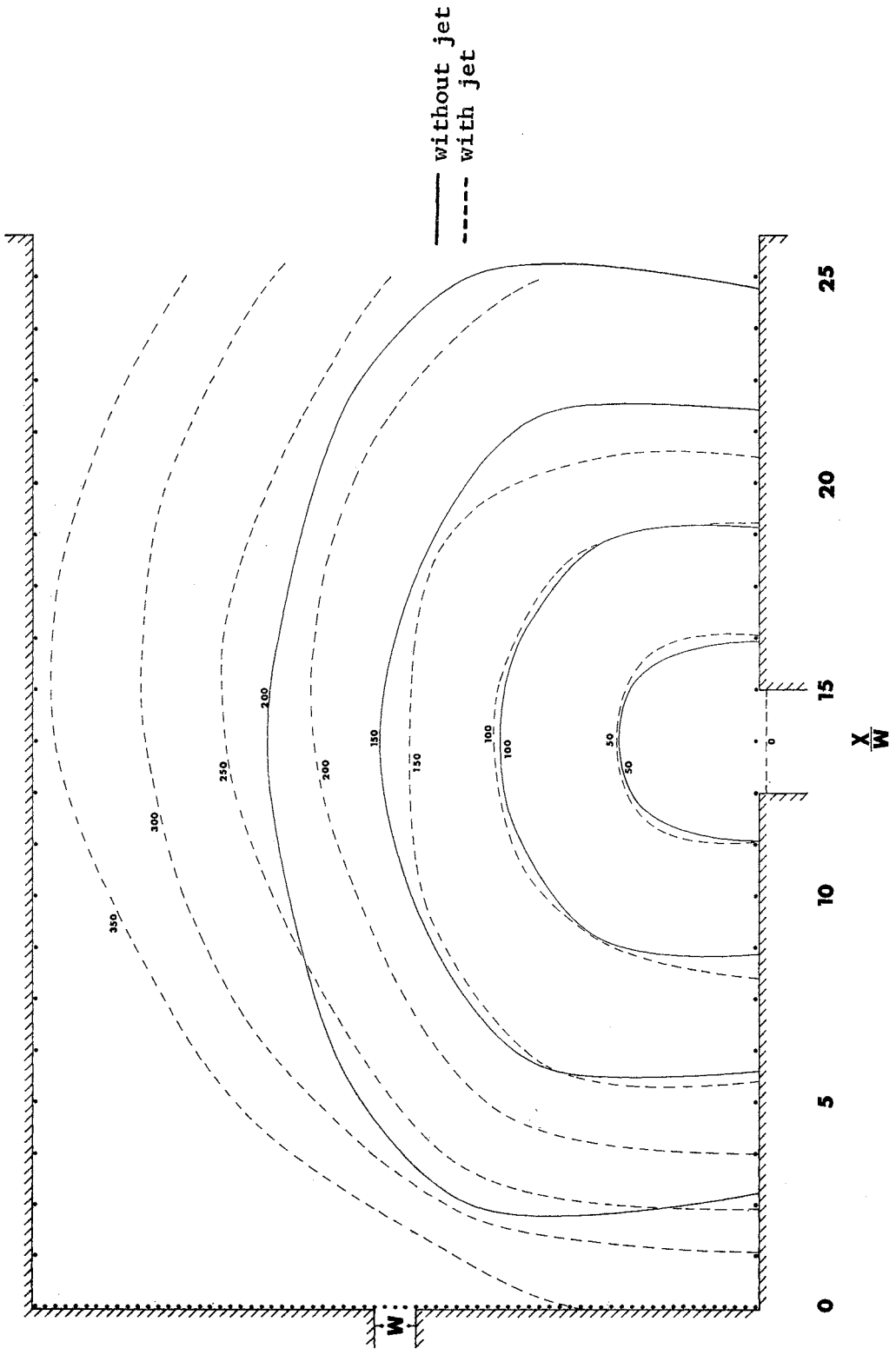

Figure 26. Wave Position with Time for Strong Shock Case.

is altered only slightly. This fact has been verified by making use of the hydraulic analogy. Plate I shows the apparatus which was used. It consists of a water table which has been equipped with a converging-diverging section capable of operating at Froude two conditions. A quick-release channel has been placed in the side of the cavity, thus allowing the water table geometry to be of the same type (but with a wider shock tube) as the geometry shown in Figure 22. Plate II shows a wave, which corresponds to the weak shock case, without the jet, emerging into the cavity. The wave profile agrees with that which has been obtained from the numerical solution (Figure 25). Plate III represents the weak shock condition for the case with the jet. The first frame shows the established mixing region before the wave has begun to emerge from the shock tube. Aluminum powder was used in order to enable the mixing region to be seen more clearly. As was indicated from the results of the numerical computations (Figure 25), the wave is seen to be both retarded and altered in profile as it proceeds through the mixing region. Though not readily apparent from Plate III, it was observed, during the water table study, that the wave actually increased in intensity beforeit proceeded through the high velocity portion of the mixing region. This is attributed to the fact that as the wave is retarded, the continual addition of mass and momentum from the shock tube causes the pressure behind the wave to increase. Thus, the pressure ratio across the wave is increased beyond that which it would otherwise have if the mixing region were not present. Therefore, it appears that even if the initial wave is not of sufficient magnitude to negotiate the mixing region, the increase in pressure due

PLATE I

WATER TABLE ARRANGEMENT FOR THE STUDY OF A SHOCK WAVE INTERACTING WITH A JET MIXING REGION

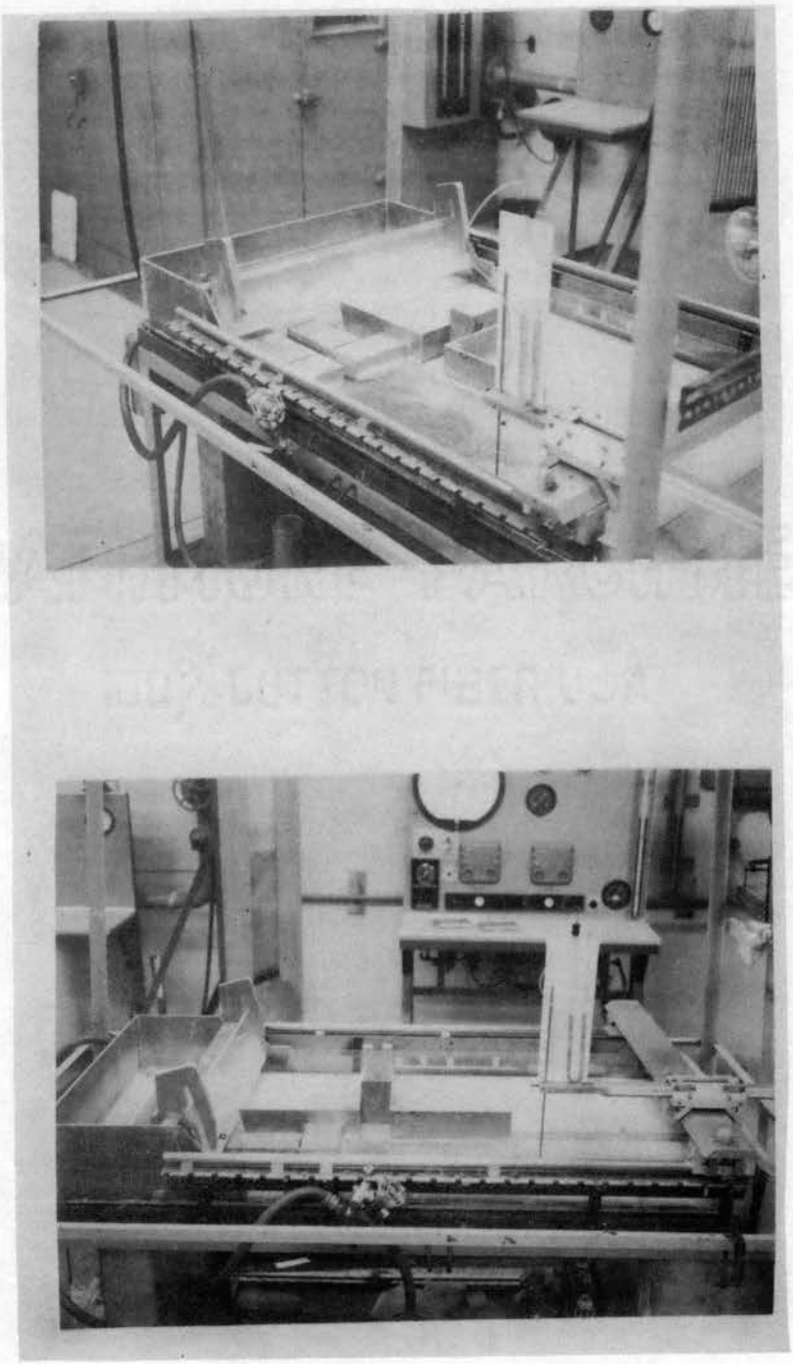

PLATE II

WATER WAVE (CORRESPONDING TO WEAK SHOCK CASE)
EMERGING INTO CAVITY WITHOUT JET


1

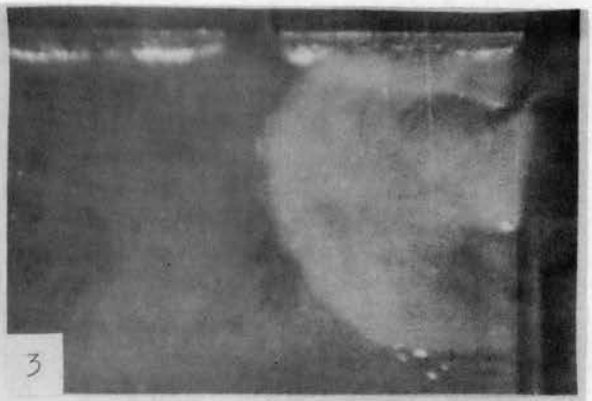
3

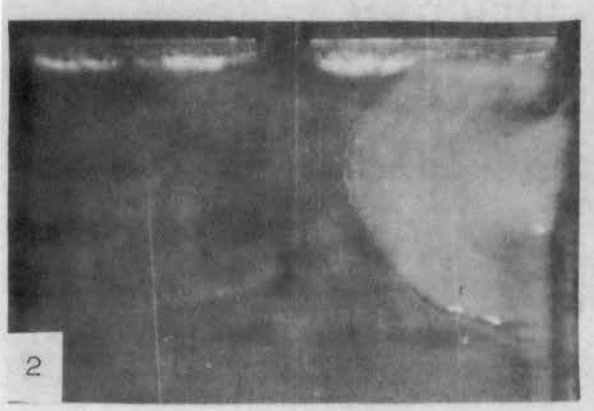
2


4

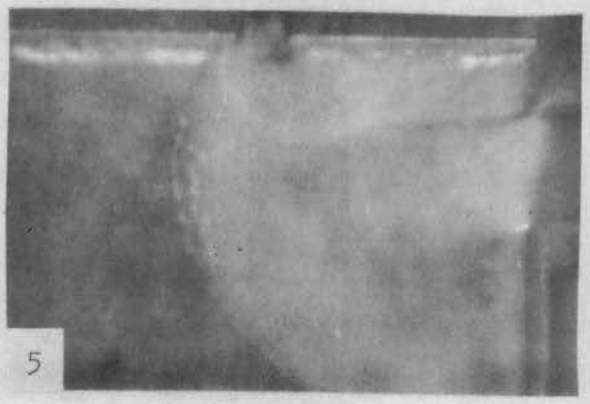
5

PLATE III

WATER WAVE (CORRESPONDING TO WEAK SHOCK CASE)
EMERGING INTO CAVITY WITH JET

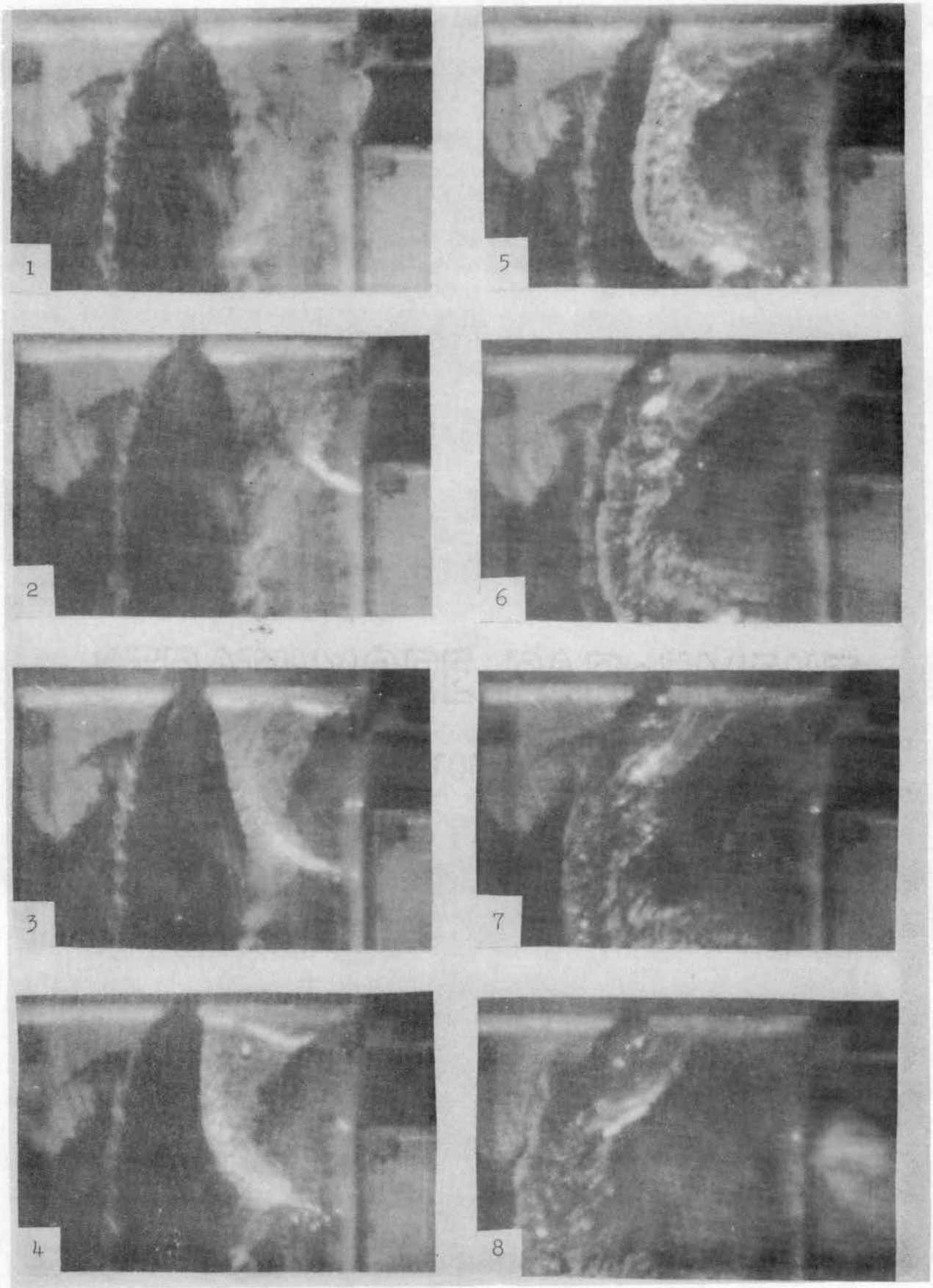
1
5
2
6
3
7
4
8

to the mass addition can provide the necessary impetus to drive the wave across. This observation has been substantiated from the numerical results and will be pointed out later.

Plate IV shows the wave emerging into the cavity without the jet for the strong shock case. Plate V shows the strong shock case with the jet. In comparing Plates IV and V it appears that the wave profile is changed only slightly because of the mixing region. The most noticeable change occurs in the vicinity of the jet. This substantiates the comment made earlier concerning Figure 26. Because of the larger wave velocity associated with the strong shock case, the pressure increase effect behind the wave was not noted during the water table study. However, as will be discussed later, the numerical results indicate a slight increase in the shock strength when the wave encounters the mixing region; but not as great an increase as for the weak shock case.

Figures 27 and 28 are crossplots from Figures 25 and 26 and show the computed shock positions with time along three rays which emanate from the intersection of the shock tube centerline and the cavity wall. For both the weak shock and the strong shock cases the shock wave is retarded first along ray 2 and later along rays 1 and 3. However, ultimately the wave experiences the most retardation along ray 1 with ray 2 being retarded less and ray 3 the least of all. As was observed in conjunction with Figures 25 and 26, the wave for the weak case experiences more retardation on the whole than does the wave for the strong shock case.

PLATE IV

WATER WAVE (CORRESPONDING TO STRONG SHOCK CASE)
EMERGING INTO CAVITY WITHOUT JET

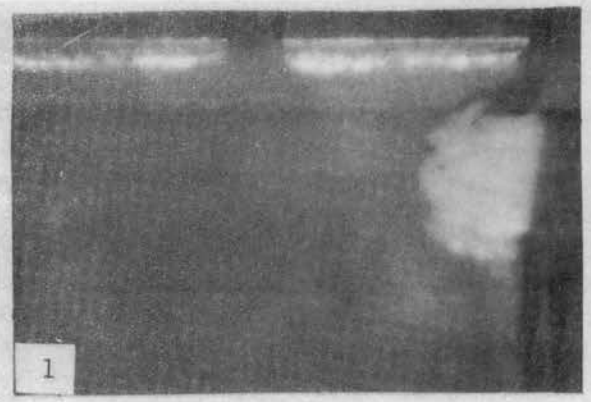
1


5

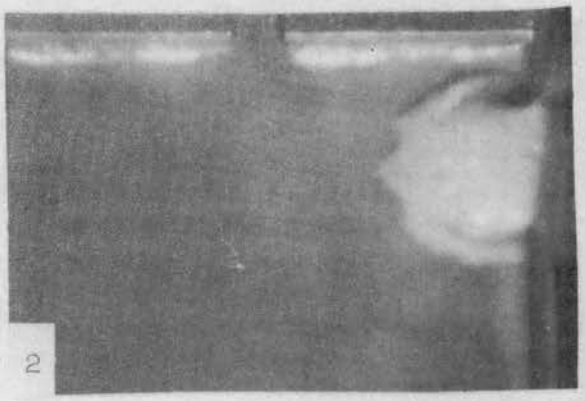
2


6


3

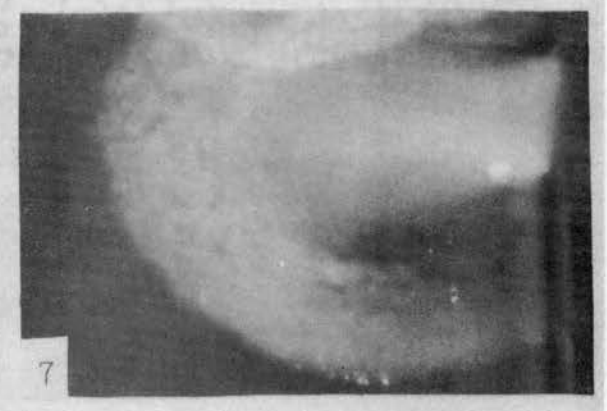
7

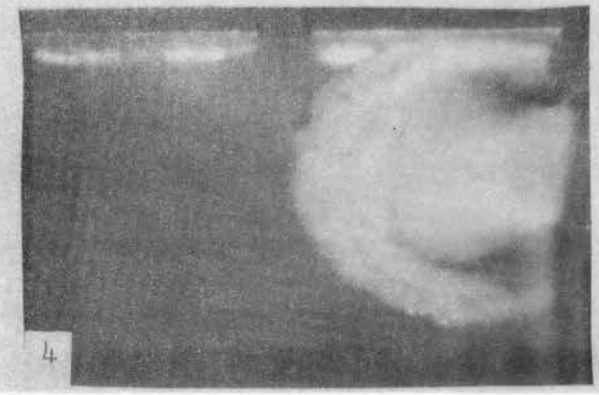
4

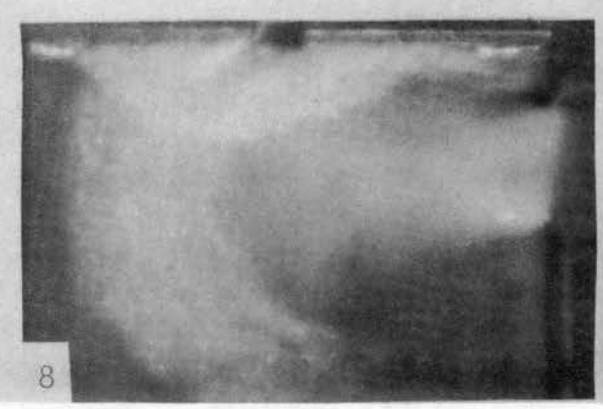
8

PLATE V

WATER WAVE (CORRESPONDING TO STRONG SHOCK CASE)
EMERGING INTO CAVITY WITH JET


1

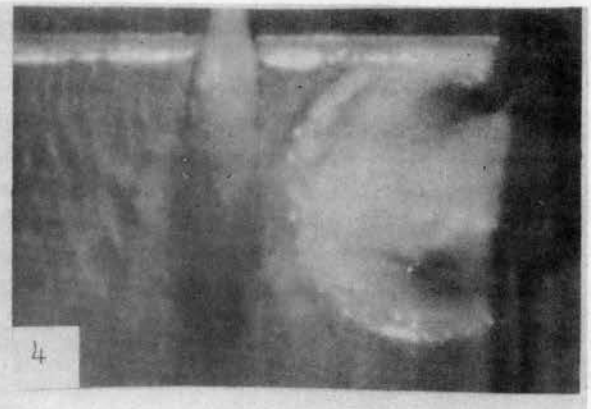
4

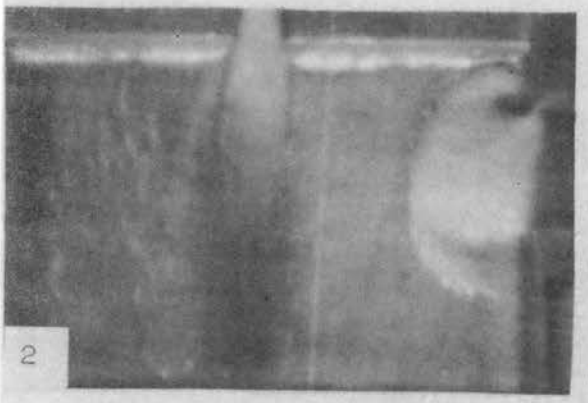
2


5


3


6


7

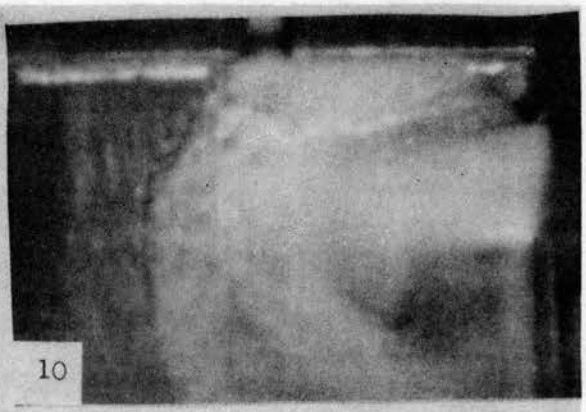
10

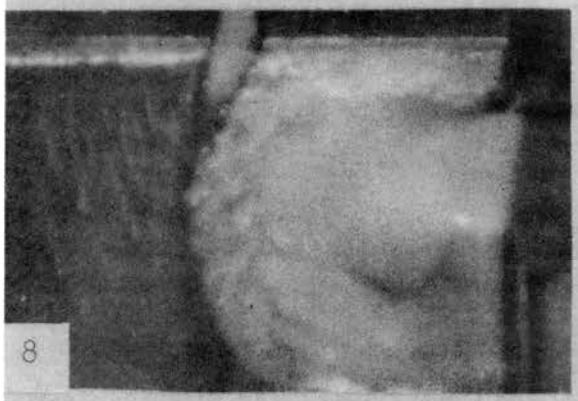
8

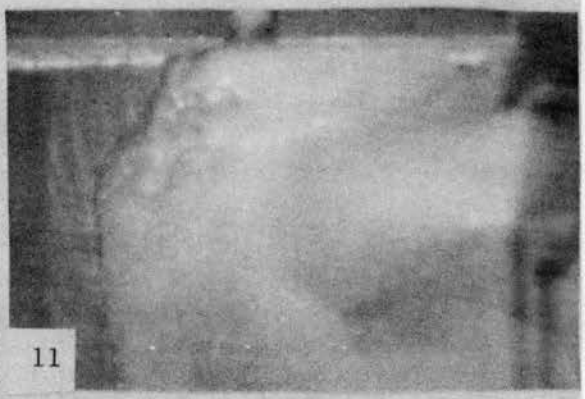
11

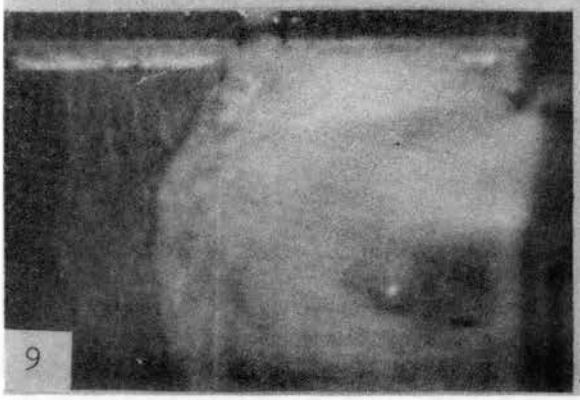
9

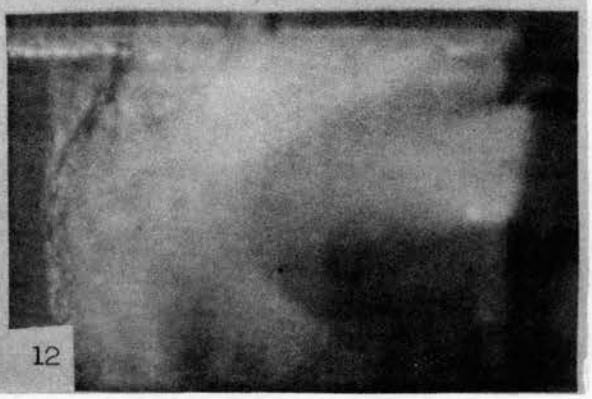
12

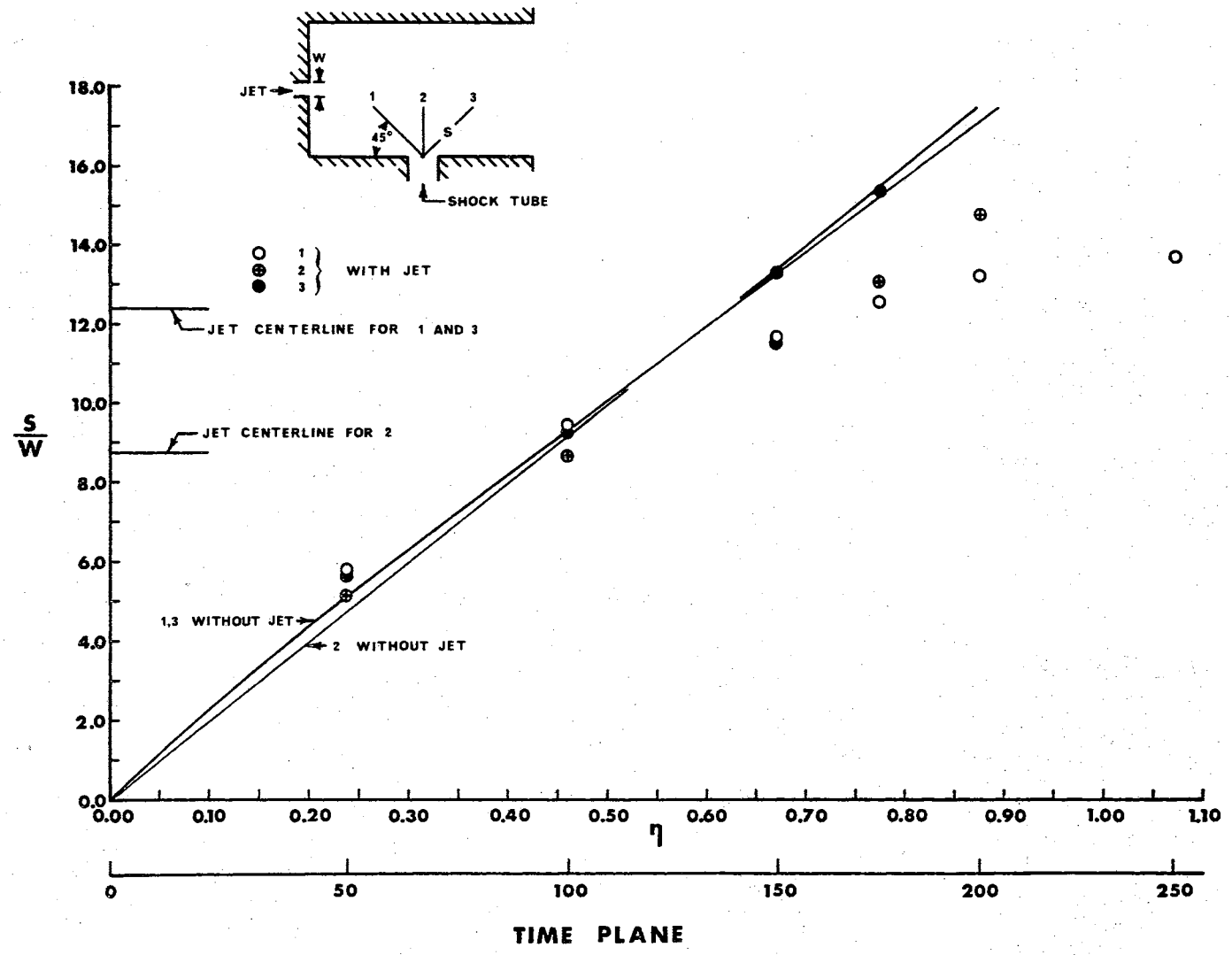

Figure 27. Computed Shock Positions with Time along Rays Emanating from Shock Tube Centerline--Weak Shock Case.

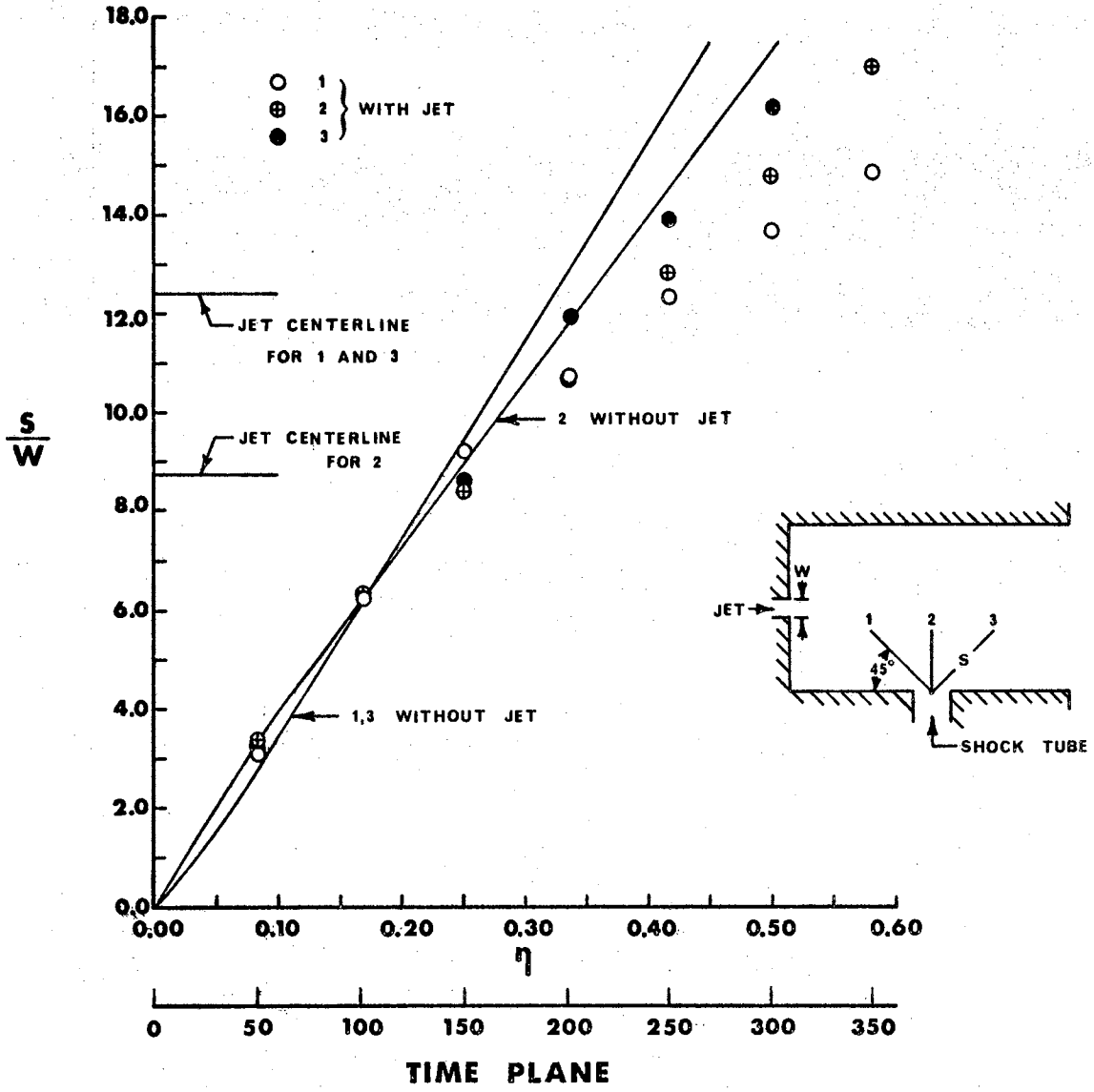

Figure 28. Computed Shock Positions with Time along Rays Emanating from Shock Tube Centerline--Strong Shock Case.

In order to obtain more information concerning the shock wave-mixing region interaction the distribution of pressure along the shock tube centerline was graphed for each of the various cases considered. Figure 29 shows the pressure distributions with time for the weak shock case without the jet. The dashed line denotes the envelop of these pressure distributions. Figure 30 shows the distribution for the weak shock case with the jet. Figure 31 is a summary graph of the pressure envelops for the two cases. As was indicated in the discussion of the water table study, there appears to be a pressure increase when the wave encounters the mixing region. The explanation which was given for this was that the addition of mass and momentum behind the wave, combined with the retardation of the wave front, produced an increase in pressure behind the wave. This explanation seems to be substantiated very well by the pressure distributions shown in Figure 30. The pressure distributions exhibit an inflection after the wave has encountered the mixing region. Thus, it appears that two shock waves are present after the interaction has occurred. The first is characterized by a lower maximum pressure and evidently corresponds to the initial wave front. The second raises the pressure to still higher values and is due to the mass and momentum addition from the shock tube. Since the shock wave with the higher back pressure will travel at a greater velocity, then it seems reasonable to expect the second wave to coalesce with the first. From the pressure distributions in Figure 30 this coalescing does in fact seem to be occurring.

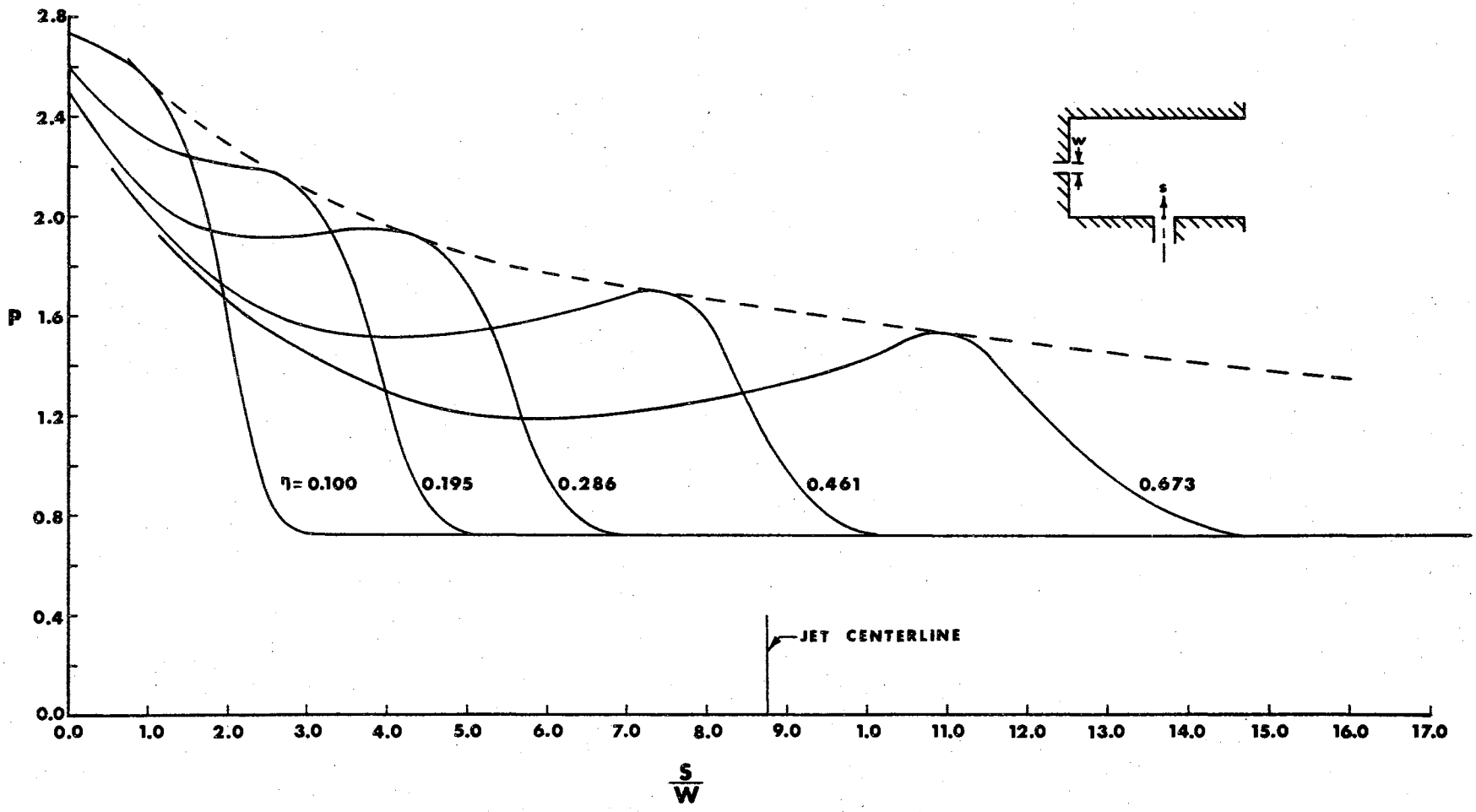

Figure 29. Pressure Distributions along Shock Tube Centerline--Weak Shock Case, without Jet.

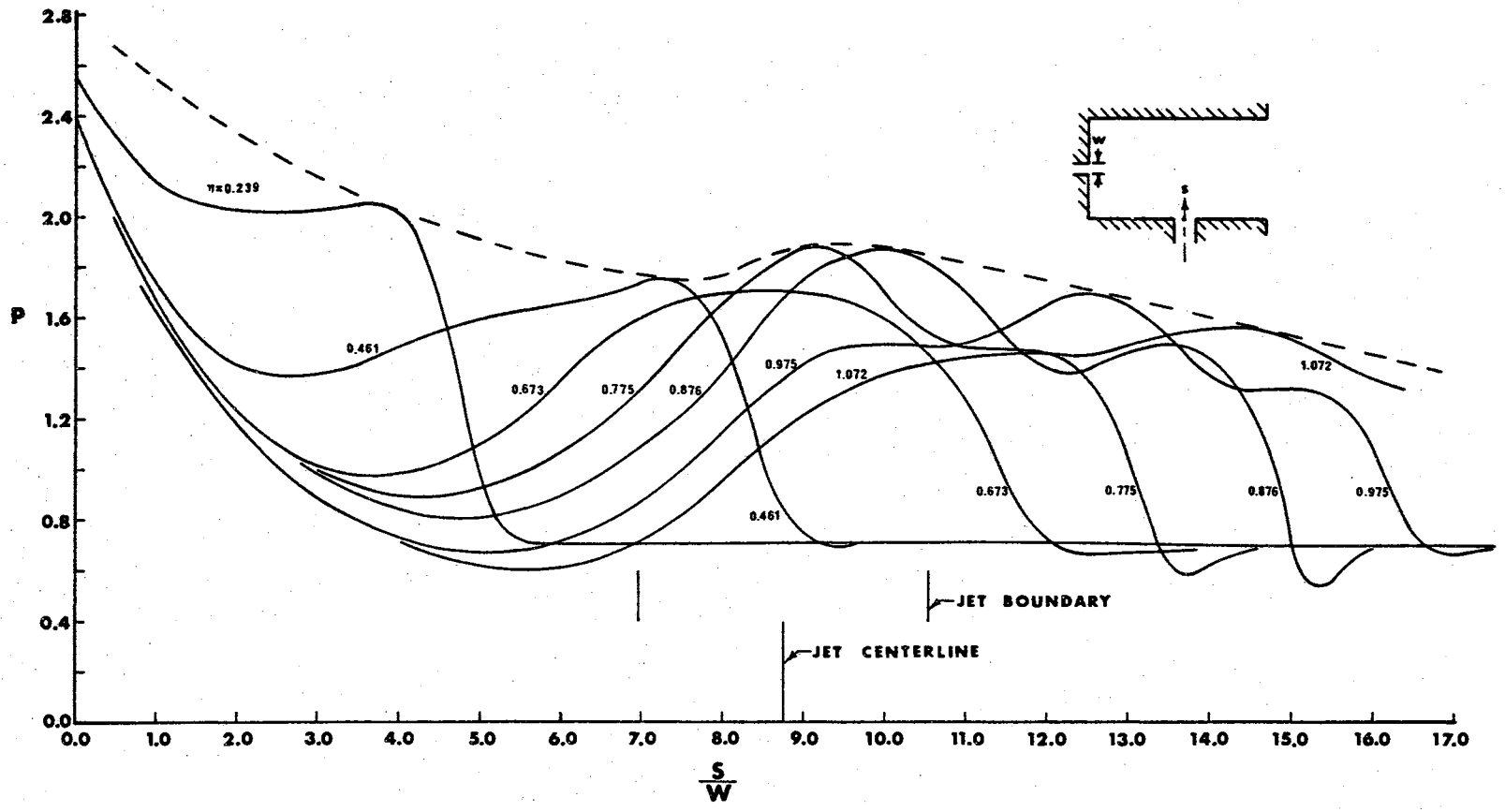

Figure 30. Pressure Distributions along Shock Tube Centerline--Weak Shock Case, with Jet.

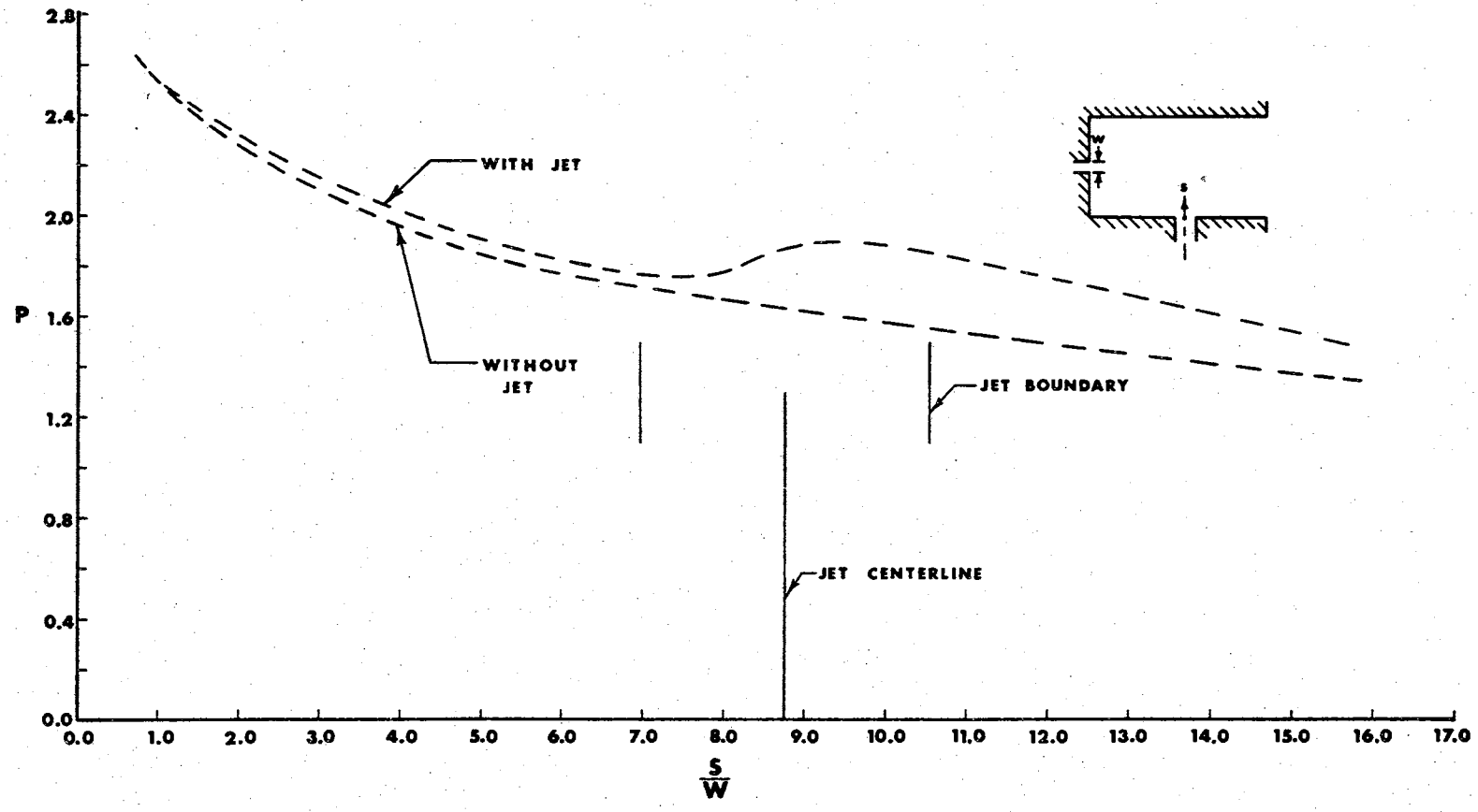

Figure 31. Envelop of Pressure Distributions along Shock Tube Centerline--Weak Shock Case.

Figure 32 shows the pressure distributions for the strong shock case with the jet. Figure 33 shows the pressure envelops for the strong shock cases both with and without the jet. For these cases the shock wave intensity seems to increase somewhat because of the mixing region, but not to nearly as large an extent as for the weak shock case. Apparently then, the retardation of the wave, for the strong shock case, is not sufficient to allow the back pressure to build up significantly as a result of the mass and momentum addition from the shock tube.

In obtaining the results which have been presented in this chapter, no undue difficulties were experienced as a result of the numerical method. It was necessary in order to compute the strong shock case, however, to change the values of $\bar{\sigma}_o$ and ω from 0.5 and 0.5 to 0.3 and 1.50 respectively. This was not entirely unexpected. The strong shock case represents a more severe non-linearity than does the weak shock case and, as implied by von Neumann (23), should require a more severe stability criteria.

The results have indicated that in passing across a mixing region, a shock wave is retarded and its profile is altered. The amount of retardation and profile change is a function of the original intensity of the wave. In both the weak shock case and the strong shock case, the wave intensities were increased when the mixing region was encountered. As was mentioned, this effect seems to be due to the combined wave retardation and efflux of mass and momentum from the shock tube.

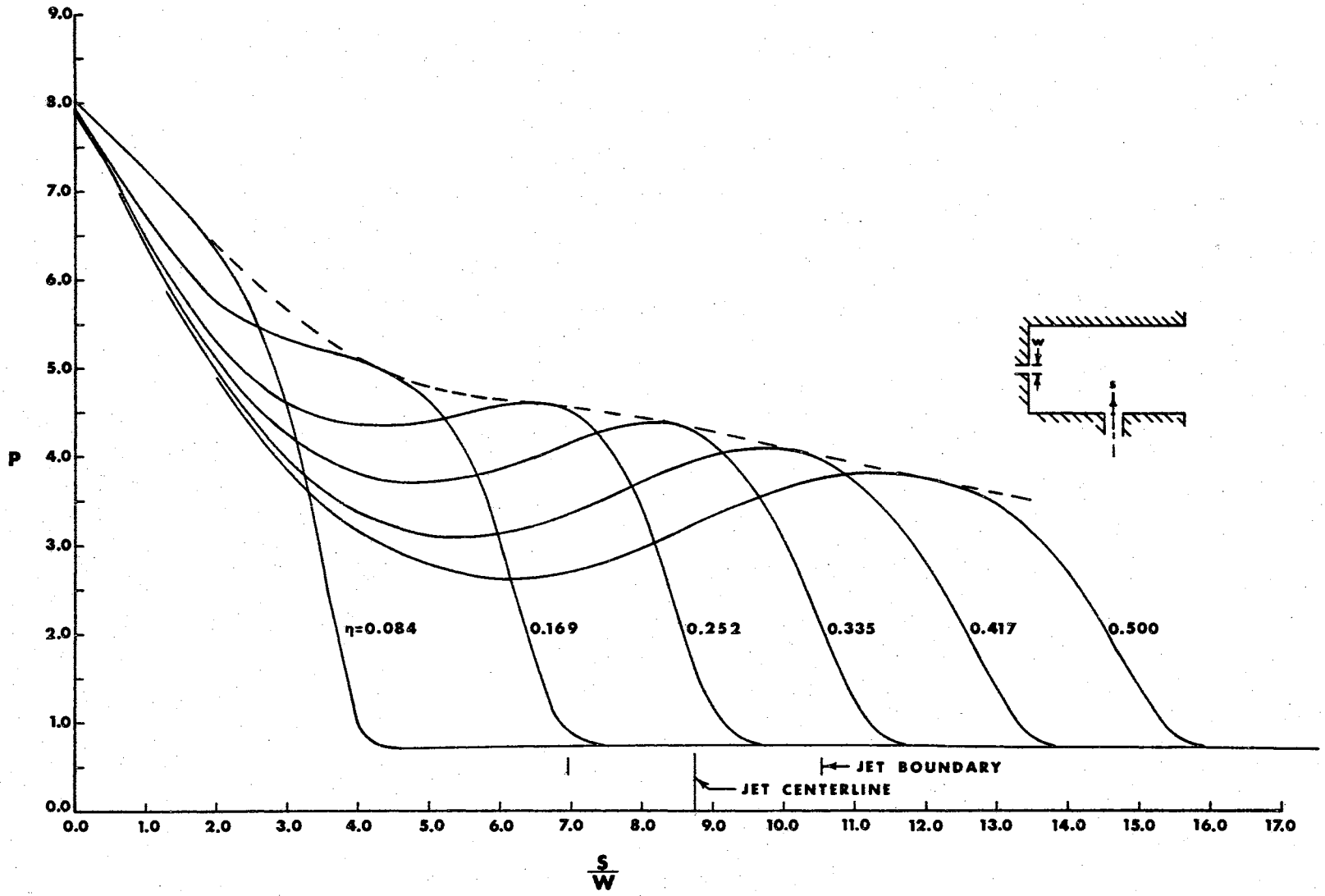

Figure 32. Pressure Distributions along Shock Tube Centerline--Strong Shock Case, with Jet.

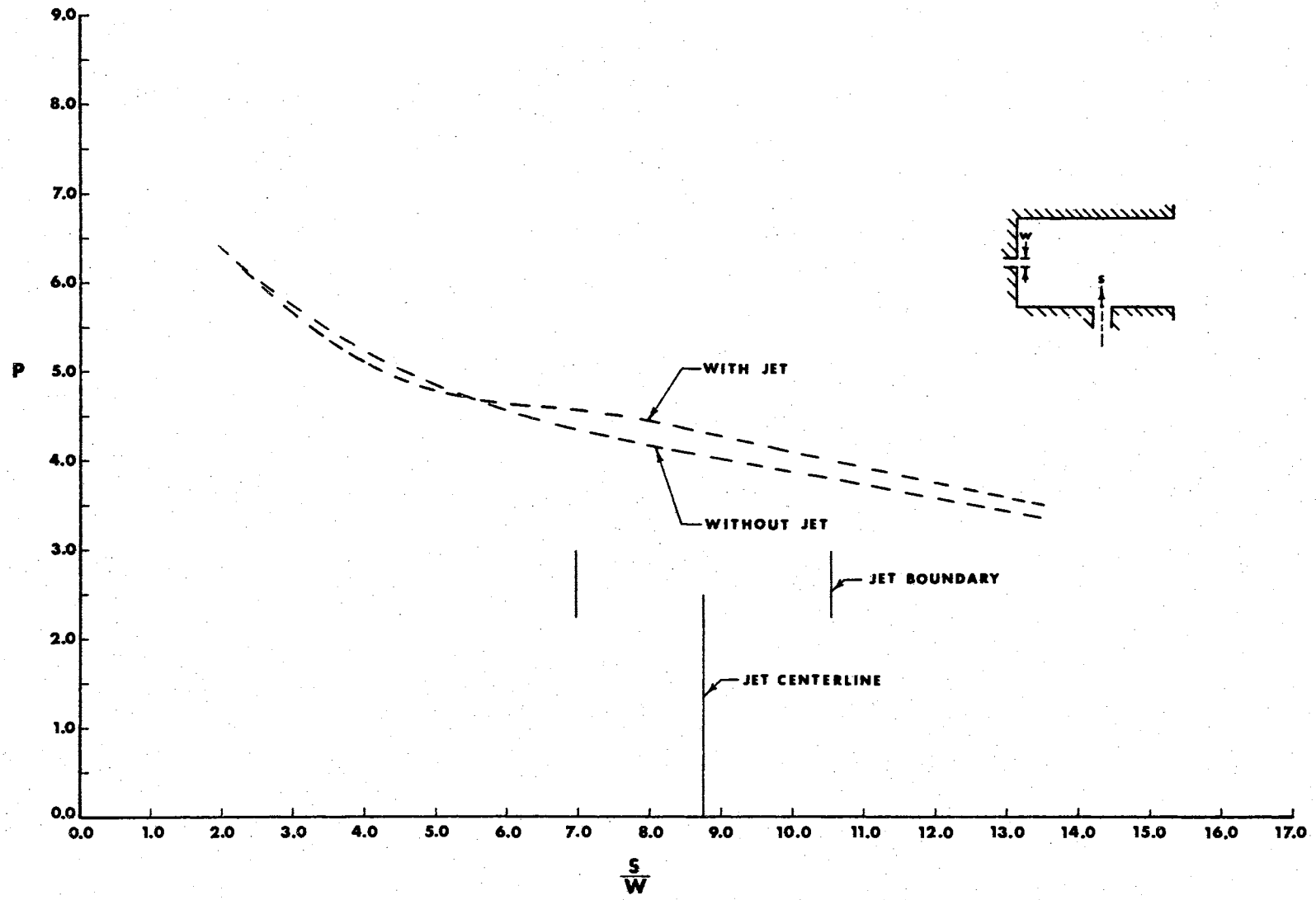

Figure 33. Envelop of Pressure Distributions along Shock Tube Centerline--Strong Shock Case.

CHAPTER VIII

CONCLUSIONS AND RECOMMENDATIONS

Conclusions

The primary objective of this investigation has been to devise a method whereby the phenomenon associated with the interaction of a moving shock wave with a turbulent mixing region could be studied. This objective has been accomplished. In addition a complete mathematical description of the two-dimensional turbulent mixing process has been given. The method of artificial viscosity was adapted to the requirements of the study and a turbulent mixing region described from the numerical solution. Shock waves of two different strengths were passed over the established turbulent mixing region and qualitative experimental verification was obtained.

Two important observations can be made from the results of the numerical computations. First, the passing of a shock wave across a turbulent mixing region occurs in a fashion much as one would expect. The wave experiences both a retardation and a change in profile, the magnitude of these being dependent upon the strength of the wave. The one unexpected phenomenon which was seen to occur was an increase in the wave intensity as it encountered the high velocity portion of the mixing region. Thus, as a shock wave passes across a mixing region,

pressures can occur which are actually greater than those which existed behind the wave prior to its entry into the high velocity region.

The second observation to be made concerns the description of the mixing region from the numerical solution. It was found that the velocity profiles which were obtained from the numerical solution showed excellent agreement with the experimentally verified Gaussian distribution. Because of this agreement, and the generality of the governing equations, it appears that the method of analysis which has been formulated holds great promise for the solution of many complicated viscous flow problems which have heretofore proved too difficult for analysis.

Recommendations for Future Work

On the basis of that which was learned from the investigation which has just been presented, the following recommendations are made:

1. An extensive investigation should be initiated in order to obtain quantitative experimental data; first, for the purpose of providing better verification of the present analysis, and second, for determining the bounds of reliability of the artificial viscosity method for solving problems of shock dynamics.
2. The present investigation has dealt entirely with the two-dimensional case. The analysis should be extended to the case of axial symmetry, with shock waves intercepting the mixing region at various angles.
3. In the development of this analysis, the need became apparent for more numerical information concerning the finite difference stability

requirements. It is therefore recommended that a simple problem involving a moving shock wave be postulated; and then a parametric study initiated for the purpose of defining numerically the limits of $\bar{\sigma}_o$ and ω for various strength shock waves. A study such as this could also furnish information concerning certain mathematical difficulties which have been encountered; namely, the description of certain boundary conditions, and the numerical means by which singular points and stagnation points can be treated.

4. The results of this analysis have indicated that the numerical approach which was adopted has great potential for the solution of complex viscous flow problems. It is therefore recommended that the method be applied to several two-dimensional turbulent mixing problems for which there is extensive experimental data available for comparison. If the numerical results compare favorably with the experimental data, and there is presently no reason for suspecting that they will not, then the method should be modified to account for laminar effects, thus enabling laminar and turbulent boundary layer and jet mixing problems to be investigated.

A SELECTED BIBLIOGRAPHY

1. Wolff, W. S., "Transient Flow Field Analysis Around a Conical Body Exposed to a Blast Wave," Lockheed Corp. Report LMSC No. 4-70-64-1, 1964.

2. Jackomis, W. M., "Transient Flow Field Analysis of a Plane Blast Wave Intercepting a Stationary Cone at Zero Angle of Attack," Ph.D. Dissertation, Oklahoma State University, May, 1965; Published as Engineering Research Report SBW-9 by Jackomis, W. N., and Zumwalt, G. W., August 1965.

3. _____. DASA/AFFDL Shock-on-Shock Interaction Conference, 2-3 Feb. 1963, Air Force Flight Dynamics Laboratory, Wright-Patterson Air Force Base, Ohio; Proceedings to be published.

4. Tyler, L. D., "Numerical Solutions of the Flow Field Produced by a Plane Shock Wave Emerging into a Crossflow," Ph.D. Dissertation, Oklahoma State University, May, 1965; Published as Eng. Res. Rpt. SWB-10 by Tyler, L. D., and Zumwalt, G. W.

5. Walker, W. F., and Tyler, L. D., "Literature Survey on Shock Wave Interactions with Shocks and Bodies," Oklahoma State University Research Report SBW-7, 1965.

6. Charczenko, N., and Hennessey, K. W., "Investigation of a Retrorocket Exhausting from the Nose of a Blunt Body into a Supersonic Stream," NASA Technical Note D-751, 1961.

7. Romeo, D. J., and Sterrett, J. R., "Exploratory Investigation of the Effect of a Forward-Facing Jet on the Bow Shock of a Blunt Body in a Mach Number 6 Free Stream," NASA Technical Note D-1605, 1962.

8. Moeckel, W. E., "Interaction of Oblique Shock Waves with Regions of Variable Pressure, Entropy, and Energy," NACA Technical Note 2725, 1952.

9. Whitham, G. B., "On the Propagation of Shock Waves through Regions of Nonuniform Area or Flow," J. Fluid Mech., Vol. 4, 1958, p. 337.

10. Riley, N., "Interaction of a Shock Wave with a Mixing Region," J. Fluid Mech., Vol. 7, 1959, p. 321.

11. Dosanjh, D. S., "Experiments on Interaction between a Traveling Shock Wave and a Turbulent Jet," J. Aero. Sci., 1957, p. 838.

12. Dosanjh, D. S., "Interaction of Traveling Shock Waves with Turbulent Flow Fields," Syracuse University College of Engineering Report No. ME 6101Q13, 1961.

13. Weeks, T. M., and Dosanjh, D. S., "Interaction between an Advancing Shock Wave and Opposing Jet Flow," AIAA J., Vol. 1, No. 7, 1963, p. 1527.

14. Zumwalt, G. W., and Tang, H. H., "Transient Base Pressure Study of an Axi-Symmetric Supersonic Missile Flying Head-on through a Blast Wave," Oklahoma State University School of Mechanical Engineering Research Report SBW-6, 1964.

15. Van Driest, E. R., "Turbulent Boundary Layer in Compressible Fluids," J. Aero Sci., Vol. 18, No. 3, 1951, p. 145.

16. Schlichting, H., Boundary Layer Theory, McGraw-Hill, New York, 1960.

17. Prandtl, L., "Bemerkungen zur Theorie der freien Turbulenz," Zamm 22, 1942, p. 241-243.

18. Boussinesq, J., "Theory de l'escoulement tourbillant," Mem. Pre. par, div. Sav. XXIII, 1877.

19. Korst, H. H., Page, R. H., and Childs, M. E., "Compressible Two-Dimensional Jet Mixing at Constant Pressure," Univ. of Illinois Engr. Expr. Sta. Rpt. ME-TN-392-1, OSR-TN-55-99, Contract AF18(600)32, 1955.

20. Maydew, R. C., and Reed, J. F., "Turbulent Mixing of Axisymmetric Compressible Jets (in the Half-Jet Region) with Quiescent Air," Sandia Corp. Research Report SC-4764(RR), 1963.

21. Chrisman, C. C., and Zumwalt, G. W., "Evaluation of the Free Jet Spreading Rate Parameter for Axi-Symmetric Air Flow at M=3," Oklahoma State Univ. School of Mech. Engr. Report SBW-3, 1962.

22. Abramovich, G. N., The Theory of Turbulent Jets, M. I. T. Press, Cambridge, Mass., 1963.

23. von Neumann, J., and Richtmyer, R. D., "A Method for the Numerical Calculation of Hydrodynamic Shocks," J. Appl. Physics, Vol. 21, 1950, p. 232.

24. Rusanov, V. V., "The Calculation of the Interaction of Non-Stationary Shock Waves and Obstacles," National Research Council of Canada Library, Ottawa, Canada, Tech. Translation by D. A. Sinclair, 1962. Translated from: Zhurnal Vychislitelnoi Fiziki, Akademiya Nauk, SSSR 1, Vol. 1, No. 2, 1961, p. 267.

25. Lax, P., "Weak Solutions of Nonlinear Hyperbolic Equations and Their Numerical Computation," Comm. Pure and Appl. Math., Vol. VII, 1954, p. 159.

26. Burstein, S. Z., "Numerical Methods in Multidimensional Shocked Flows," AIAA J., Vol. 2, No. 12, 1964, p. 2111.

27. Ricktmyer, R. D., Difference Methods for Initial-Value Problems, Interscience, New York, 1957.

28. Olsen, R. E., and Miller, D. P., "Aerodynamic Studies of Free and Attached Jets," United Aircraft Corp. Res. Rpt. for Harry Diamond Lab., Contract DA-49-186-ORD-912; Rpt. A-1771-24 from Dept. of Commerce, Office of Tech. Services, Washington 25, D. C., 1963.

29. Pai, S. I., Viscous Flow Theory, D. Van Nostrand, New York, 1957.

APPENDIX A

PLOTTED COMPUTER RESULTS

The results of the numerical computations for the weak shock and strong shock cases are presented in graphical form in this appendix. The results are presented as velocity vector plots and as graphs of constant pressure lines for various times during the progression of a wave across the cavity. The symbol, n_B, is used to denote the time plane number after the introduction of a shock wave into the system.

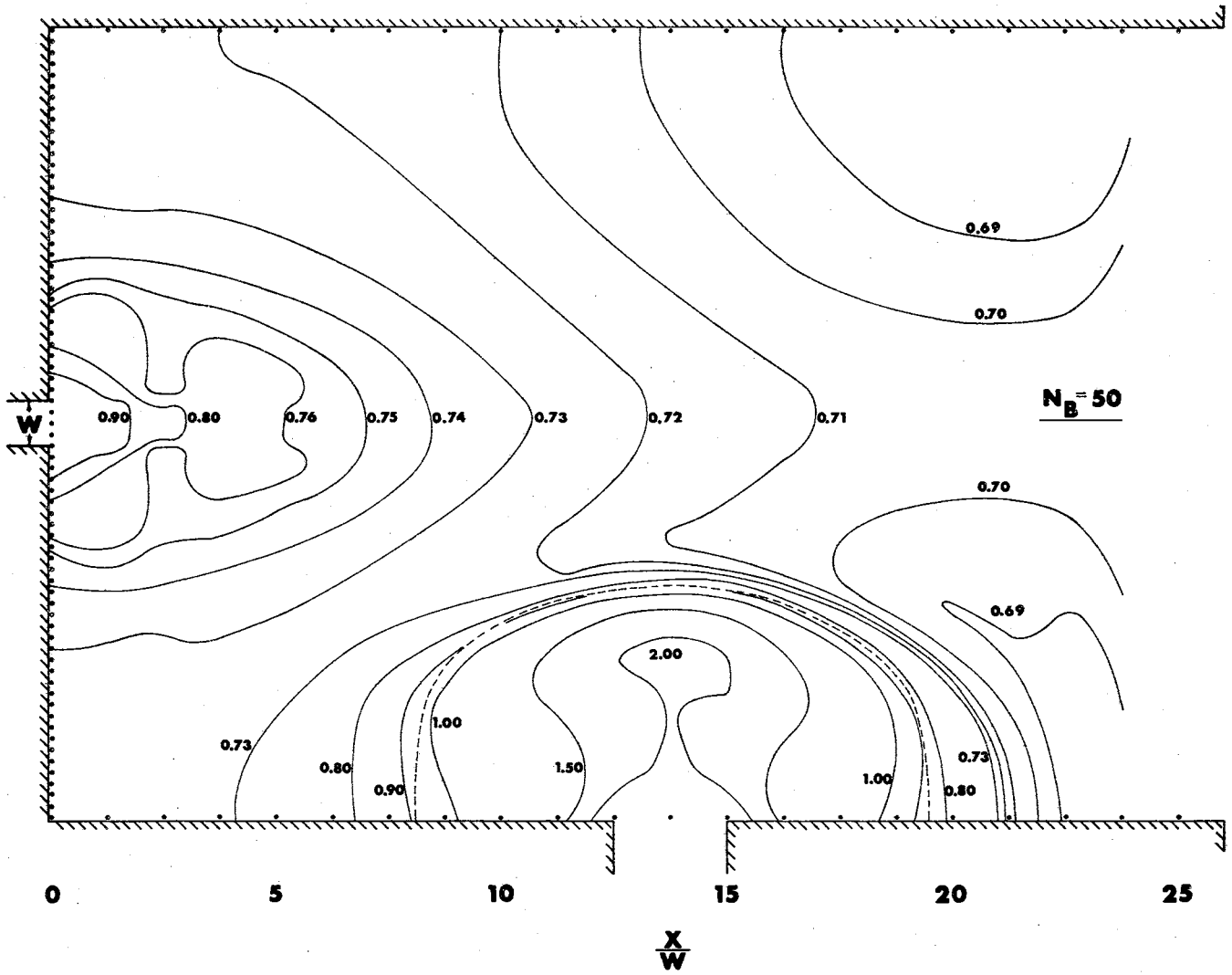

Figure 34. Constant Pressure Lines for Weak Shock Case, $\eta = 0.239$.

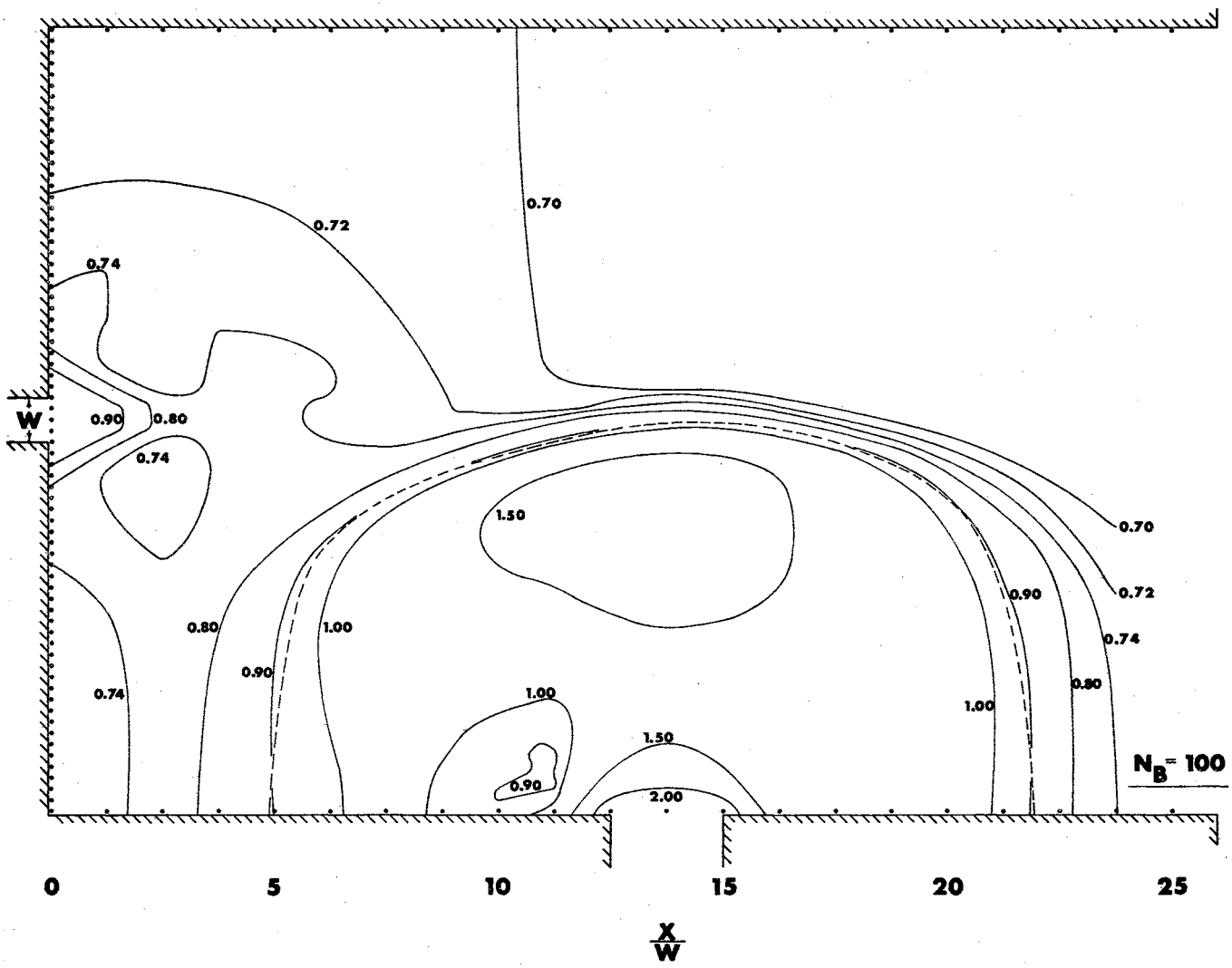

Figure 35. Constant Pressure Lines for Weak Shock Case, η = 0.461.

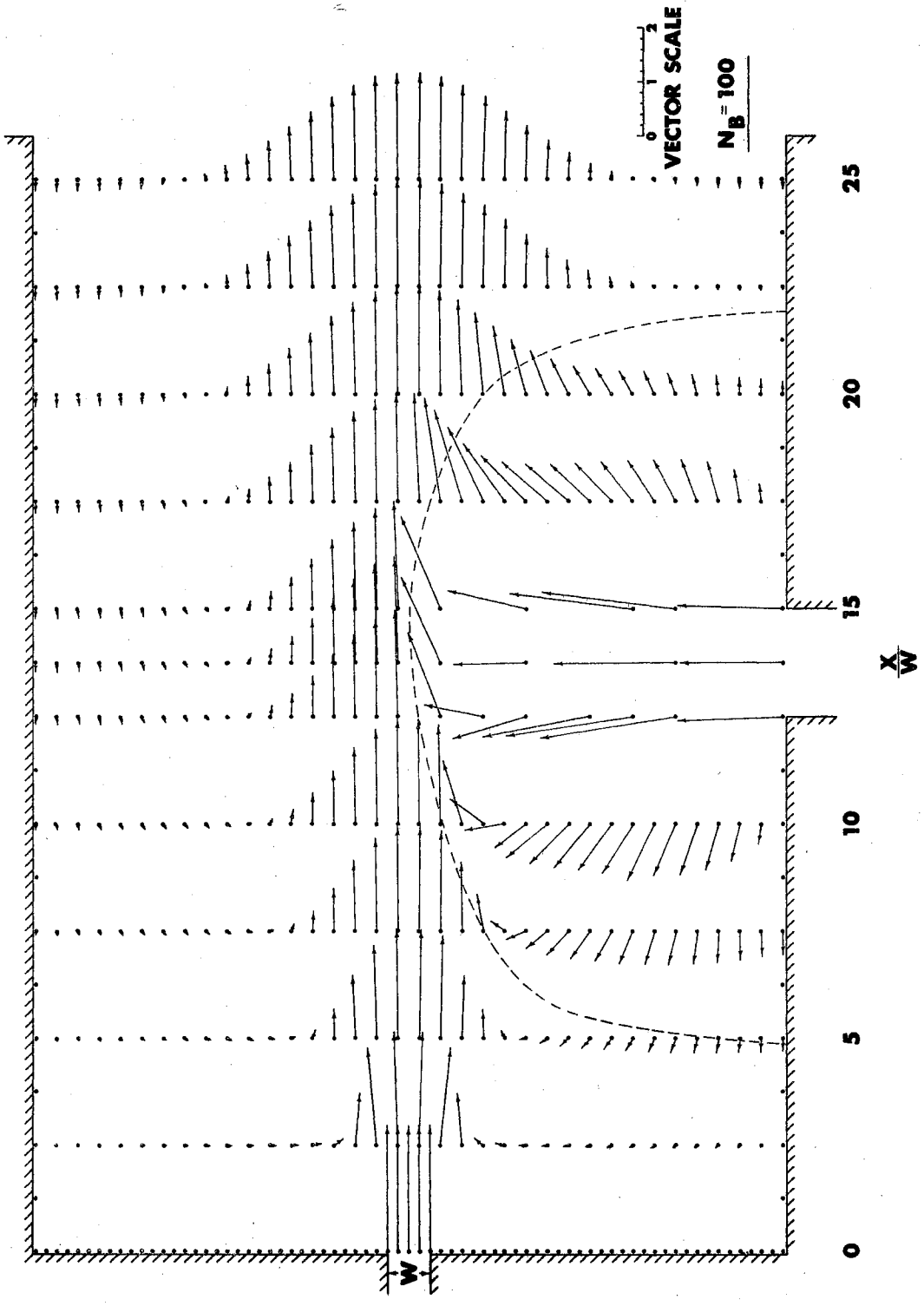

Figure 36. Velocity Vector Field for Weak Shock Case, $\eta = 0.461$.

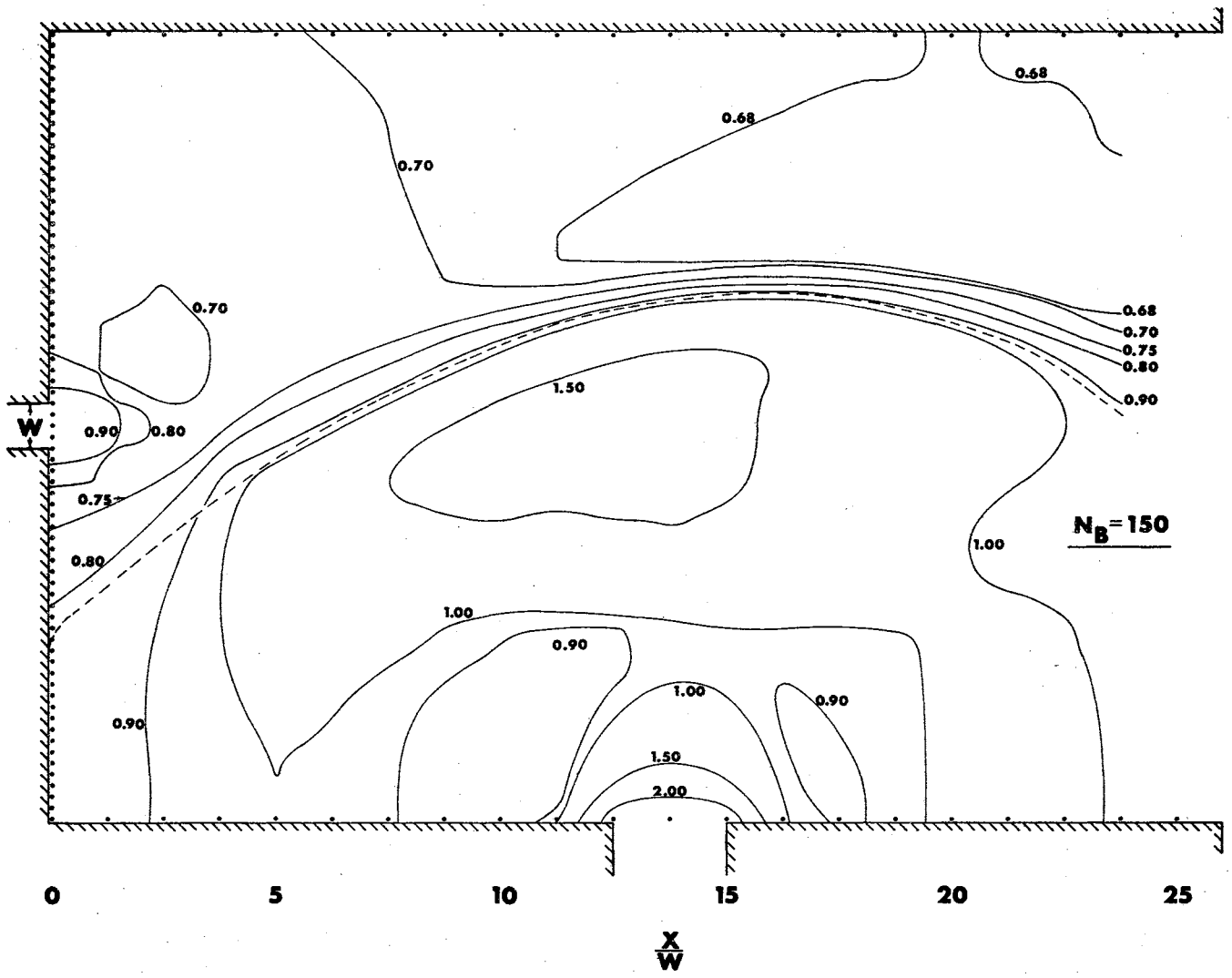

Figure 37. Constant Pressure Lines for Weak Shock Case, η = 0.673.

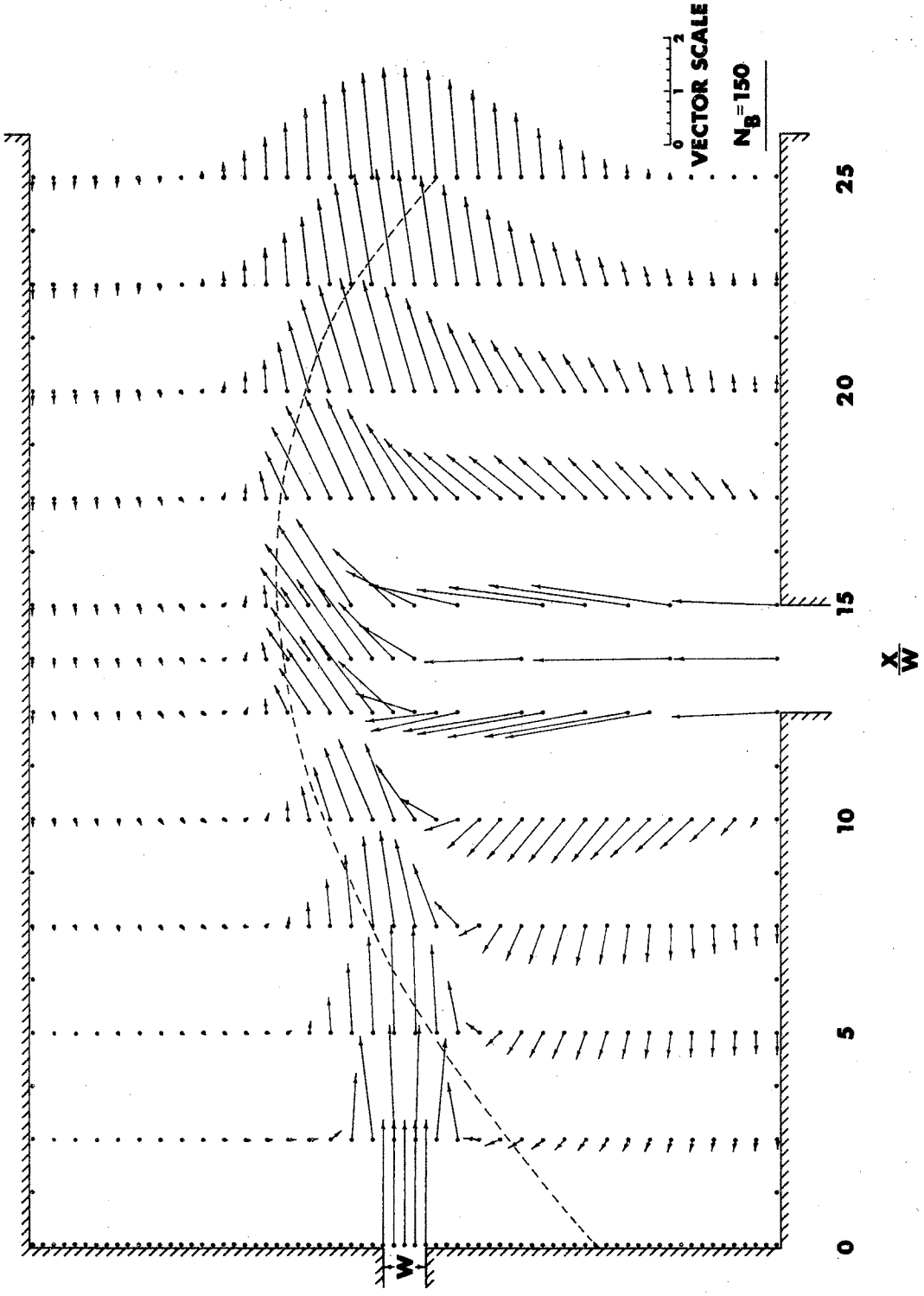

Figure 38. Velocity Vector Field for Weak Shock Case, η = 0.673.

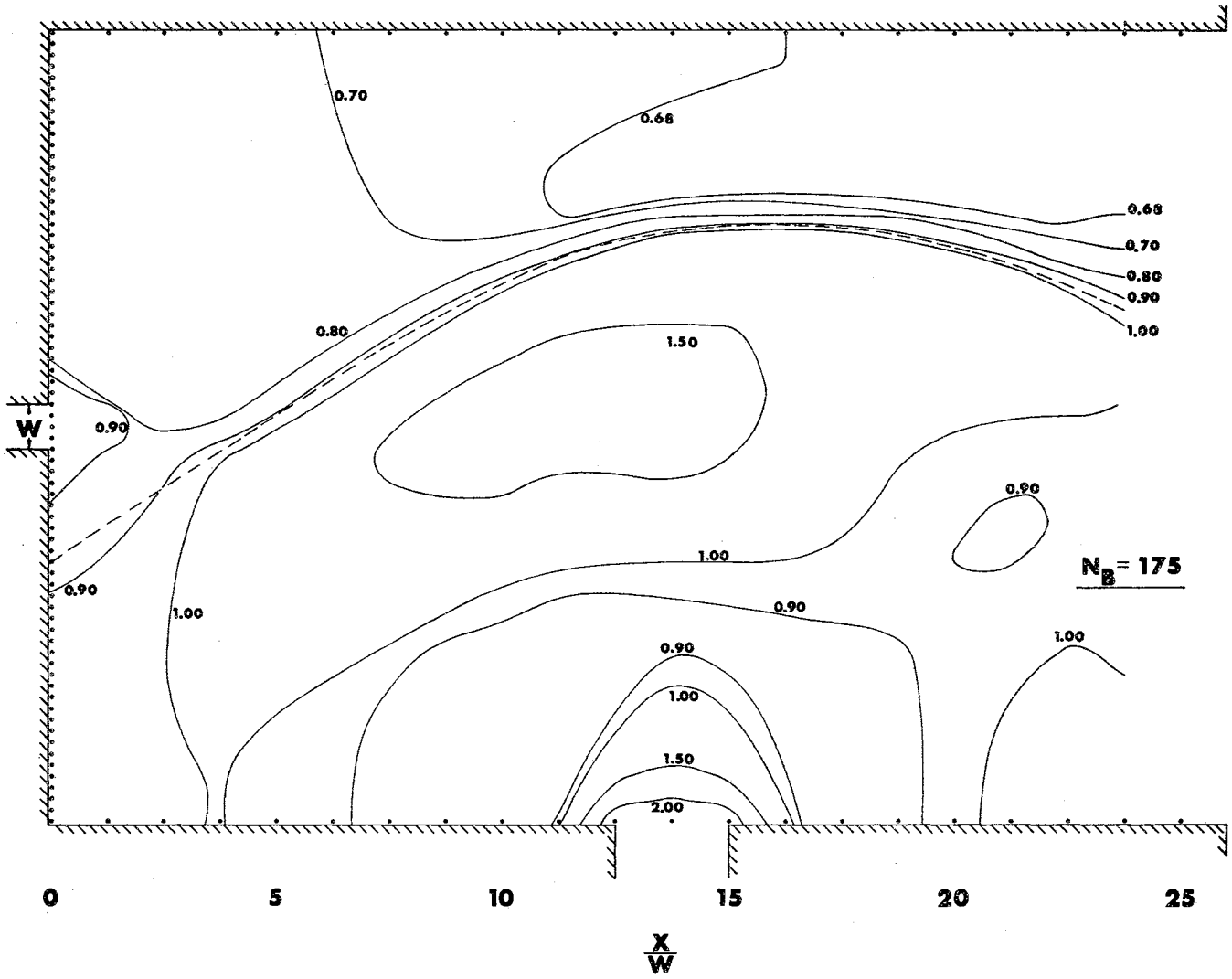

Figure 39. Constant Pressure Lines for Weak Shock Case, $\eta = 0.773$.

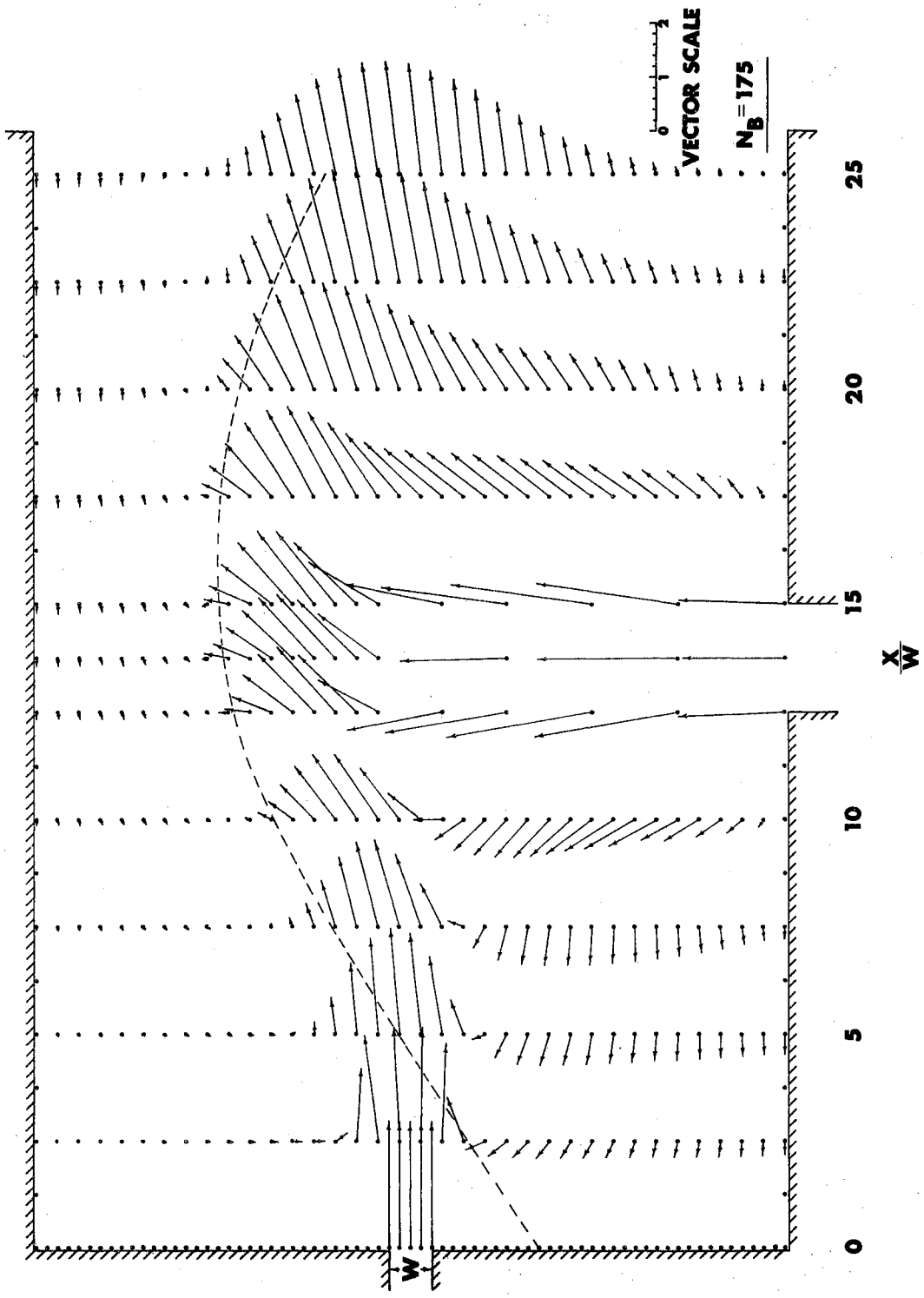

Figure 40. Velocity Vector Field for Weak Shock Case, η = 0.773.

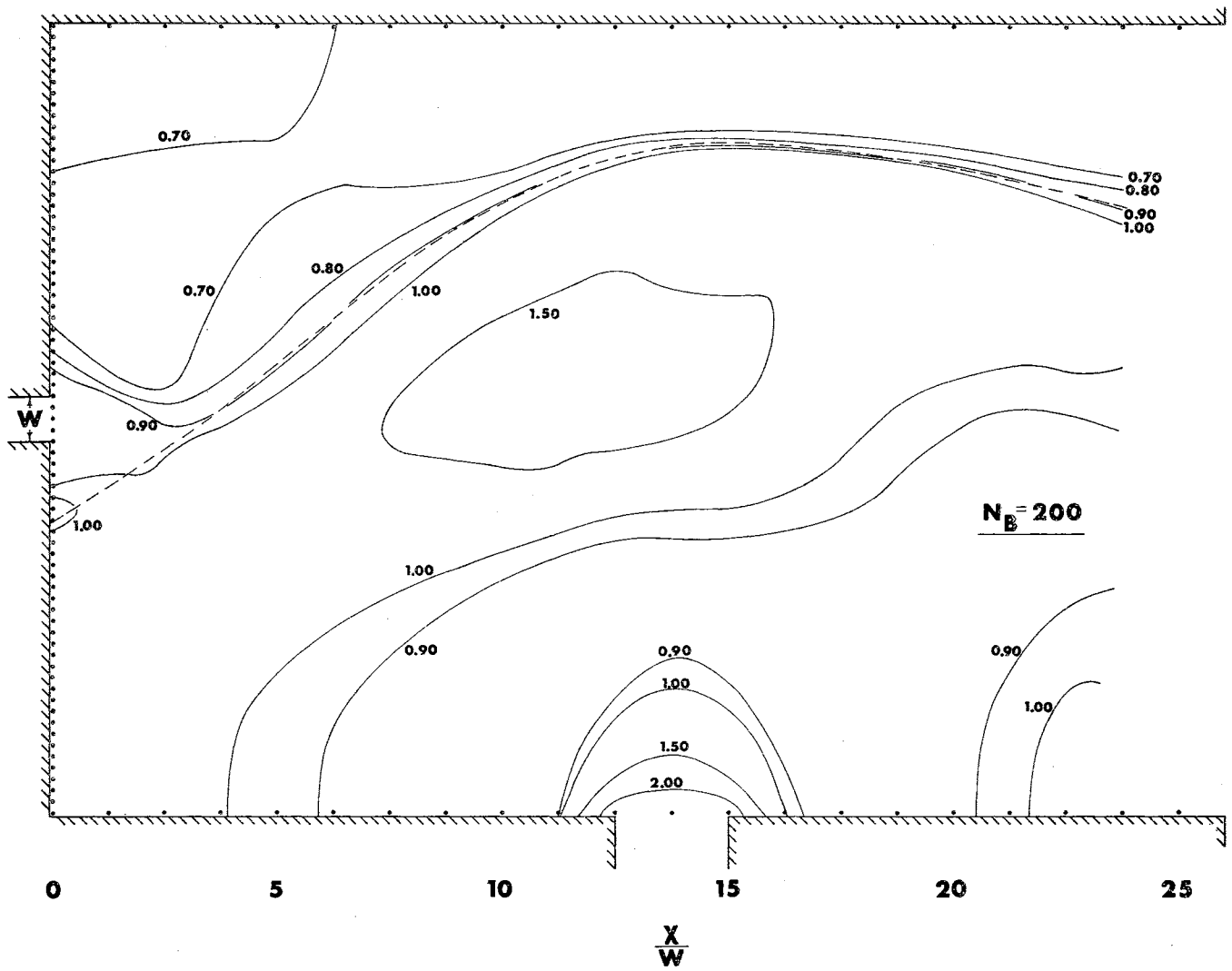

Figure 41. Constant Pressure Lines for Weak Shock Case, $\eta = 0.876$.

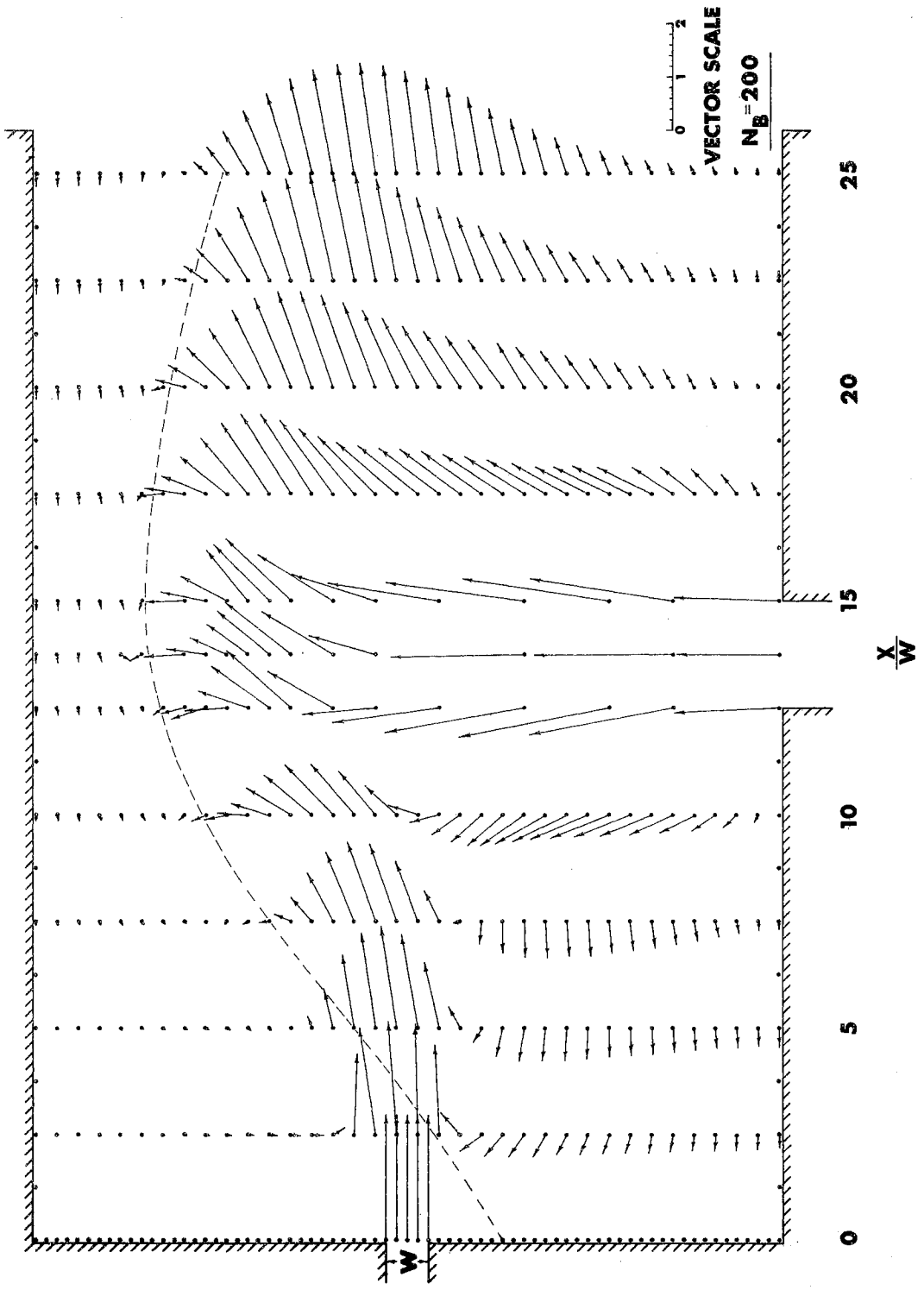

Figure 42. Velocity Vector Field for Weak Shock Case, η = 0.876.

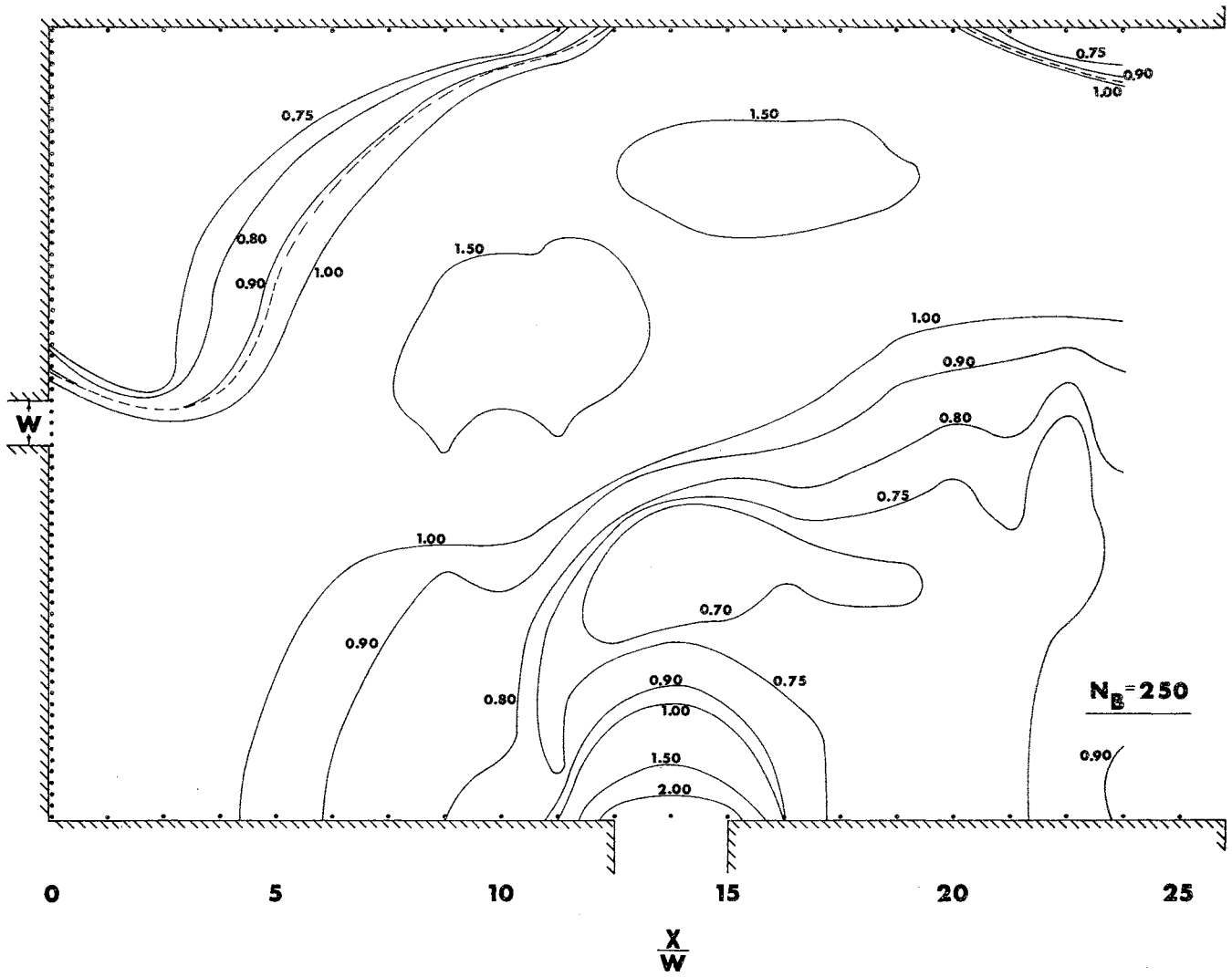

Figure 43. Constant Pressure Lines for Weak Shock Case, $\eta = 1.072$.

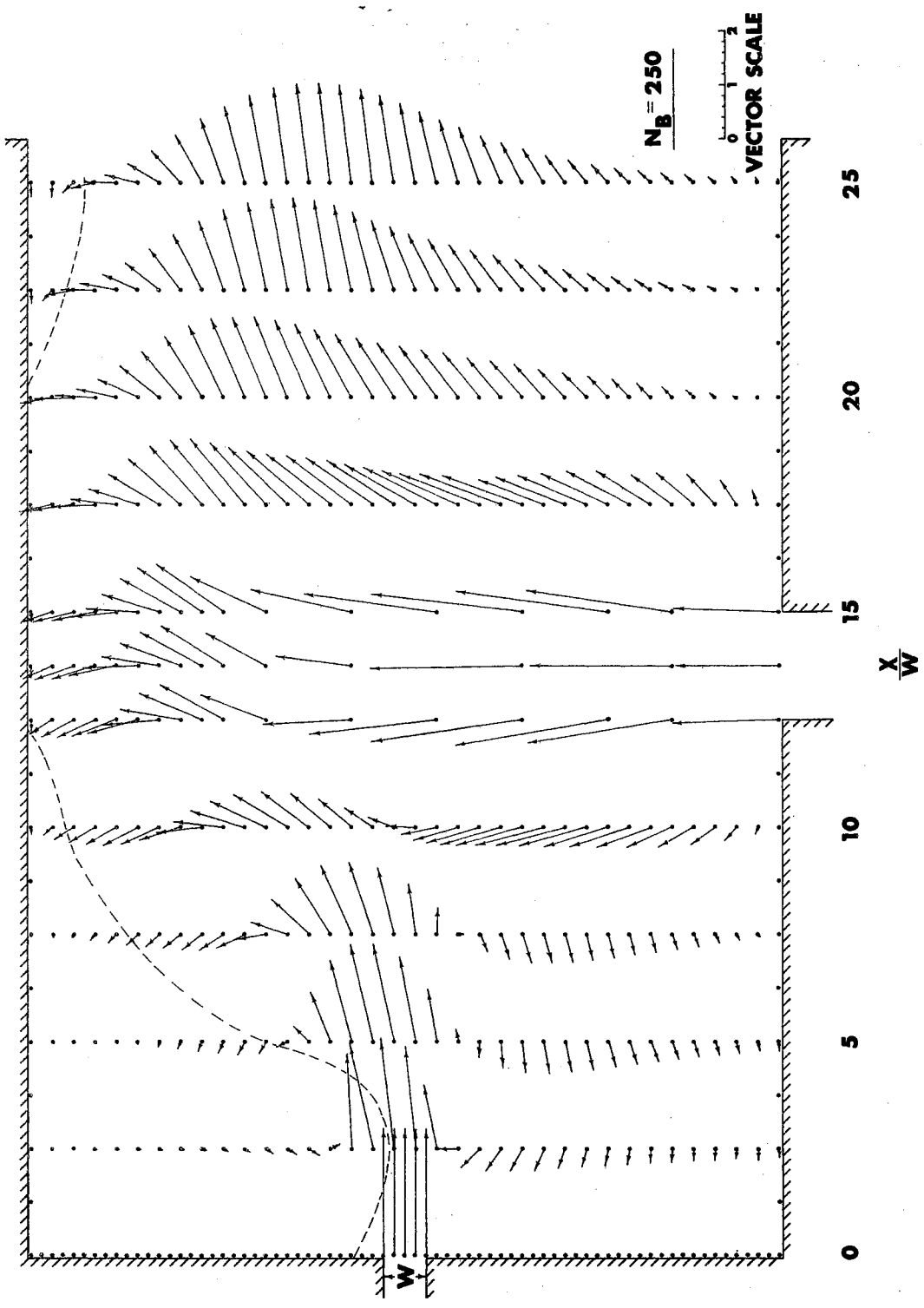

Figure 44. Velocity Vector Field for Weak Shock Case, $\eta = 1.072$.

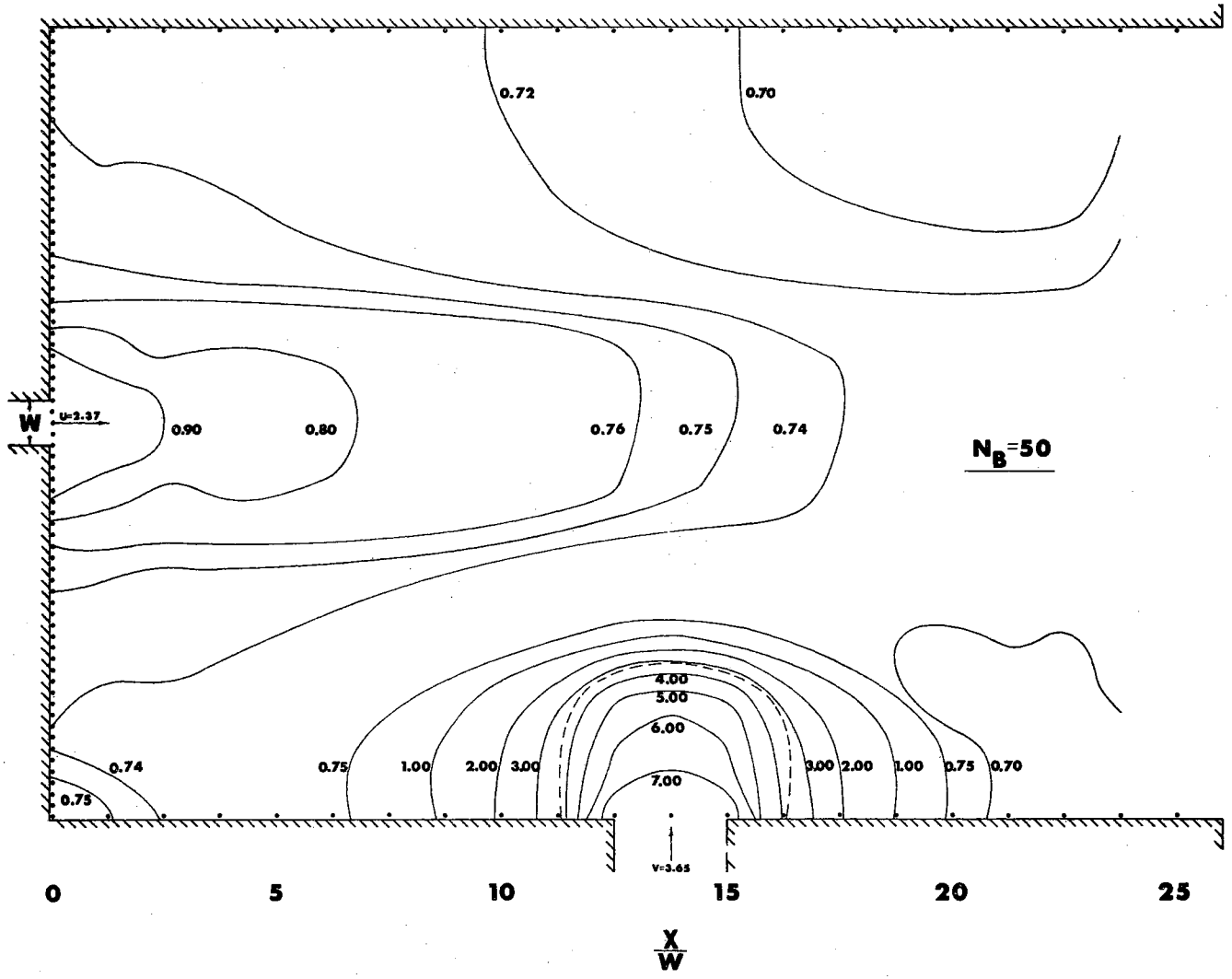

Figure 45. Constant Pressure Lines for Strong Shock Case, η = 0.084.

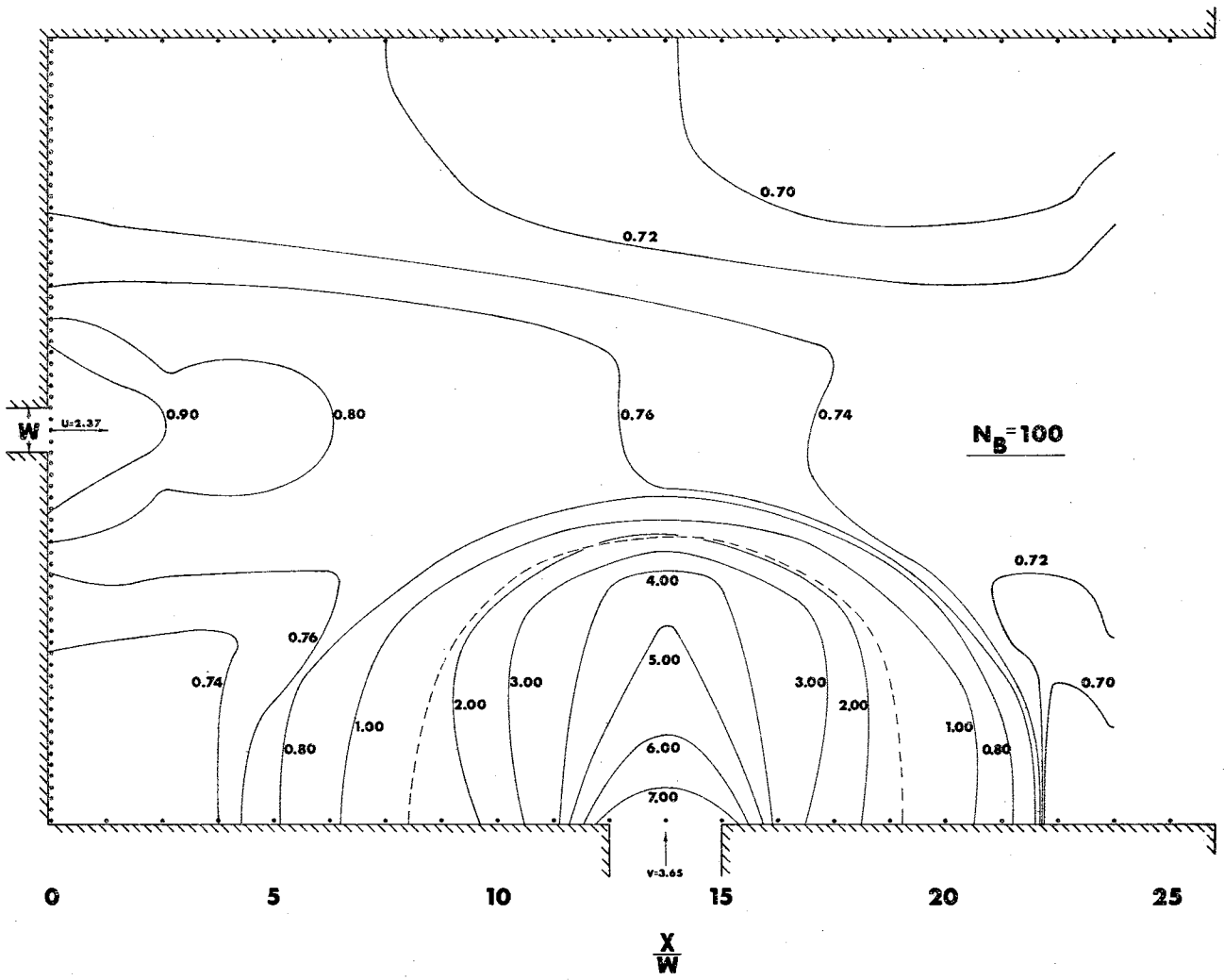

Figure 46. Constant Pressure Lines for Strong Shock Case, $\eta = 0.169$.

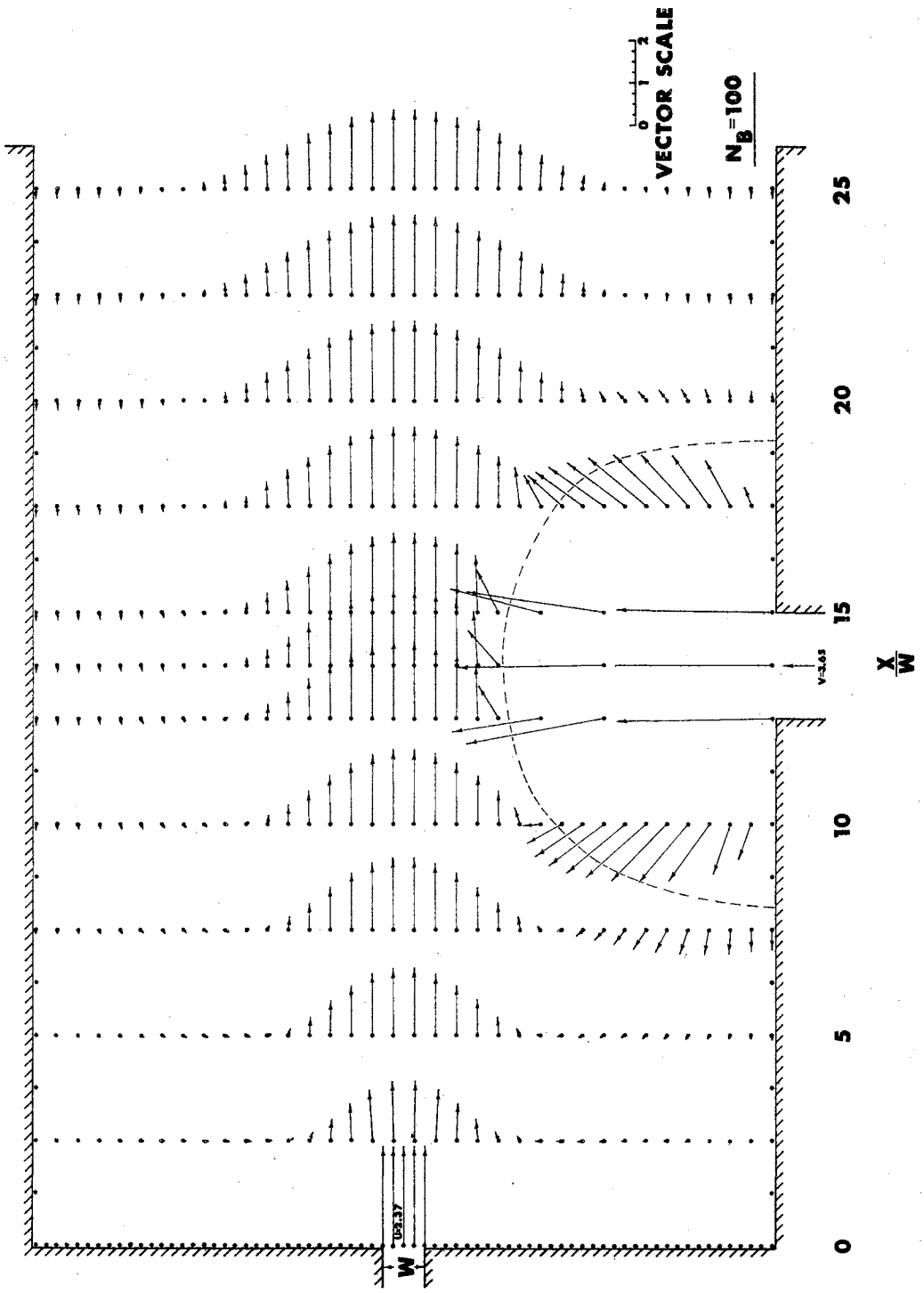

Figure 47. Velocity Vector Field for Strong Shock Case, η = 0.169.

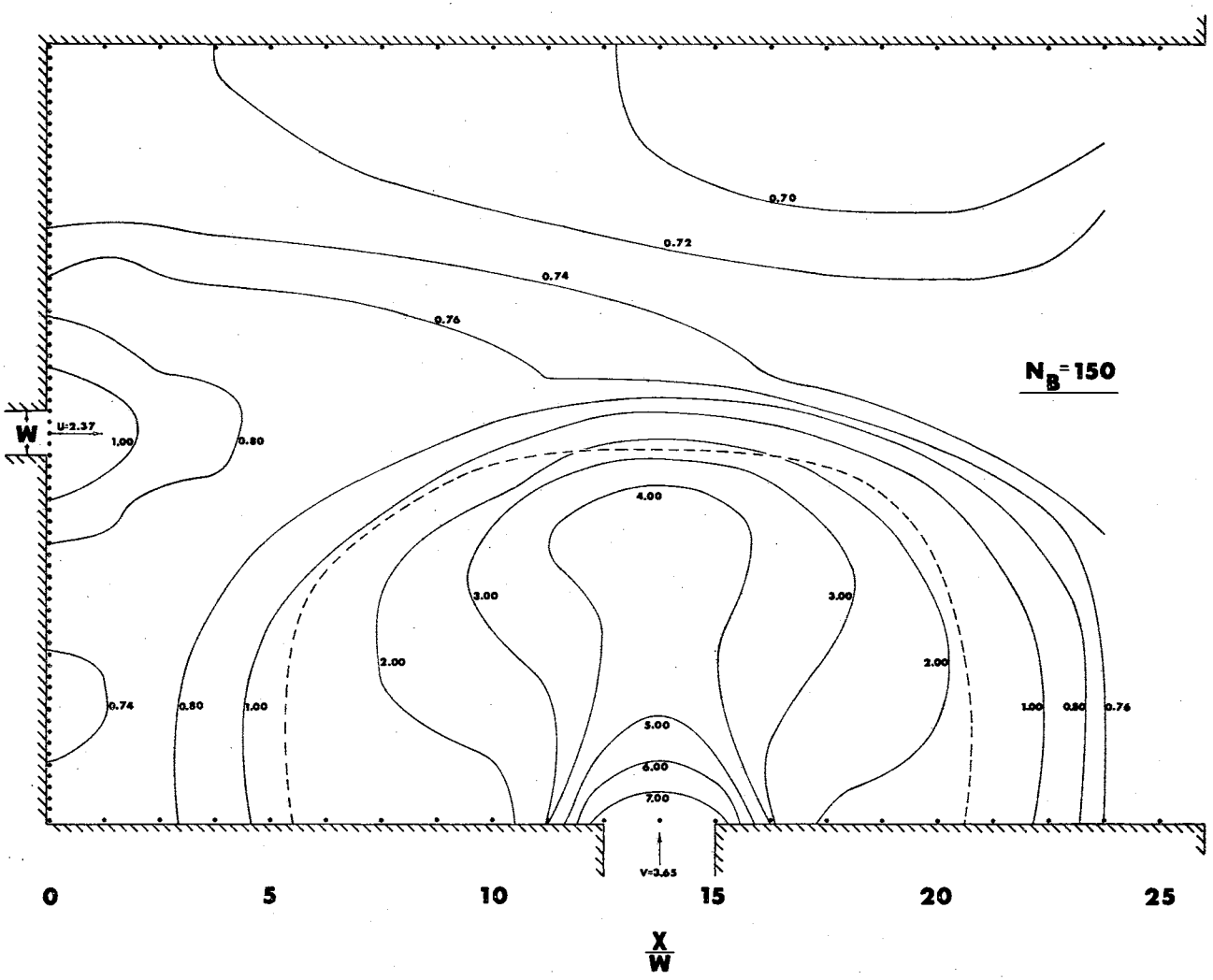

Figure 48. Constant Pressure Lines for Strong Shock Case, η = 0.252.

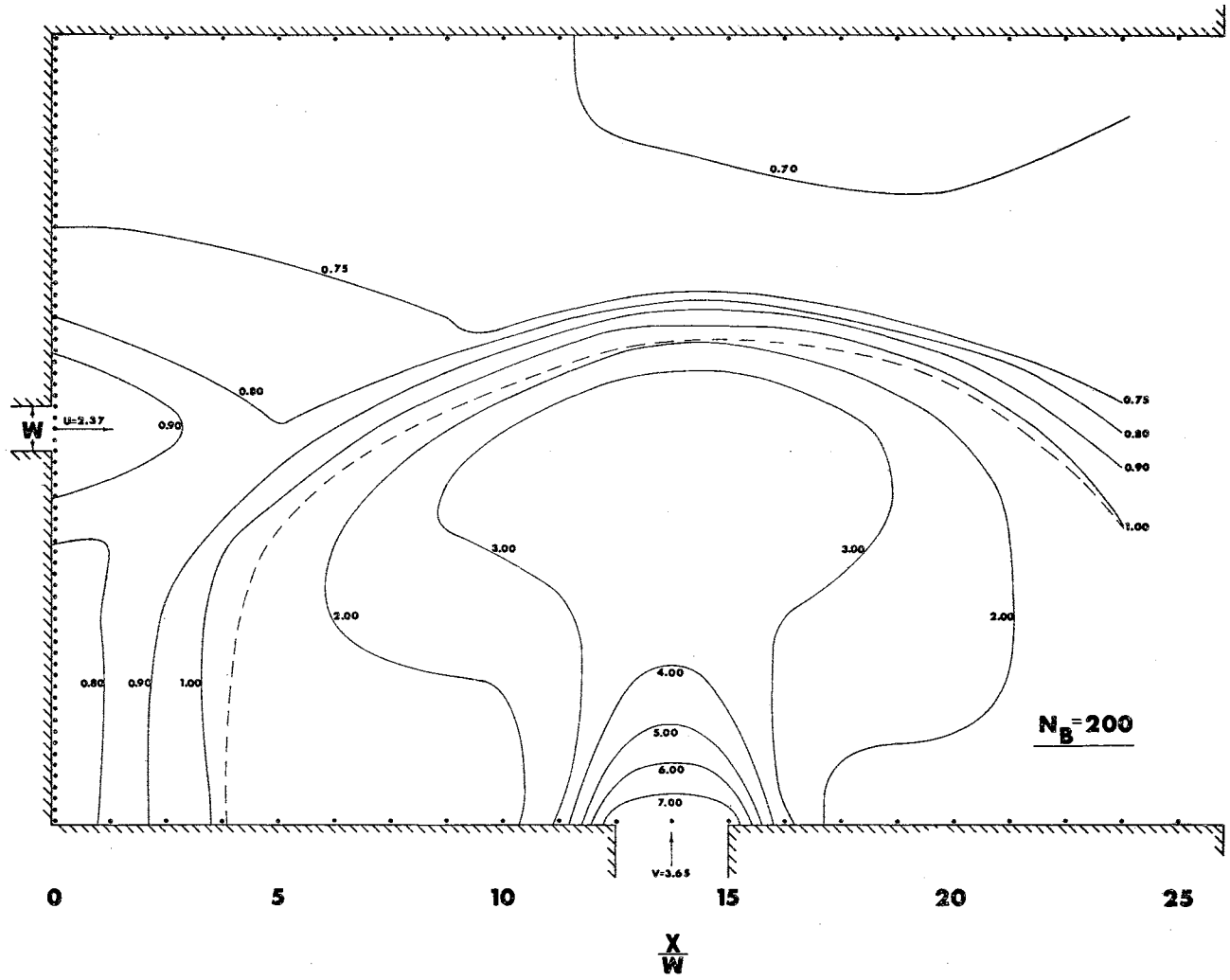

Figure 49. Constant Pressure Lines for Strong Shock Case, η = 0.335.

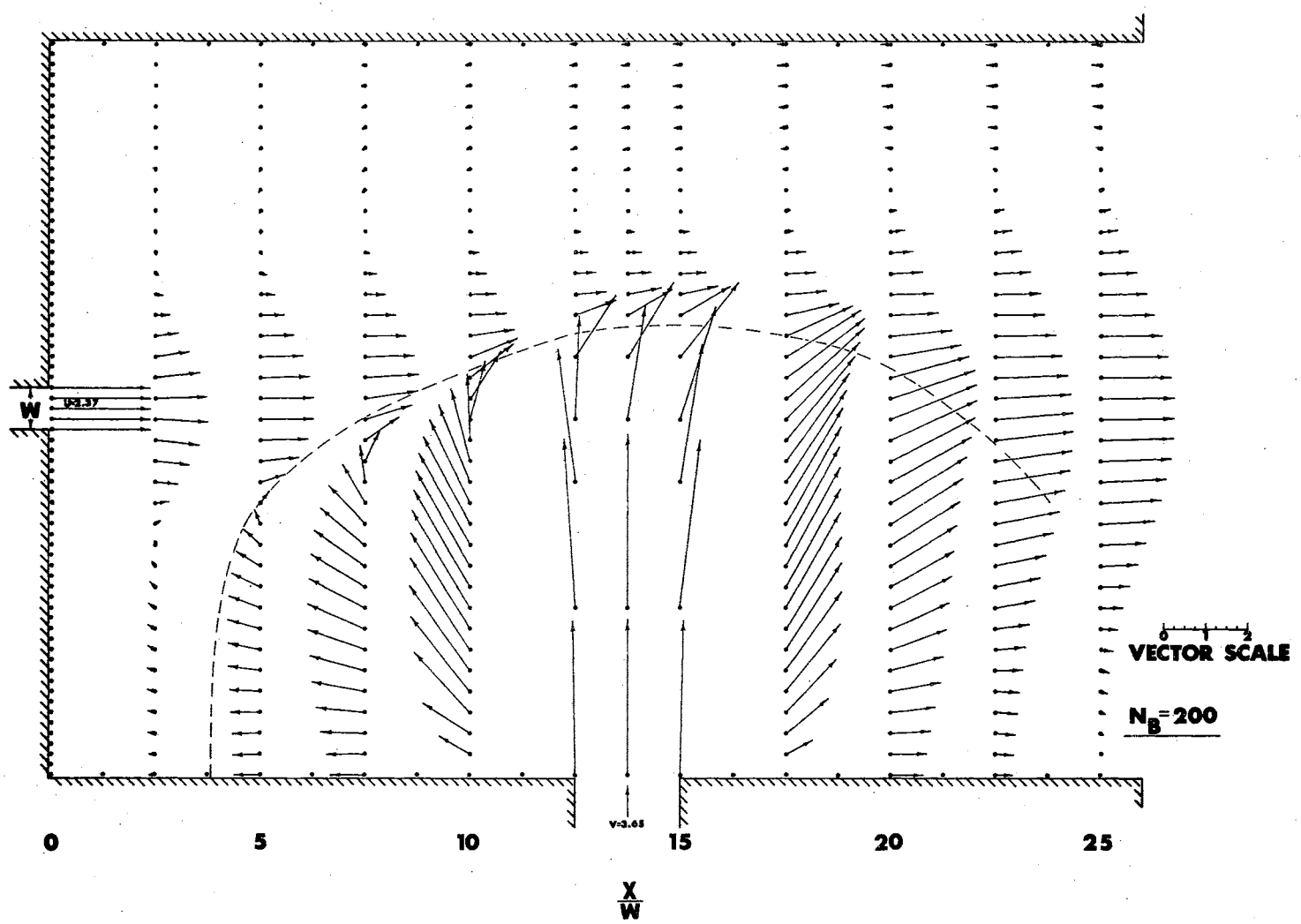

Figure 50. Velocity Vector Field for Strong Shock Case, $\eta = 0.335$.

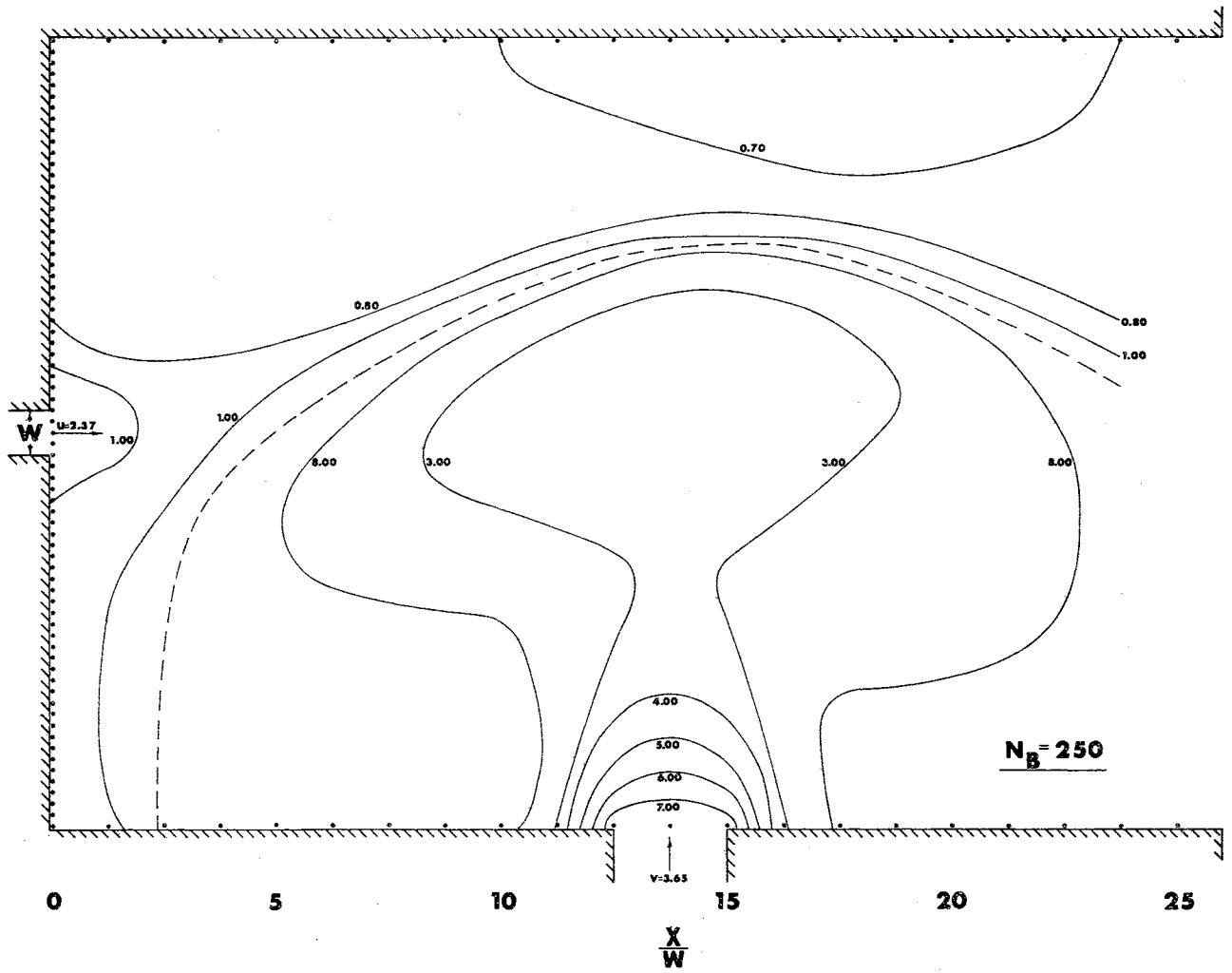

Figure 51. Constant Pressure Lines for Strong Shock Case, $\eta = 0.417$.

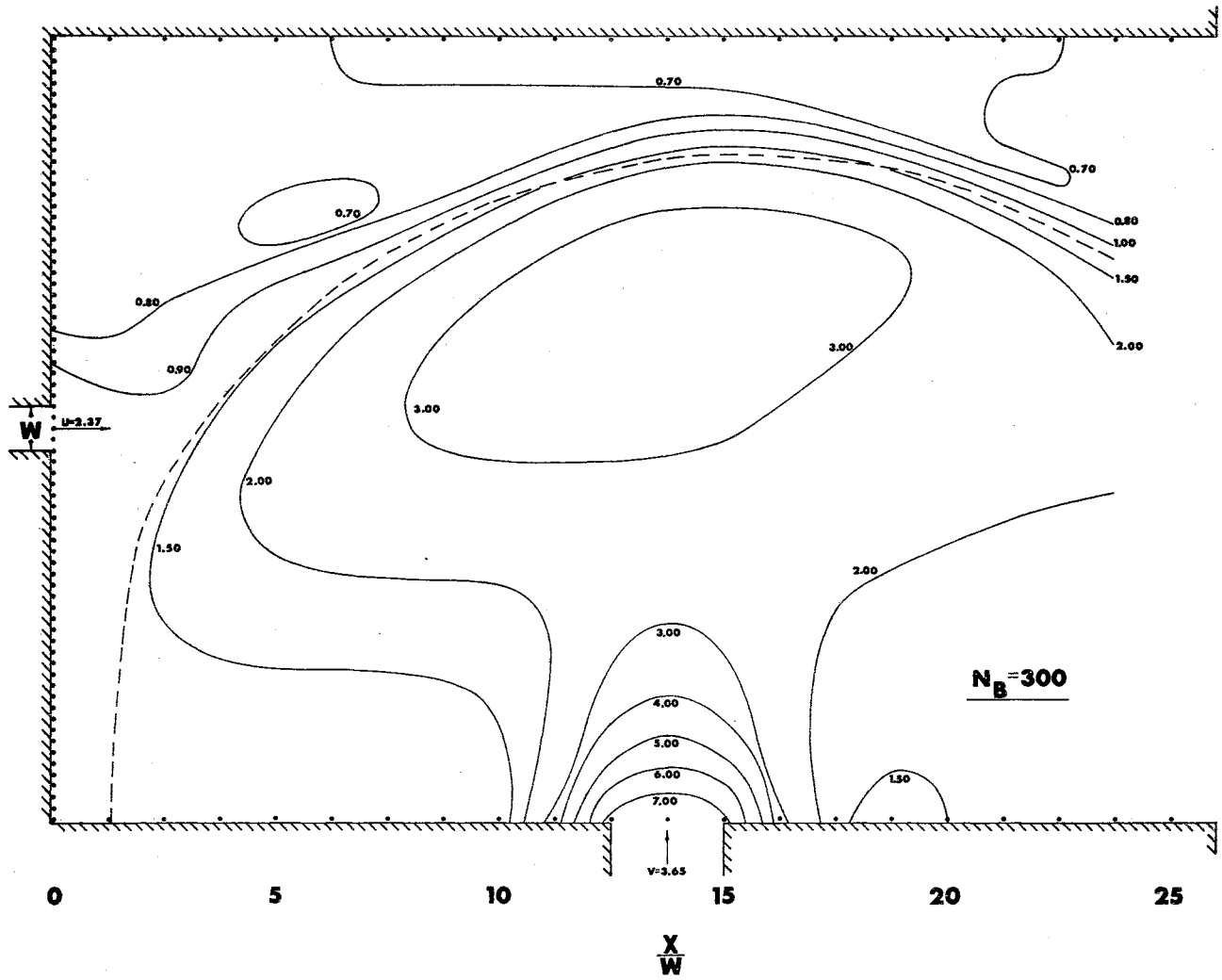

Figure 52. Constant Pressure Lines for Strong Shock Case, $\eta = 0.500$.

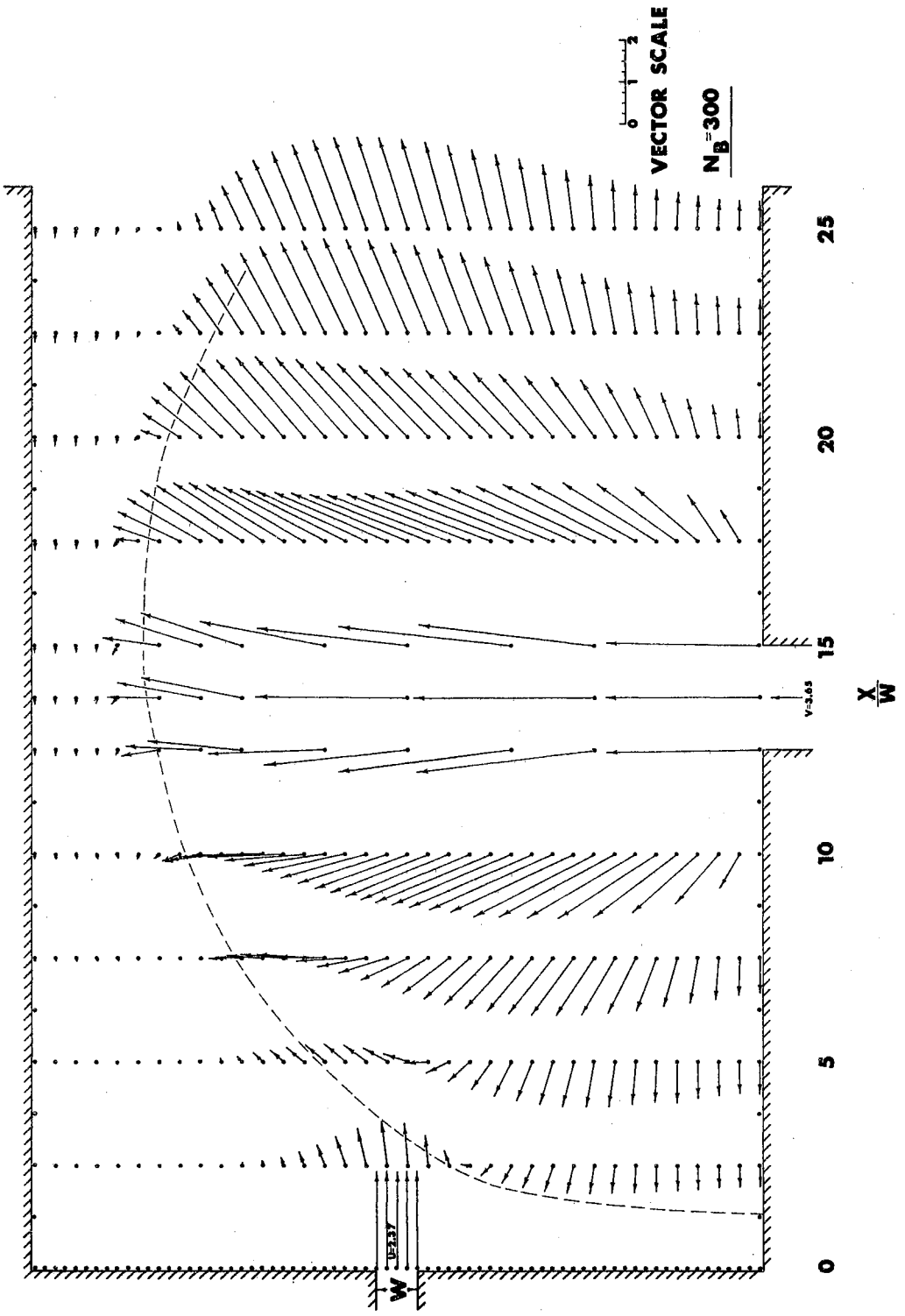

Figure 53. Velocity Vector Field for Strong Shock Case, η = 0.500.

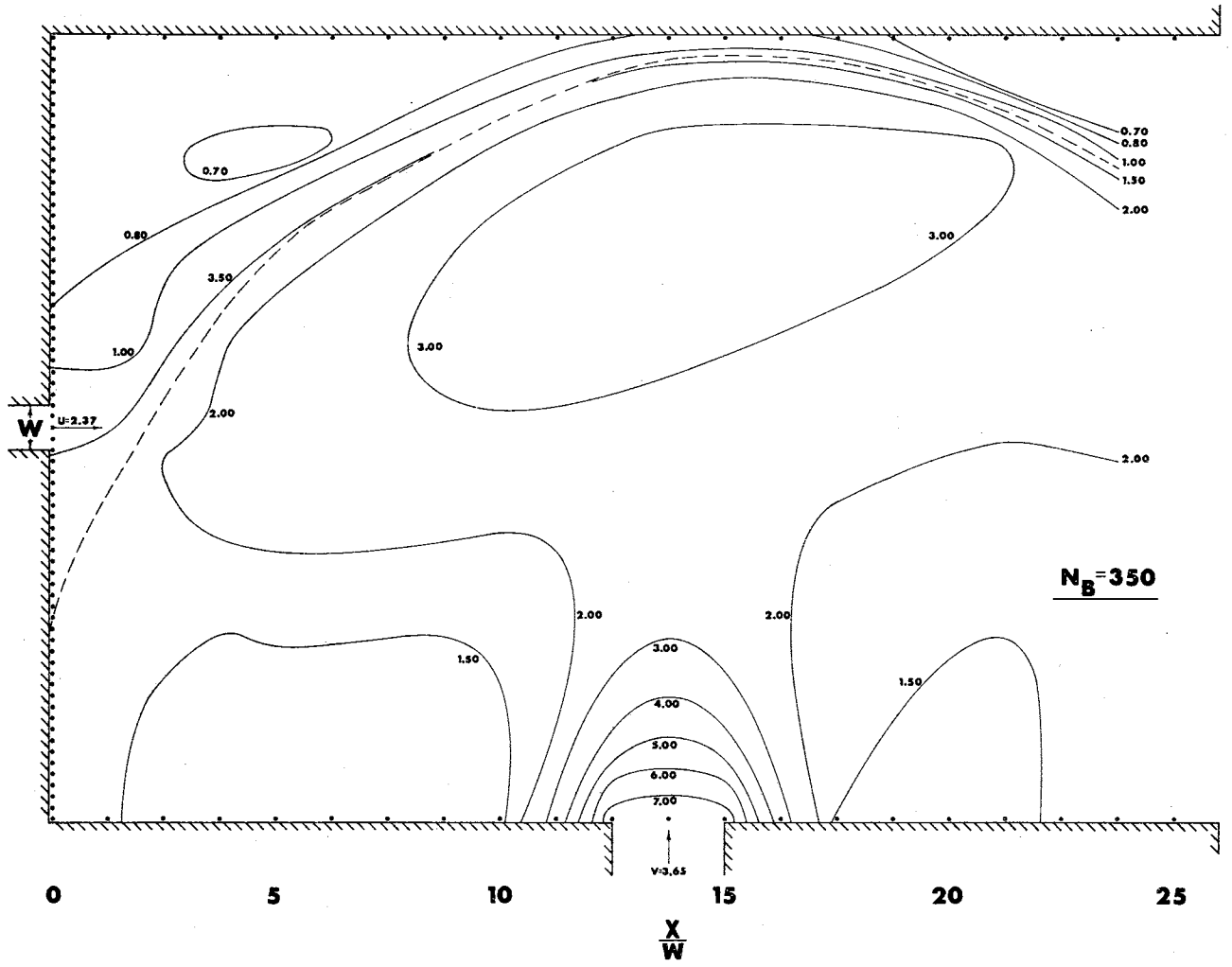

Figure 54. Constant Pressure Lines for Strong Shock Case, $\eta = 0.582$.

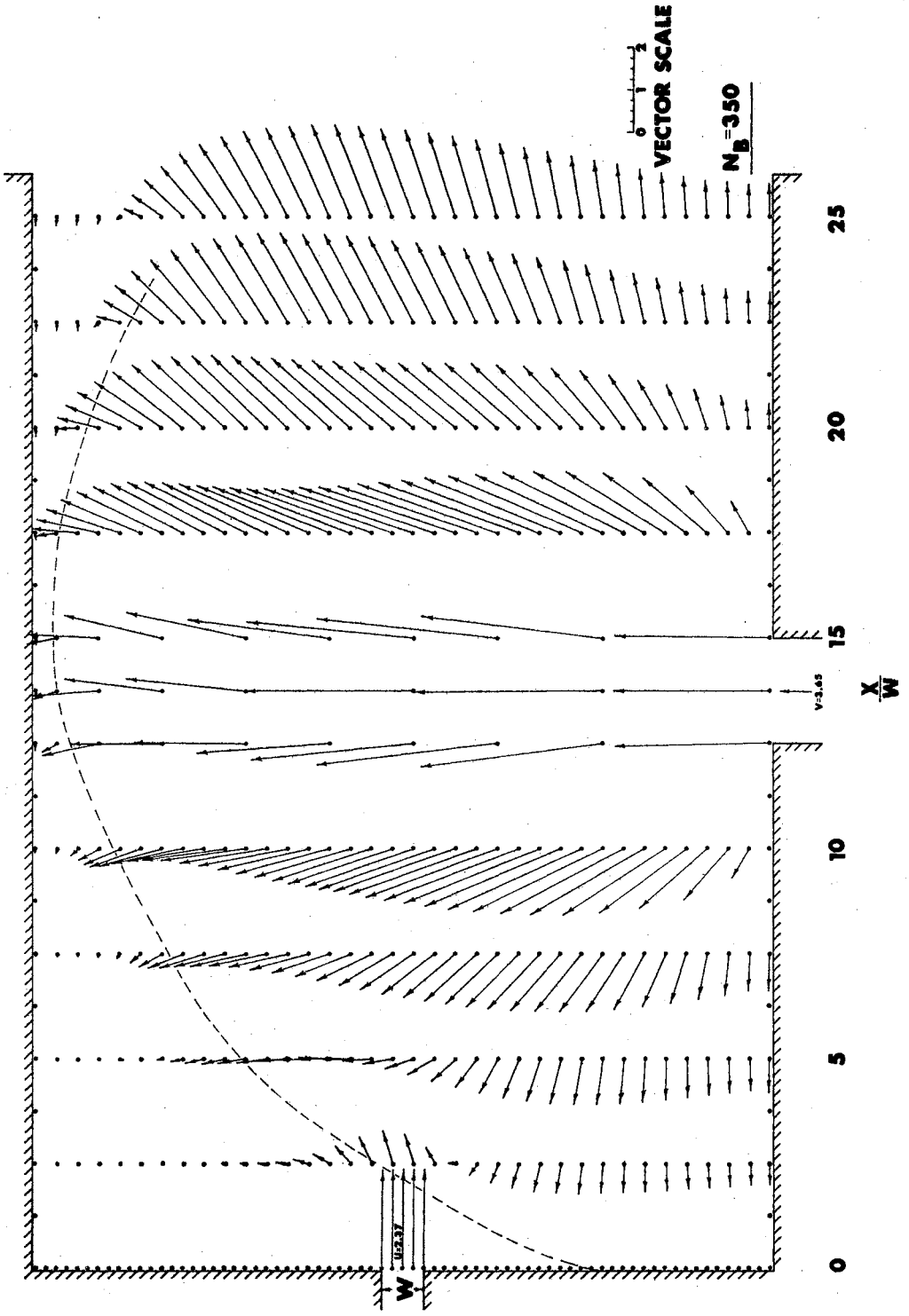

Figure 55. Velocity Vector Field for Strong Shock Case, η = 0.582.

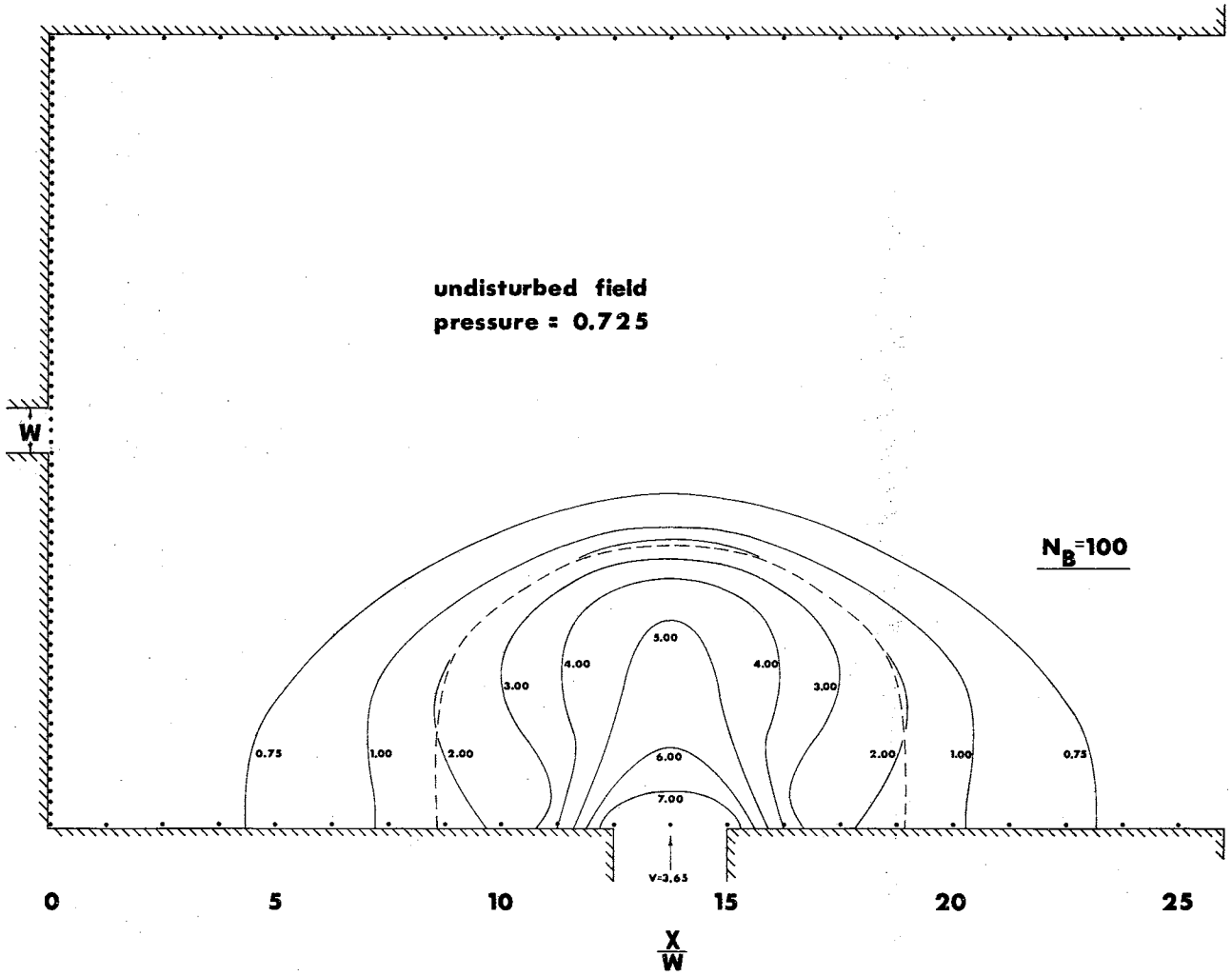

Figure 56. Constant Pressure Lines for Strong Shock Case without Jet, $\eta = 0.169$.

APPENDIX B

DERIVATION OF LAMINAR HYDRODYNAMIC EQUATIONS IN CONSERVATION FORM

The principles of conservation of mass, momentum, and energy will be utilized to derive the hydrodynamic equations in Eulerian coordinates for the unsteady flow of a viscous, compressible fluid. In accordance with the method of solution used in the present study, the equations will be written in the conservation form discussed by Tyler (4).

Conservation of Mass

Figure 57 shows a two-dimensional control volume of unit depth. For such a control volume the principle of conservation of mass can be expressed in the manner of equation (B-1)

$$\left[\begin{array}{l}\text{rate of mass}\\ \text{accumulation}\\ \text{in control}\\ \text{volume}\end{array}\right] = \left[\begin{array}{l}\text{rate of}\\ \text{mass in}\end{array}\right] - \left[\begin{array}{l}\text{rate of}\\ \text{mass out}\end{array}\right] \qquad \text{(B-1)}$$

The rate of mass accumulation in the control volume is $(\Delta x \Delta y)\frac{\partial \rho}{\partial t}$, where ρ is the mass per unit volume (density) of the fluid and x, y, and t are the space and time variables. From Figure 57 the difference between the rate of mass entering and the rate of mass leaving the control volume is easily seen to be

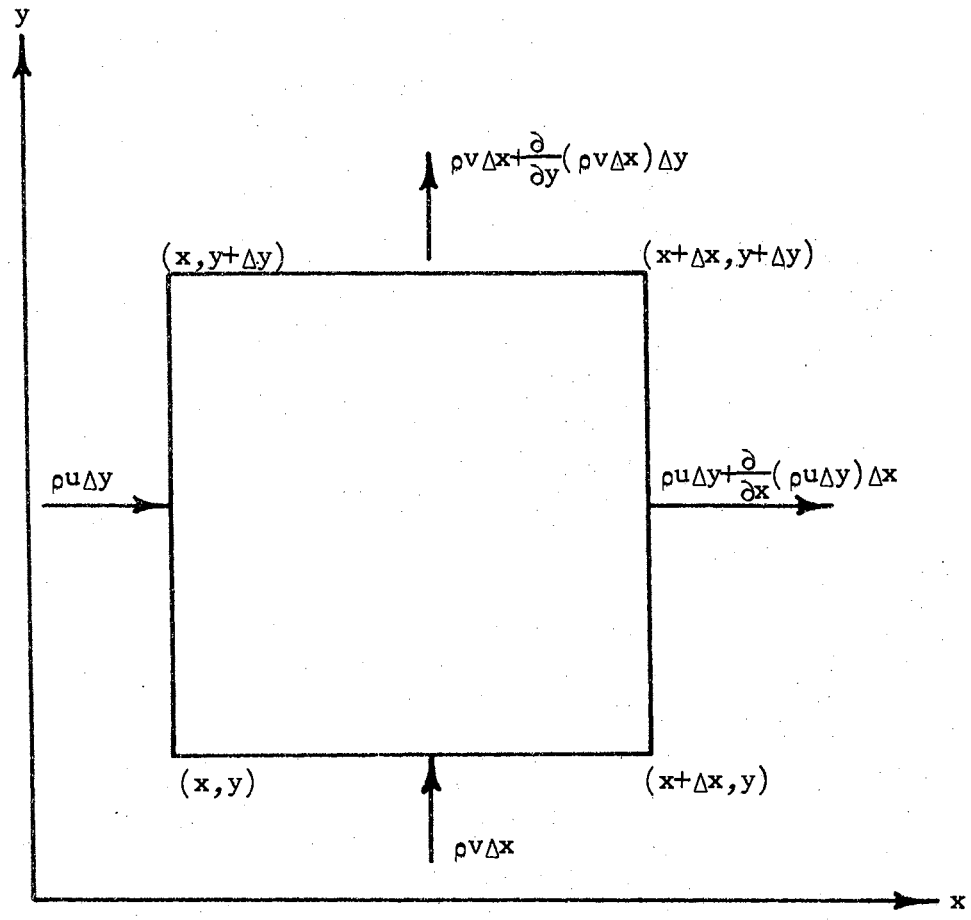

Figure 57. Control Volume for Derivation of Continuity Equation.

$$-\Delta x\Delta y\frac{\partial(\rho u)}{\partial x} - \Delta x\Delta y\frac{\partial(\rho v)}{\partial y} ,$$

where u is the component of velocity in the x-direction and v is the component of velocity in the y-direction. Therefore, by substituting these quantities into equation (B-1) and dividing through by the product $\Delta x\Delta y$, one obtains equation (B-2), the continuity equation in conservation form.

$$\frac{\partial \rho}{\partial t} + \frac{\partial(\rho u)}{\partial x} + \frac{\partial(\rho v)}{\partial y} = 0 \qquad \text{(B-2)}$$

Conservation of Momentum

For a differential volume of fluid at a point in space, the principle of conservation of momentum may be expressed as shown in equation (B-3).

$$\left[\begin{array}{l}\text{Rate of}\\ \text{Momentum}\\ \text{Accumulation}\end{array}\right] = \left[\begin{array}{l}\text{Rate of}\\ \text{Momentum}\\ \text{In}\end{array}\right] - \left[\begin{array}{l}\text{Rate of}\\ \text{Momentum}\\ \text{Out}\end{array}\right] + \left[\begin{array}{l}\text{Net Sum of}\\ \text{Forces Acting}\\ \text{on the System}\end{array}\right] \qquad \text{(B-3)}$$

Equation (B-3) is a vector equation with components, for the two-dimensional case, in both the x and the y directions. Since the derivations are very similar for the conservation of x and y momentum, only the derivation for the x component of momentum will be presented.

Figure 58 illustrates the terms which appear on the right-hand side of equation (B-3). The quantity (ρu) represents the momenta per unit mass in the x-direction while (ρv) represents the momenta per unit

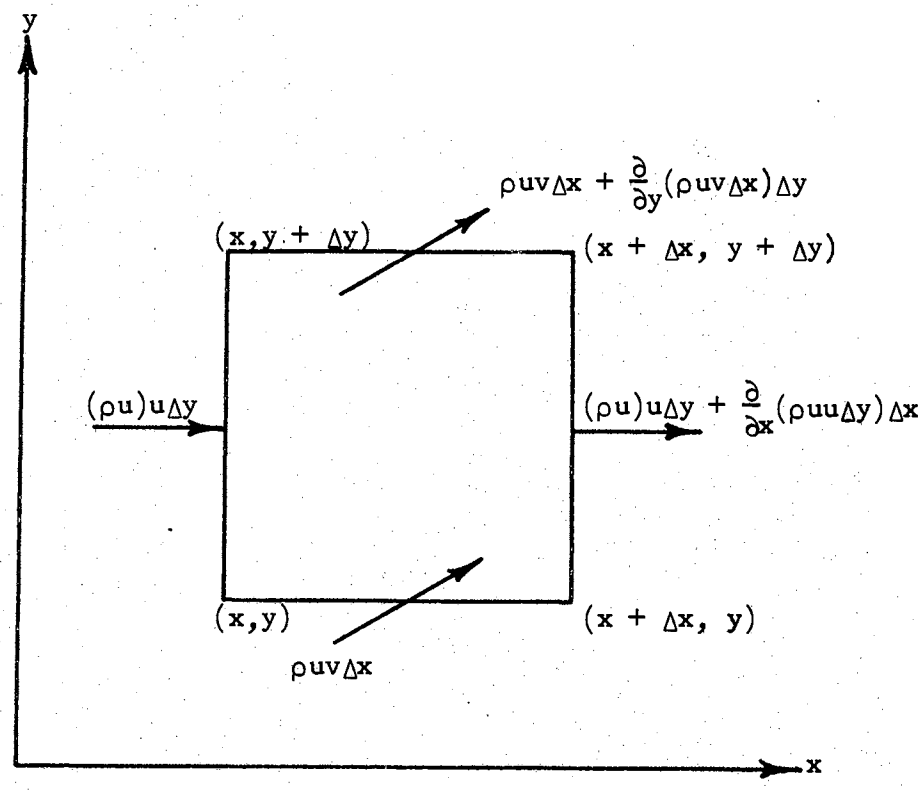

(a) Fluxes of Momentum in the x Direction

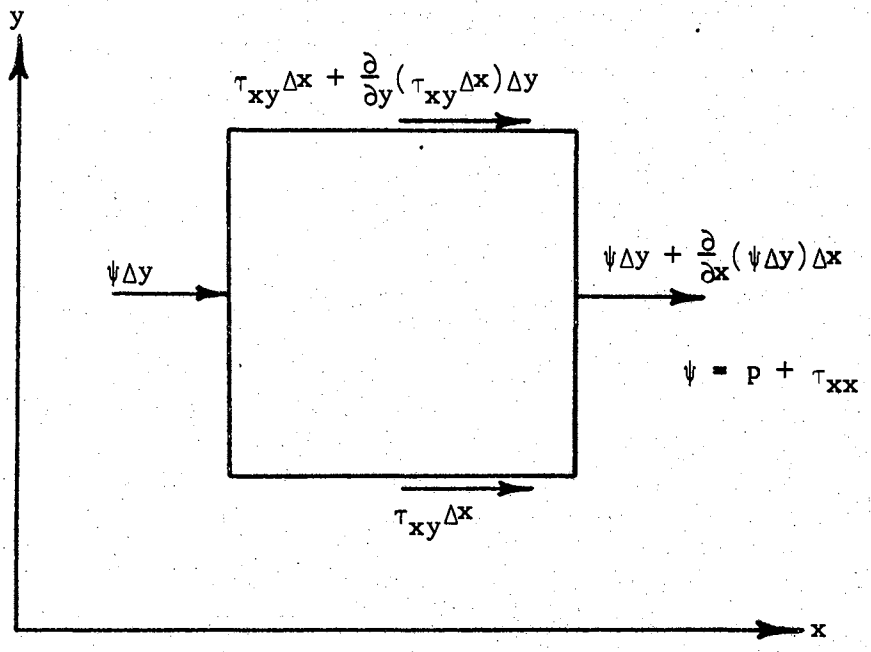

(b) Forces Acting in the x Direction

Figure 58. Control Volumes for Momentum Fluxes and Forces in the x Direction.

mass in the y-direction. The pressure at the point under consideration is denoted as p. The shearing stresses acting on the fluid element are divided into normal, τ_{xx}, and tangential, τ_{xy}, components. Figure 58(a) shows the fluxes of momentum entering and leaving the control volume with respect to the x-direction. Figure 58(b) shows the forces acting on the control volume in the x-direction. The normal force Ψ shown in Figure 58(b) is composed of both the pressure force and the normal shearing force acting on the vertical faces.

The rate of accumulation of x-momentum within the fluid element is $\Delta x \Delta y \frac{\partial(\rho u)}{\partial t}$. Upon substituting the appropriate values from Figure 58 into equation (B-3), equation (B-4) is obtained.

$$\Delta x \Delta y \frac{\partial(\rho u)}{\partial t} = - \Delta x \Delta y \frac{\partial(\rho u^2)}{\partial x} - \Delta x \Delta y \frac{\partial(\rho uv)}{\partial y}$$

$$- \Delta x \Delta y \frac{\partial p}{\partial x} - \Delta x \Delta y \frac{\partial \tau_{xx}}{\partial x} - \Delta x \Delta y \frac{\partial(\tau_{xy})}{\partial y} \quad . \qquad \text{(B-4)}$$

Equation (B-5), which represents the conservation of x-momentum, is obtained by dividing equation (B-4) by the product $\Delta x \Delta y$ and by grouping together quantities whose derivatives are taken in the same spatial direction.

$$\frac{\partial(\rho u)}{\partial t} + \frac{\partial(\rho u^2 + p + \tau_{xx})}{\partial x} + \frac{\partial(\rho uv + \tau_{xy})}{\partial y} = 0 \quad . \qquad \text{(B-5)}$$

Equation (B-5) is in the conservation form required. Equation (B-6), whose derivation is similar to that of equation (B-5), represents the

conservation of momentum in the y-direction.

$$\frac{\partial(\rho v)}{\partial t} + \frac{\partial(\rho uv + \tau_{xy})}{\partial x} + \frac{\partial(\rho v^2 + p + \tau_{yy})}{\partial y} = 0 \quad . \qquad \text{(B-6)}$$

Conservation of Energy

For a differential volume of fluid at a point in space, the principle of conservation of energy may be represented in the manner shown in equation (B-7).

$$\begin{bmatrix}\text{Rate of Accumulation of Internal and Kinetic Energy}\end{bmatrix} = \begin{bmatrix}\text{Net Rate of Internal and Kinetic Energy Addition by Convection}\end{bmatrix} + \begin{bmatrix}\text{Net Rate of Heat Addition by Conduction}\end{bmatrix} - \begin{bmatrix}\text{Net Rate of Work Done by System on the Surroundings}\end{bmatrix} \qquad \text{(B-7)}$$

Figure 59(a) illustrates the control volume depicting the rate of convected internal and kinetic energies. As noted in Figure 59(a) the sum of the internal and kinetic energies is written as

$$e = \rho U + \tfrac{1}{2}\rho w^2 \ ,$$

where U is the specific internal energy and w is the velocity modulus which is given as

$$w = [u^2 + v^2]^{\frac{1}{2}} \ .$$

Figure 59(b) shows the net rate of heat addition by conduction. The heat flux in the x-direction is q_x and that in the y-direction is q_y.

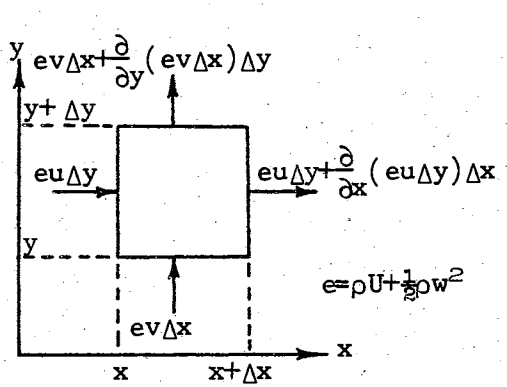

(a) Rates of Internal and Kinetic Energies Transferred by Convection

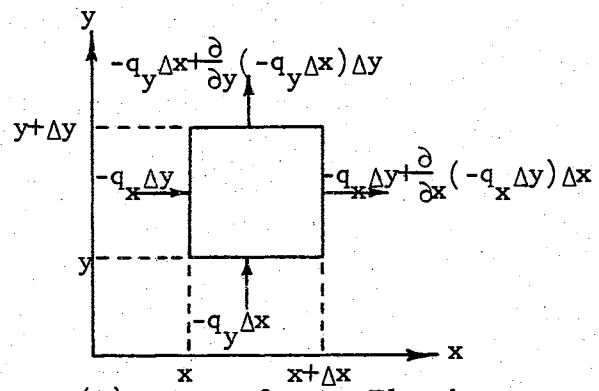

(b) Rates of Heat Flux by Conduction

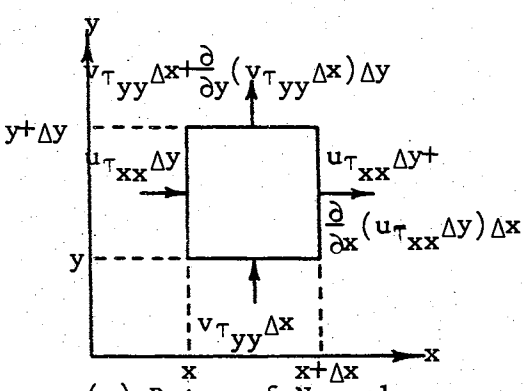

(c) Rates of Normal Shearing Work

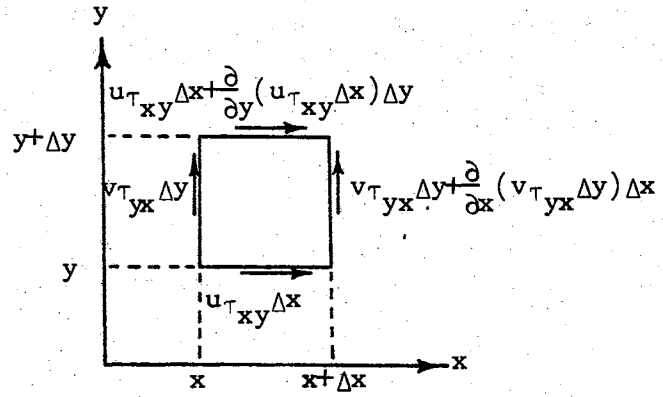

(d) Rates of Tangential Shearing Work

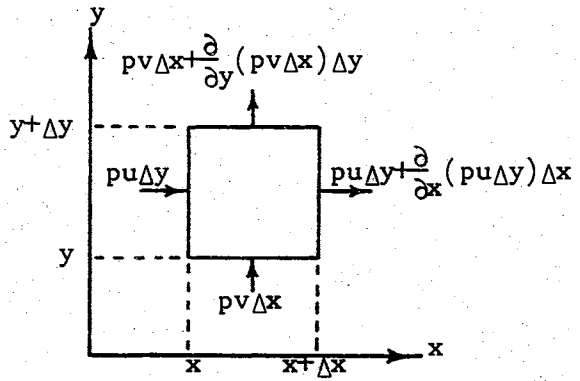

(e) Rates of Work Due to Pressure Forces

Figure 59. Control Volumes for Energy Equation

The rate at which work is done by the system on the surroundings is illustrated in figures 59(c), 59(d), 59(e). The rate of the accumulation of the internal and kinetic energies is $\Delta x \Delta y \frac{\partial e}{\partial t}$. The quantities on the right hand side of equation (B-7) may be taken from the illustrations in Figure 59. In so doing, equation (B-8) is obtained.

$$\Delta x \Delta y \frac{\partial e}{\partial t} = - \Delta x \Delta y \frac{\partial (eu)}{\partial x} - \Delta x \Delta y \frac{\partial (ev)}{\partial y} - \Delta x \Delta y \frac{\partial q_x}{\partial x} - \Delta x \Delta y \frac{\partial q_y}{\partial y} -$$

$$- \Delta x \Delta y \frac{\partial (u\tau_{xx})}{\partial x} - \Delta x \Delta y \frac{\partial (v\tau_{yy})}{\partial y} - \Delta x \Delta y \frac{\partial (v\tau_{yx})}{\partial x} - \Delta x \Delta y \frac{\partial (u\tau_{xy})}{\partial y} -$$

$$- \Delta x \Delta y \frac{\partial (up)}{\partial x} - \Delta x \Delta y \frac{\partial (vp)}{\partial y} \quad . \tag{B-8}$$

By dividing equation (B-8) by $\Delta x \Delta y$ and grouping terms as was done before, one obtains equation (B-9), which is the energy equation in conservation form.

$$\frac{\partial e}{\partial t} + \frac{\partial [(e + p)u + q_x + u\tau_{xx} + v\tau_{xy}]}{\partial x} +$$

$$+ \frac{\partial [(e + p)v + q_y + v\tau_{yy} + u\tau_{xy}]}{\partial y} = 0 \quad . \tag{B-9}$$

The shear stress and heat flux terms which have appeared in the preceeding equations must now be expressed in equation form. For Newtonian fluids, the normal and tangential shearing stresses are given by equations (B-10).

$$\tau_{xx} = -2\mu\frac{\partial u}{\partial x} + \frac{2}{3}\mu\left(\frac{\partial u}{\partial x} + \frac{\partial v}{\partial y}\right)$$

$$\tau_{yy} = -2\mu\frac{\partial v}{\partial y} + \frac{2}{3}\mu\left(\frac{\partial u}{\partial x} + \frac{\partial v}{\partial y}\right) \qquad \text{(B-10)}$$

$$\tau_{xy} = \tau_{yx} = \mu\left(\frac{\partial u}{\partial y} + \frac{\partial v}{\partial x}\right)$$

The coefficient of viscosity, μ, may be either constant or a function of the fluid temperature.

The heat flux terms in equation (B-9) may be evaluated as shown in equation (B-11) with the aid of the Fourier heat conduction equation.

$$q_x = -k\frac{\partial T}{\partial x}$$

$$\qquad \text{(B-11)}$$

$$q_y = -k\frac{\partial T}{\partial y}$$

The coefficient of thermal conductivity, k, may be either constant or a function of the fluid temperature, T.

From the physical principles of conservation of mass, momentum, and energy four equations have been derived. Associated with these equations are the five variables, p, ρ, u, v, and e. The additional equation necessary is, of course, an equation of state such as

$$p = p(\rho, e) \; . \qquad \text{(B-12)}$$

Equations (B-2), (B-5), (B-6), (B-9), (B-10), (B-11), and (B-12) are the equations which govern the unsteady flow of a compressible, viscous fluid.

APPENDIX C

SIGNIFICANCE OF MOLECULAR TRANSPORT TERMS IN THE HYDRODYNAMIC EQUATIONS

The equations derived in Appendix B are the governing equations for the unsteady flow of a viscous, compressible fluid. Since the present investigation is concerned with the description of a turbulent mixing region, the question arises as to which of the molecular transport terms, if any, can be neglected for large Reynolds numbers. In order to answer this question it is necessary to non-dimensionalize the equations of Appendix B with respect to some reference conditions. These conditions will be denoted by the subscript "1". A "bar" will denote non-dimensionalized quantities. Since, for two-dimensional considerations, there is no intrinsic characteristic length, the reference length R will be taken to be one foot. The non-dimensionalized quantities are given in equation (C-1).

$$\bar{\rho} = \frac{\rho}{\rho_1} \quad ; \quad \bar{v} = \frac{v}{V_1} \quad ; \quad \bar{u} = \frac{u}{V_1} \quad ;$$

$$\bar{T} = \frac{T}{T_1} \quad ; \quad \bar{\mu} = \frac{\mu}{\mu_1} \quad ; \quad \bar{k} = \frac{k}{k_1} \quad ; \qquad \text{(C-1)}$$

$$\bar{x} = \frac{x}{R} \quad ; \quad \bar{y} = \frac{y}{R} \quad ; \quad \bar{t} = \frac{t}{R/V_1} \quad .$$

Equations (C-2) give the relationships to be used in non-dimensionalizing the space and time derivatives.

$$\frac{\partial}{\partial x} = \frac{\partial}{\partial \bar{x}} \frac{\partial \bar{x}}{\partial x} = \frac{1}{R} \frac{\partial}{\partial \bar{x}}$$

$$\frac{\partial}{\partial y} = \frac{\partial}{\partial \bar{y}} \frac{\partial \bar{y}}{\partial y} = \frac{1}{R} \frac{\partial}{\partial \bar{y}} \qquad \text{(C-2)}$$

$$\frac{\partial}{\partial t} = \frac{\partial}{\partial \bar{t}} \frac{\partial \bar{t}}{\partial t} = \frac{V_1}{R} \frac{\partial}{\partial \bar{t}}$$

Continuity Equation

By substituting equations (C-1) and (C-2) into equation (B-2), equation (C-3) is obtained.

$$\frac{\rho_1 V_1}{R} \frac{\partial \bar{\rho}}{\partial \bar{t}} + \frac{\rho_1 V_1}{R} \frac{\partial(\bar{\rho}\bar{u})}{\partial \bar{x}} + \frac{\rho_1 V_1}{R} \frac{\partial(\bar{\rho}\bar{v})}{\partial \bar{y}} = 0 \qquad \text{(C-3)}$$

Thus, the non-dimensional continuity equation is:

$$\frac{\partial \bar{\rho}}{\partial \bar{t}} + \frac{\partial(\bar{\rho}\bar{u})}{\partial \bar{x}} + \frac{\partial(\bar{\rho}\bar{v})}{\partial \bar{y}} = 0 \; . \qquad \text{(C-4)}$$

Momentum Equations

Before non-dimensionalizing the momentum equations, it will facilitate matters to obtain the normal and tangential shear stress equations in terms of the non-dimensional and reference values. This is accomplished by substituting equations (C-1) and (C-2) into equations (B-10).

$$\tau_{xx} = \frac{\mu_1 V}{R}\left[-2\bar{\mu}\frac{\partial \bar{u}}{\partial \bar{x}} + \frac{2}{3}\bar{\mu}\left(\frac{\partial \bar{u}}{\partial \bar{x}} + \frac{\partial \bar{v}}{\partial \bar{y}}\right)\right]$$

$$\tau_{yy} = \frac{\mu_1 V}{R}\left[-2\bar{\mu}\frac{\partial \bar{v}}{\partial \bar{y}} + \frac{2}{3}\bar{\mu}\left(\frac{\partial \bar{u}}{\partial \bar{x}} + \frac{\partial \bar{v}}{\partial \bar{y}}\right)\right] \qquad \text{(C-5)}$$

$$\tau_{xy} = \frac{\mu_1 V}{R}\left[-\bar{\mu}\left(\frac{\partial \bar{u}}{\partial \bar{y}} + \frac{\partial \bar{v}}{\partial \bar{x}}\right)\right]$$

The quantities inside the brackets in equations (C-5) are nothing more than non-dimensional normal and tangential shearing stresses. Therefore if the non-dimensional quantities

$$\bar{\tau}_{xx} = -2\bar{\mu}\frac{\partial \bar{u}}{\partial \bar{x}} + \frac{2}{3}\bar{\mu}\left(\frac{\partial \bar{u}}{\partial \bar{x}} + \frac{\partial \bar{v}}{\partial \bar{y}}\right),$$

$$\bar{\tau}_{yy} = -2\bar{\mu}\frac{\partial \bar{v}}{\partial \bar{y}} + \frac{2}{3}\bar{\mu}\left(\frac{\partial \bar{u}}{\partial \bar{x}} + \frac{\partial \bar{v}}{\partial \bar{y}}\right),$$

$$\bar{\tau}_{xy} = -\bar{\mu}\left(\frac{\partial \bar{u}}{\partial \bar{y}} + \frac{\partial \bar{v}}{\partial \bar{x}}\right),$$

are defined, equations (C-5) may be expressed as in equation (C-6).

$$\tau_{xx} = \frac{\mu_{1\,1} V}{R} \bar{\tau}_{xx}$$

$$\tau_{yy} = \frac{\mu_{1\,1} V}{R} \bar{\tau}_{yy} \qquad \text{(C-6)}$$

$$\tau_{xy} = \frac{\mu_{1\,1} V}{R} \bar{\tau}_{xy}$$

x-Momentum

If one substitutes equations (C-1), (C-2), and (C-6) into equation (B-5) for the x component of momentum, equation (C-7) is obtained.

$$\frac{\rho_{1\,1} V^2}{R} \frac{\partial(\bar{\rho}\bar{u})}{\partial t} + \frac{1}{R} \frac{\partial}{\partial \bar{x}} \left[\rho_{1\,1} V^2 \bar{\rho}\bar{u}^2 + p + \frac{\mu_{1\,1} V}{R} \bar{\tau}_{xx} \right] +$$

$$+ \frac{1}{R} \frac{\partial}{\partial \bar{y}} \left[\rho_{1\,1} V^2 \bar{\rho}\bar{u}\bar{v} + \frac{\mu_{1\,1} V}{R} \bar{\tau}_{xy} \right] = 0 \qquad \text{(C-7)}$$

Upon dividing equation (C-7) by $\rho_{1\,1} V^2/R$ it is noted that the non-dimensionalizing quantity for the pressure is $\rho_{1\,1} V^2$. Thus the non-dimensional pressure is expressed as

$$\bar{p} = \frac{p}{\rho_{1\,1} V^2} \,. \qquad \text{(C-8)}$$

When the coefficients of the shear stress terms are divided by $\rho_1 V_1^2$ the Reynolds number (N_{Re}) appears, where for this investigation the Reynolds number is defined as

$$N_{Re} = \frac{\rho_1 V_1 R}{\mu_1} \quad , \tag{C-9}$$

The resulting non-dimensionalized equation of x-momentum takes the form of equation (C-10).

$$\frac{\partial(\bar{\rho}\bar{u})}{\partial t} + \frac{\partial}{\partial \bar{x}}\left[\bar{\rho}\,\bar{u}^2 + \bar{p} + \frac{\bar{\tau}_{xx}}{N_{Re}} \right] +$$

$$+ \frac{\partial}{\partial \bar{y}}\left[\bar{\rho}\,\bar{u}\,\bar{v} + \frac{\bar{\tau}_{xy}}{N_{Re}} \right] = 0 \tag{C-10}$$

y-Momentum

By non-dimensionalizing equation (B-6) in the same manner as was done for equation (B-5), the non-dimensionalized equation (C-11) for y-momentum is obtained.

$$\frac{\partial(\bar{\rho}\,\bar{v})}{\partial t} + \frac{\partial}{\partial \bar{x}}\left[\bar{\rho}\,\bar{u}\,\bar{v} + \frac{\bar{\tau}_{xy}}{N_{Re}} \right] +$$

$$+ \frac{\partial}{\partial \bar{y}}\left[\bar{\rho}\,\bar{v}^2 + \bar{p} + \frac{\bar{\tau}_{yy}}{N_{Re}} \right] = 0 \tag{C-11}$$

Energy Equation

The energy equation (B-9) will be non-dimensionalized with the aid of equations (C-1), (C-2), and (C-6). However it will be advantageous to write the energy term, e, from equation (B-9) in terms of non-dimensional and reference quantities. As previously noted, e is defined as the sum of the specific internal energy and the kinetic energy, or

$$e = \rho U + \rho \frac{u^2 + v^2}{2} \quad . \tag{C-12}$$

For an ideal gas, equation (C-12) may be written as

$$e = \frac{p}{\gamma - 1} + \rho \left(\frac{u^2 + v^2}{2} \right) , \tag{C-13}$$

where γ denotes the ratio of specific heats.

If the appropriate non-dimensional and reference quantities from equations (C-1) and (C-8) are substituted into equation (C-13), the result is

$$e = \rho_1 V_1^2 \left[\frac{\bar{p}}{\gamma - 1} + \bar{\rho} \frac{\bar{u}^2 + \bar{v}^2}{2} \right] . \tag{C-14}$$

If a non-dimensional e is defined as

$$\bar{e} = \frac{\bar{p}}{\gamma - 1} + \bar{\rho} \frac{\bar{u}^2 + \bar{v}^2}{2} \quad , \tag{C-15}$$

then equation (C-14) may be written as

$$e = \rho_1 V_1^2 \bar{e} \quad . \tag{C-16}$$

In order to non-dimensionalize the energy equation, the non-dimensional quantities previously defined, along with equations (C-6) and (C-16), must be incorporated into equation (B-9). If one makes the indicated substitutions, and divides the resulting equation by $\rho_1 V_1^3/R$, equation (C-17) will be obtained.

$$\frac{\partial \bar{e}}{\partial t} + \frac{\partial}{\partial x}\left[(\bar{e} + \bar{p})\,\bar{u} - \frac{k_1 T_1 \bar{k}}{\rho_1 V_1^3 R}\frac{\partial \bar{T}}{\partial \bar{x}} + \frac{\bar{u}\,\bar{\tau}_{xx}}{N_{Re}} + \frac{\bar{v}\,\bar{\tau}_{xy}}{N_{Re}} \right] +$$

$$+ \frac{\partial}{\partial \bar{y}}\left[(\bar{e} + \bar{p})\,\bar{v} - \frac{k_1 T_1 \bar{k}}{\rho_1 V_1^3 R}\frac{\partial \bar{T}}{\partial \bar{y}} + \frac{\bar{v}\,\bar{\tau}_{yy}}{N_{Re}} + \frac{\bar{u}\,\bar{\tau}_{xy}}{N_{Re}} \right] = 0 \qquad \text{(C-17)}$$

As was done in the momentum equations, the Reynolds number (N_{Re}) has been used in equation (C-17). The coefficients of the terms representing molecular energy transport in equation (C-17) can be written, as shown in equation (C-18), in terms of the Reynolds number (N_{Re}), Prandtl number (N_{Pr}), Mach number (M_1), and ratio of specific heats, where

$$N_{Pr} = \frac{\mu_1 c_p}{k_1}$$

and

$$M = \frac{V_1}{C_1} .$$

$$\frac{k_1 T_1}{\rho_1 V_1^3 R} \frac{\mu_1}{\mu_1} = \frac{1}{N_{Re}} \frac{k_1 T_1}{V_1^2 \mu_1} \frac{c_p}{c_p} = \frac{1}{N_{Re} N_{Pr}} \frac{T_1 c_p}{V_1^2} \frac{\gamma R}{\gamma R}$$

$$= \frac{1}{N_{Re} N_{Pr} M_1^2 \gamma R} c_p = \frac{1}{N_{Re} N_{Pr} M_1^2 (\gamma - 1)} \qquad \text{(C-18)}$$

If equation (C-18) is substituted into equation (C-17), the non-dimensionalized form of the energy equation (C-19) is obtained.

$$\frac{\partial \bar{e}}{\partial t} + \frac{\partial}{\partial \bar{x}} \left[(\bar{e} + \bar{p}) \bar{u} - \frac{\bar{k}}{N_{Re} N_{Pr} M_1^2 (\gamma - 1)} \frac{\partial \bar{T}}{\partial \bar{x}} + \frac{\bar{u} \bar{\tau}_{xx}}{N_{Re}} + \right.$$

$$\left. + \frac{\bar{v} \bar{\tau}_{xy}}{N_{Re}} \right] + \frac{\partial}{\partial \bar{y}} \left[(\bar{e} + \bar{p}) \bar{v} - \frac{\bar{k}}{N_{Re} N_{Pr} M_1^2 (\gamma - 1)} \frac{\partial \bar{T}}{\partial \bar{y}} + \right.$$

$$\left. + \frac{\bar{v} \tau_{yy}}{N_{Re}} + \frac{\bar{u} \bar{\tau}_{xy}}{N_{Re}} \right] = 0 \qquad \text{(C-19)}$$

As was pointed out previously, the purpose of this appendix is to ascertain which, if any, of the molecular transport terms, for the equations of Appendix B, can be neglected under the assumptions of the present investigation. Since no molecular transport terms occur in the continuity equation, only the momentum and energy equations will be considered. In both the momentum equations, (C-10) and (C-11), there appear normal and tangential shearing stresses divided by the Reynolds number. For all cases to be considered, it will be assumed that the Reynolds number is not less than 10^5.

Therefore since

$$O\left[\bar{\rho}\right] = O\left[\bar{u}\right] = O\left[\bar{v}\right] = O\left[\bar{p}\right] = O\left[\bar{\tau}\right], \quad \text{(C-20)}$$

then

$$O\left[\bar{\rho}\,\bar{u}^2 + \bar{p}\right] \gg O\left[\frac{\bar{\tau}_{xx}}{N_{Re}}\right] \quad \text{(C-21)}$$

and

$$O\left[\rho\, u\, v\right] \gg O\left[\frac{\bar{\tau}_{xy}}{N_{Re}}\right].$$

The same conclusions hold for the y-momentum equation. Thus, so long as the Reynolds number remains at a sufficiently large value, the terms representing molecular transport are small compared to the terms representing overall momentum transport.

Similar reasoning applies to the energy equation. The terms which represent the shearing work are divided by the Reynolds number and are, therefore, small when compared with $(e + p)u$ or $(e + p)v$. The coefficients of the temperature gradient terms, though not as small as the coefficients of the shearing work terms, are sufficiently small to be considered negligible when compared with $(e + p)u$ or $(e + P)v$. Therefore in the energy equation the terms representing molecular effects are small when compared with the terms which represent the fluxes of internal and kinetic energy and pressure work.

The equations which describe the two-dimensional jet mixing process are derived in Chapter III. These equations contain terms which

represent the turbulent transport phenomenon. Van Driest (15) and Pai (29) have noted that the contributions to momentum and energy transport made by the turbulence terms outweigh any contributions on the molecular scale. This fact, in conjunction with the previous analysis, provides sufficient justification for completely neglecting any laminar contribution in the turbulent jet mixing analysis. Therefore, the equations upon which the turbulent jet mixing analysis will be based are:

Continuity,

$$\frac{\partial \rho}{\partial t} + \frac{\partial(\rho u)}{\partial x} + \frac{\partial(\rho v)}{\partial y} = 0 \quad ; \qquad \text{(C-22)}$$

x-Momentum,

$$\frac{\partial(\rho u)}{\partial t} + \frac{\partial(\rho u^2 + p)}{\partial x} + \frac{\partial(\rho uv)}{\partial y} = 0 \quad ; \qquad \text{(C-23)}$$

y-Momentum,

$$\frac{\partial(\rho v)}{\partial t} + \frac{\partial(\rho uv)}{\partial x} + \frac{\partial(\rho v^2 + p)}{\partial y} = 0 \quad ; \qquad \text{(C-24)}$$

Energy,

$$\frac{\partial e}{\partial t} + \frac{\partial(e + p)u}{\partial x} + \frac{\partial(e + p)v}{\partial y} = 0 \quad . \qquad \text{(C-25)}$$

APPENDIX D

REPRESENTATION OF (ρu), (ρv), AND e AS FLUID PROPERTIES

The representation of (ρu) and (ρv) as fluid properties was originally suggested by Van Driest (15) as a mathematical simplification in turbulence analysis. The author has chosen to represent the fluid energy, e, in the same manner in the present investigation. The requirements which must be met by the turbulent fluctuating components, whenever this representation is utilized, is presented in this appendix. Only the x-momenta per unit mass, (ρu), and the specific fluid energy, e, will be discussed since the requirements for (ρv) will be similar to those for (ρu).

In order to be able to represent the instantaneous value of (ρu) as

$$\rho u = \overline{(\rho u)} + (\rho u)' \qquad \text{(D-1)}$$

it must be established that the instantaneous value of (ρu) obtained in the more familiar form

$$\rho u = (\bar{\rho} + \rho')(\bar{u} + u') \qquad \text{(D-2)}$$

is identical to that given in equation (D-1). From equation (D-2) therefore

$$\rho u = \bar{\rho}\bar{u} + \bar{\rho}u' + \rho'\bar{u} + \rho'u' \quad ; \qquad \text{(D-3)}$$

the time average of equation (D-3) is (see equation (3-6)),

$$\overline{\rho u} = \bar{\rho}\bar{u} + \overline{\rho' u'} \quad . \tag{D-4}$$

If equations (D-3) and (D-1) are equated, the result is

$$\overline{\rho u} + (\rho u)' = \bar{\rho}\bar{u} + \bar{\rho}u' + \rho'\bar{u} + \rho' u' \quad . \tag{D-5}$$

By adding and subtracting $\overline{\rho' u'}$ to the right side of equation (D-5), and simplifying according to equation (D-4), the necessary expression for $(\rho u)'$ is obtained.

$$(\rho u)' = \bar{\rho}u' + \rho'\bar{u} + \rho' u' - \overline{\rho' u'} \tag{D-6}$$

Equation (D-6) then shows the form which the term $(\rho u)'$ must have if the quantity (ρu) is to be represented as in equation (D-1). Similarly, the expression for $(\rho v)'$ is

$$(\rho v)' = \bar{\rho}v' + \rho'\bar{v} + \rho' v' - \overline{\rho' v'} \quad . \tag{D-7}$$

When using the shorthand form for representing the instantaneous values of (ρu) and (ρv), the question might arise as to the correct method of representing the instantaneous value of the product (ρuv). Three possible choices exist and are

$$\rho uv = (\bar{\rho} + \rho')(\bar{u} + u')(\bar{v} + v') \tag{D-8}$$

$$\rho uv = [\,\overline{(\rho u)} + (\rho u)'\,](\bar{v} + v') \tag{D-9}$$

$$\rho uv = [\,\overline{(\rho v)} + (\rho v)'\,](\bar{u} + u') \quad . \tag{D-10}$$

Under the assumptions of equations (D-6) and (D-7) the right hand side of equations (D-8), (D-9), and (D-10) are found to be equivalent. Thus any of the three representations may be used for expressing the instantaneous value of the product (ρuv).

In order to represent the instantaneous value of the fluid energy as the sum of a temporal mean and fluctuating component, it will be necessary to determine the expression for the fluctuating component, e'. The defining equation for the fluid energy is

$$e = \frac{p}{\gamma - 1} + \frac{\rho u^2 + \rho v^2}{2} \quad . \tag{D-11}$$

If the instantaneous pressure, density, and velocities on the right side of equation (D-11) are replaced by their time average and fluctuating components, equation (D-12) for the instantaneous value of e is obtained.

$$e = \frac{\tilde{p} + p'}{\gamma - 1} + \frac{[\overline{(\rho u)} + (\rho u)'](\tilde{u} + u') + [\overline{(\rho v)} + (\rho v)'](\tilde{v} + v')}{2}$$

or

$$e = \frac{\tilde{p} + p'}{\gamma - 1} + \frac{\overline{\rho u}\,\tilde{u} + \overline{\rho u}\,u' + (\rho u)'\tilde{u} + (\rho u)'u'}{2} +$$

$$+ \frac{\overline{\rho v}\,\tilde{v} + \overline{\rho v}\,v' + (\rho v)'\tilde{v} + (\rho v)'v'}{2} \tag{D-12}$$

The time average of e is then

$$\bar{e} = \frac{\bar{p}}{\gamma - 1} + \frac{\overline{\rho u}\,\bar{u} + \overline{(\rho u)'u'} + \overline{\rho v}\,\bar{v} + \overline{(\rho v)'v'}}{2} \quad . \tag{D-13}$$

If it is assumed that the energy term can be written as the sum of a temporal mean and a fluctuating component, the fluctuation term may be expressed as

$$e' = e - \bar{e} \quad . \tag{D-14}$$

Therefore by subtracting equation (D-13) from equation (D-12) the expression for e' is obtained which allows the instantaneous value of e to be written as

$$e = \bar{e} + e' \, .$$

The resulting expression for e' is

$$e' = \frac{p'}{\gamma - 1} + \frac{1}{2}\left[\overline{\rho u}\,u' + (\rho u)'\bar{u} + (\rho u)'u' - \right.$$

$$\left. - \overline{(\rho u)'u'} + \overline{\rho v}\,v' + (\rho v)'\bar{v} + (\rho v)'v' - \overline{(\rho v)'v'}\right] \, . \tag{D-15}$$

APPENDIX E

COMPUTER LOGIC DIAGRAM

The many problem solutions which have been computed during the course of this investigation have all been obtained with the use of one basic computer program. The logic diagram for that basic program is presented in this appendix. The definitions of the terms which appear in the logic diagram are as follows:

NROW	number of rows
NCOL	number of columns
M	an arbitrary logical tape unit
NTIMES	number of time planes to be calculated
NPRINT	printout interval
DELTAX	Δx
DELTAY	Δy
GAMA	γ
CONST	$\frac{u_a}{2\sigma^2}$
XINIT	position of leftmost column of matrix with respect to an arbitrarily defined origin
SIGMA	$\bar{\sigma}_o$
ANGLE	χ
RHO	density at time plane n

U	x-component of velocity at time plane n
V	y-component of velocity at time plane n
P	pressure at time plane n
RHON	density at time plane n + 1
UN	x-component of velocity at time plane n + 1
VN	y-component of velocity at time plane n + 1
PN	pressure at time plane n + 1
PTKND	denotes kind of point under consideration, field or boundary
NT	time plane counter
NPRT	print interval counter
I	row counter
J	column counter
II	row counter

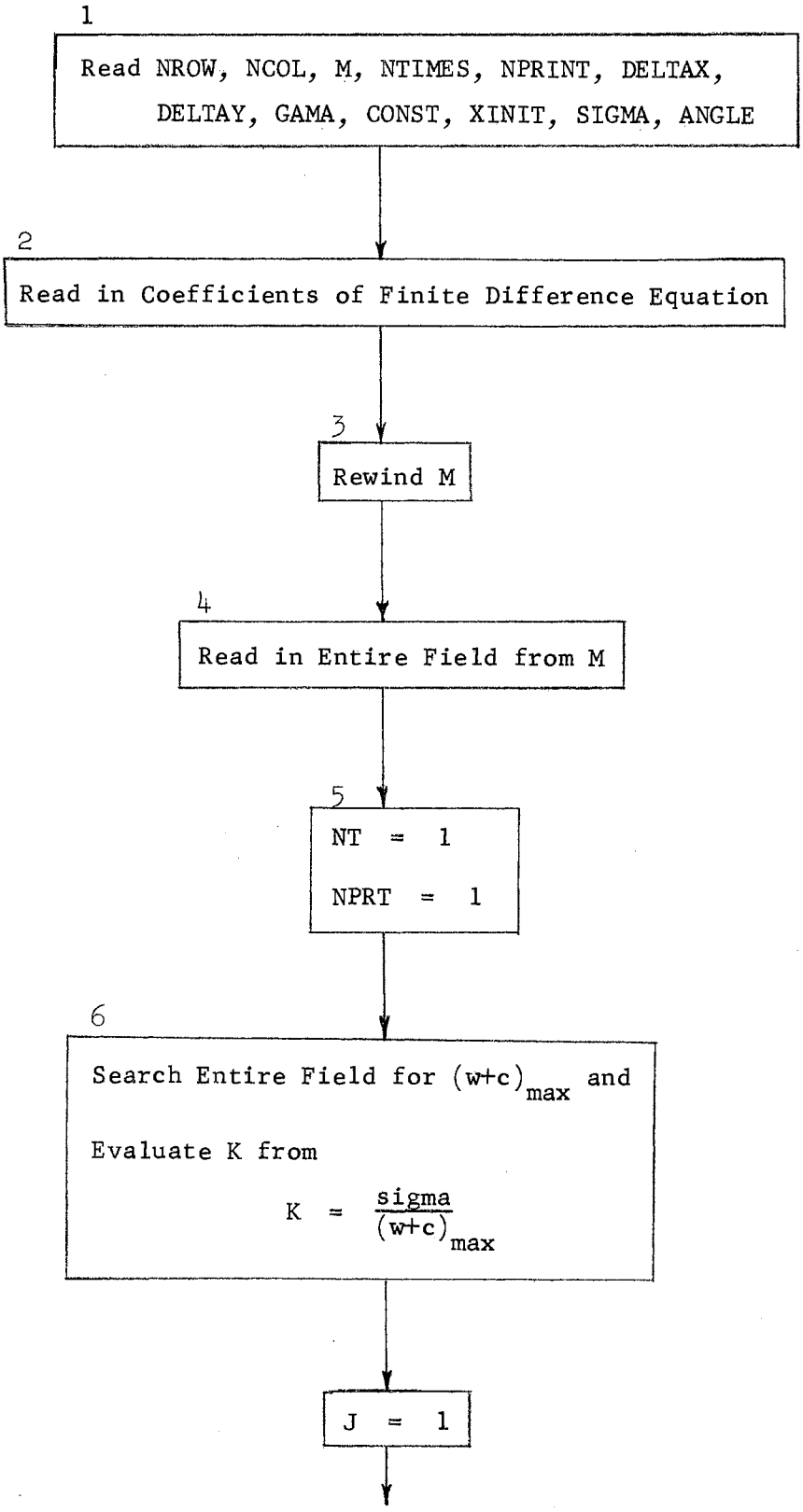
1
Read NROW, NCOL, M, NTIMES, NPRINT, DELTAX,
DELTAY, GAMA, CONST, XINIT, SIGMA, ANGLE
2
Read in Coefficients of Finite Difference Equation
3
Rewind M
4
Read in Entire Field from M
5
NT = 1
NPRT = 1
6
Search Entire Field for $(w+c)_{max}$ and
Evaluate K from
$K = \frac{sigma}{(w+c)_{max}}$
J = 1

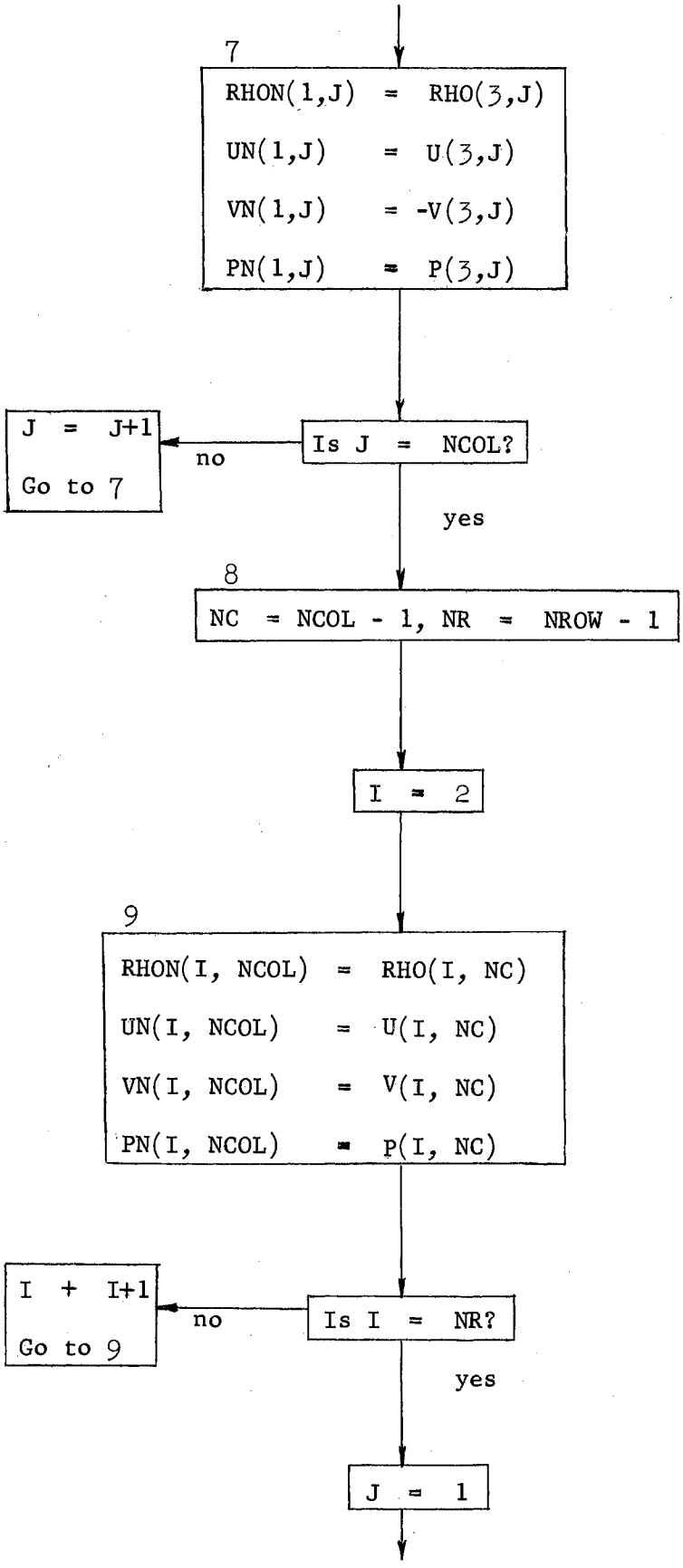
7
RHON(1,J) = RHO(3,J)
UN(1,J) = U(3,J)
VN(1,J) = -V(3,J)
PN(1,J) = P(3,J)
Is J = NCOL?
no
J = J+1
Go to 7
yes
8
NC = NCOL - 1, NR = NROW - 1
I = 2
9
RHON(I, NCOL) = RHO(I, NC)
UN(I, NCOL) = U(I, NC)
VN(I, NCOL) = V(I, NC)
PN(I, NCOL) = P(I, NC)
Is I = NR?
no
I + I+1
Go to 9
yes
J = 1

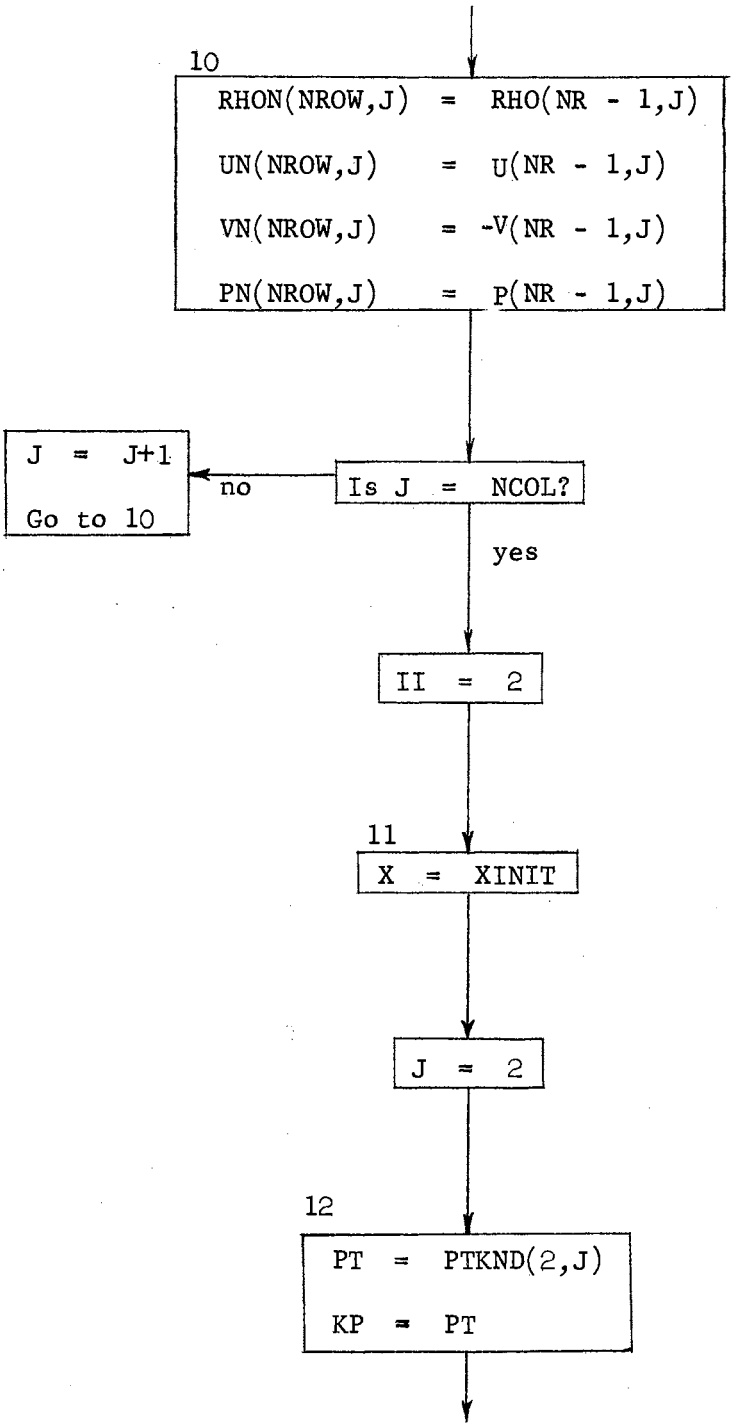
10
RHON(NROW,J) = RHO(NR - 1,J)
UN(NROW,J) = U(NR - 1,J)
VN(NROW,J) = -V(NR - 1,J)
PN(NROW,J) = P(NR - 1,J)
Is J = NCOL?
no
J = J+1
Go to 10
yes
II = 2
11
X = XINIT
J = 2
12
PT = PTKND(2,J)
KP = PT

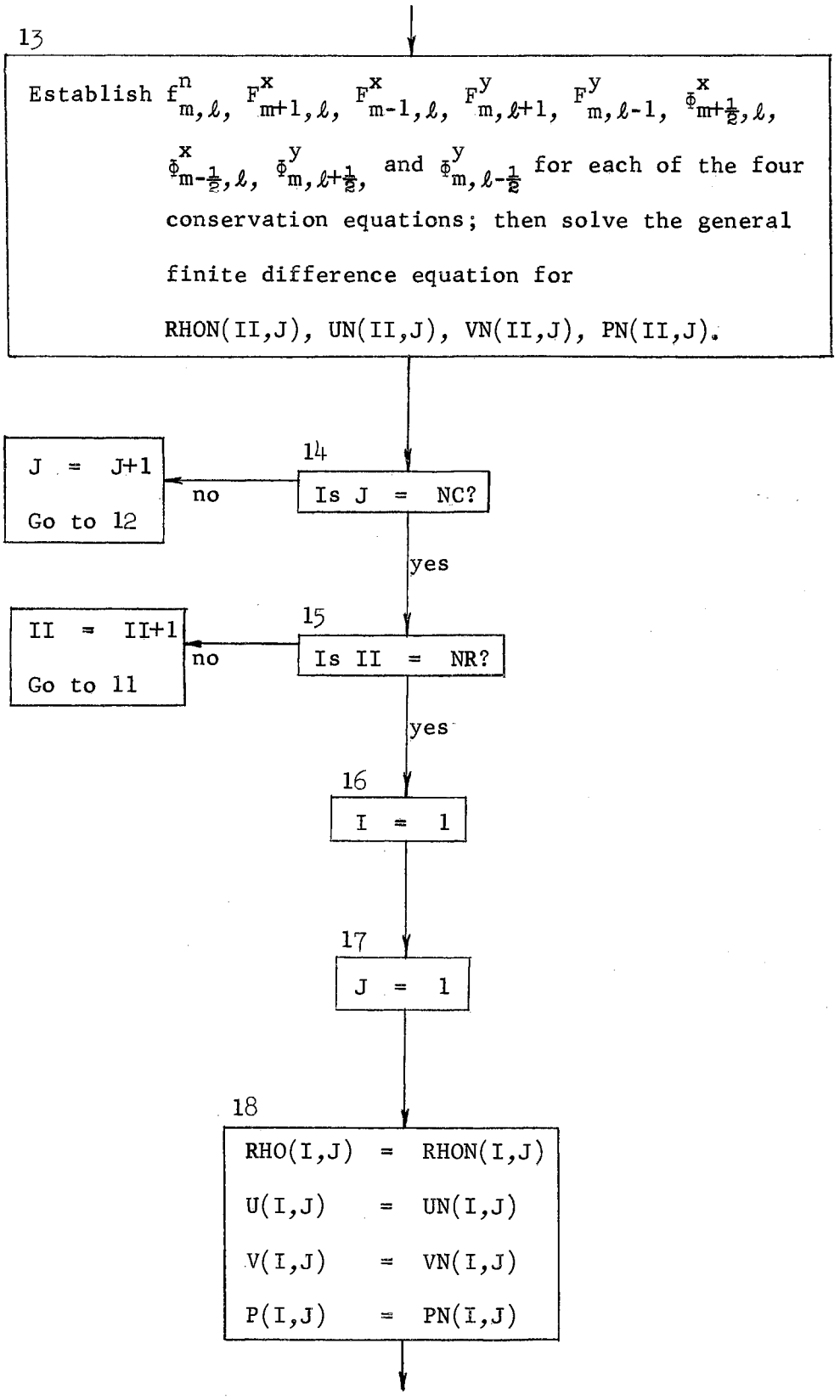
13
Establish $f^{n}_{m,\ell}$, $F^{x}_{m+1,\ell}$, $F^{x}_{m-1,\ell}$, $F^{y}_{m,\ell+1}$, $F^{y}_{m,\ell-1}$, $\Phi^{x}_{m+\frac{1}{2},\ell}$, $\Phi^{x}_{m-\frac{1}{2},\ell}$, $\Phi^{y}_{m,\ell+\frac{1}{2}}$, and $\Phi^{y}_{m,\ell-\frac{1}{2}}$ for each of the four conservation equations; then solve the general finite difference equation for RHON(II,J), UN(II,J), VN(II,J), PN(II,J).
14
Is J = NC?
no
J = J+1
Go to 12
yes
15
Is II = NR?
no
II = II+1
Go to 11
yes
16
I = 1
17
J = 1
18
RHO(I,J) = RHON(I,J)
U(I,J) = UN(I,J)
V(I,J) = VN(I,J)
P(I,J) = PN(I,J)

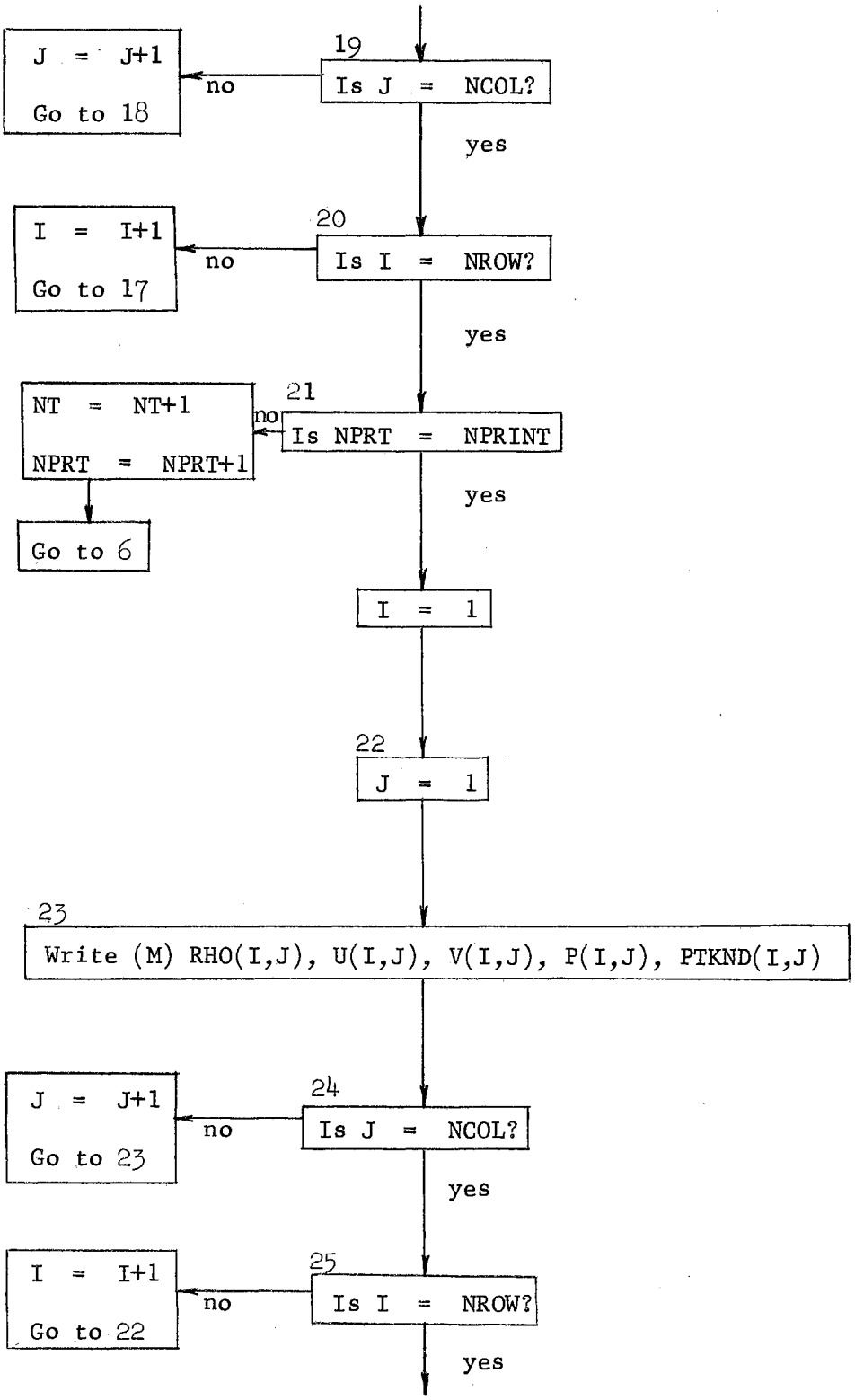
19
Is J = NCOL?
no
J = J+1
Go to 18
yes
20
Is I = NROW?
no
I = I+1
Go to 17
yes
21
Is NPRT = NPRINT
no
NT = NT+1
NPRT = NPRT+1
Go to 6
yes
I = 1
22
J = 1
23
Write (M) RHO(I,J), U(I,J), V(I,J), P(I,J), PTKND(I,J)
24
Is J = NCOL?
no
J = J+1
Go to 23
yes
25
Is I = NROW?
no
I = I+1
Go to 22
yes

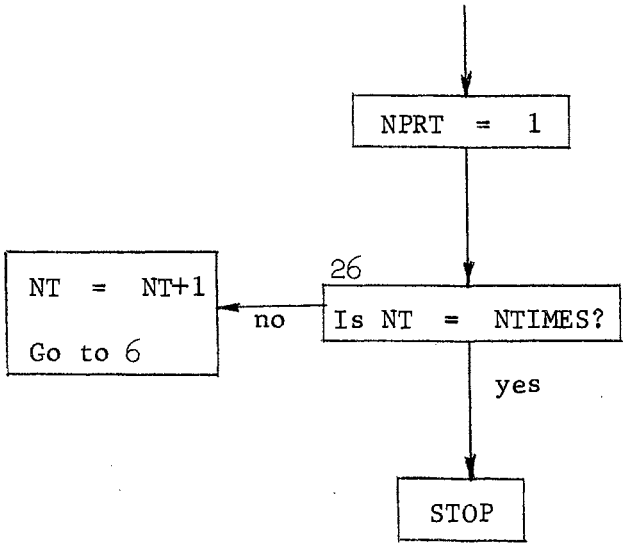
NPRT = 1
26
Is NT = NTIMES?
no
NT = NT+1
Go to 6
yes
STOP

APPENDIX F

METHOD FOR NON-DIMENSIONALIZING VARIABLES

In all of the computations which have been performed for this investigation all of the properties have been non-dimensionalized with respect to the conditions in the jet. This is somewhat different from the work of Tyler (4) who non-dimensionalized the properties with respect to the undisturbed conditions downstream of the moving shock wave. However, the method of non-dimensionalization is the same and is presented here for convenience.

Figure 60 is the schematic representation of a jet issuing into a cavity. The properties in the jet will be denoted by subscript x and those in the cavity by subscript y. The superscript * denotes dimensional quantities. If the thermodynamic properties in the entire field are non-dimensionalized with respect to the conditions in the jet, the result is

$$p_x = \frac{p_x^*}{p_x^*} = 1.0 \quad , \quad \rho_x = \frac{\rho_x^*}{\rho_x^*} = 1.0 \quad , \quad c_x = \sqrt{\gamma \frac{p_x}{\rho_x}} = \sqrt{\gamma} \quad , \tag{F-1}$$

$$p_y = \frac{p_y^*}{p_x^*} \quad , \qquad \rho_y = \frac{\rho_y^*}{\rho_x^*} \quad , \qquad c_y = \sqrt{\gamma \frac{p_y}{\rho_y}} \quad .$$

The velocities are non-dimensionalized by requiring that the Mach numbers in terms of dimensional quantities have the same values as the Mach

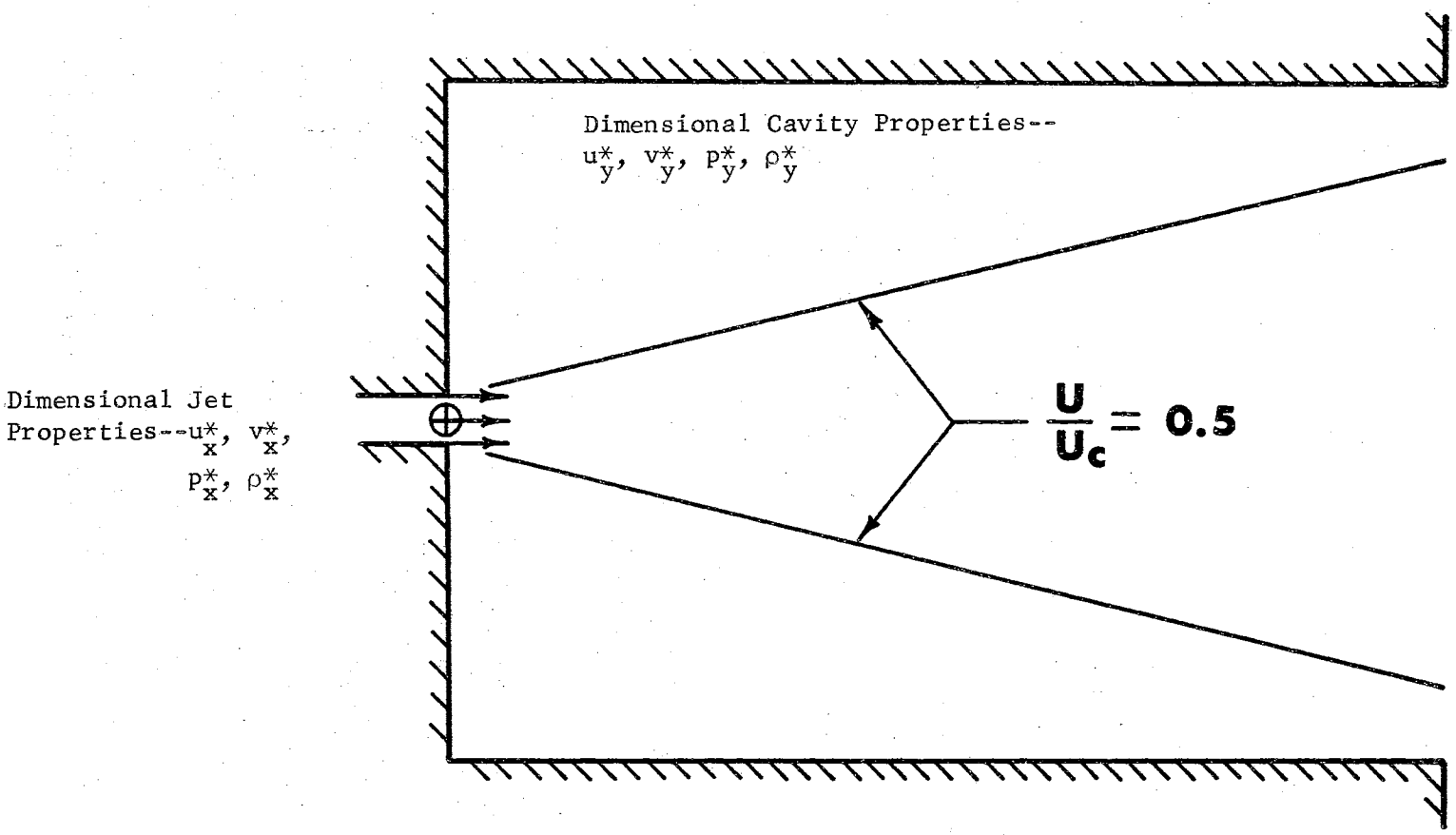

Figure 60. Jet Issuing into a Cavity.

numbers in terms of dimensionless values. For example, if the velocity in the cavity is considered,

$$M_y^* = \frac{u_y^*}{c_y^*} \qquad \text{and} \qquad M_y = \frac{u_y}{c_y}$$

but it is required that

$$M_y = M_y^*$$

therefore

$$\frac{u_y}{\sqrt{\gamma \frac{p_y}{\rho_y}}} = \frac{u_y^*}{\sqrt{\gamma \frac{p_y^*}{\rho_y^*}}}$$

By making use of equations (F-1), the dimensionless velocity can be written as

$$u_y = \frac{u_y^*}{\left[\frac{p_x^*}{\rho_x^*}\right]^{\frac{1}{2}}}. \qquad \text{(F-2)}$$

Therefore, the thermodynamic properties are non-dimensionalized as shown in equation (F-1); and the velocities are made dimensionless by dividing the dimensional velocities by the square root of the pressure-density ratio in the reference region.

VITA

William Fred Walker

Candidate for the Degree of

Doctor of Philosophy

Thesis: A NUMERICAL SOLUTION FOR THE INTERACTION OF A MOVING SHOCK WAVE WITH A TURBULENT MIXING REGION

Major Field: Mechanical and Aero Space Engineering

Biographical:

Personal Data: Born in Sherman, Texas, December 1, 1937, the son of Harry N. and Francis Olivia Walker.

Education: Attended grade school in Bowie and Arlington, Texas; graduated from Arlington High School, Arlington, Texas in 1955; received the Associate of Science degree from the Arlington State College, with a major in Aeronautical Engineering, in June, 1957; received the Bachelor of Science degree from The University of Texas, with a major in Aerospace Engineering, in January, 1960; received the Master of Science degree from The University of Texas, with a major in Aerospace Engineering, in June, 1961; completed the requirements for the Doctor of Philosophy degree in May, 1966.

Experience: Student Engineer for the United States Army Corps of Engineers, Carswell AFB, Texas, during the summers of 1957 and 1958; Student Engineer for Chance Vought Aircraft Co., Dallas, Texas, during the summer of 1959; Teaching Assistant for the Department of Aerospace Engineering of The University of Texas, from 1959 to 1961; Research Engineer for the Bureau of Engineering Research, The University of Texas for the 1959 and 1960 school years; Engineer for Ling-Temco-Vought, Inc., Dallas, Texas, from 1961 to 1962; Teaching and Research Assistant for the School of Mechanical Engineering of Oklahoma State University from 1962 to 1965; Engineer for Sandia Corporation, Albuquerque, New Mexico, for the summer of 1964.

Professional organizations: The author is a member of the following professional organizations: American Institute of Aeronautics and Astronautics, and the Society of Sigma Xi.